

# Full Validation Report LOTOS-EUROS

Open-Source v3.0.000

Authors	H.J. Jonas, R. Kranenburg		
Date	2025-02-05		
Run ID	EUgrid-v3-0-000 (open source version 3.0)		
Reference run ID	EUgrid-v2-3-000 (open source version 2.3)		
Project	LOTOS-EUROS Validation		
Location	Europe, MACC grid		

# All rights reserved

No part of this publication may be reproduced and/or published by print, photoprint, microfilm or any other means without the previous written consent of TNO.

© 2025 TNO

# Contents

Full V	alidation Report LOTOS-EUROS Open-Source v3.0.000	1
1. 1.1.1. 1.1.2. 1.1.3.	Changes  Functional Changes  Technical Changes  Bug Fixes	1 1
2.	Detailing of functional changes	2
3.	Evaluation Approach	4
4. 4.1. 4.2. 4.2.1.	Results and Discussion.  Harmonization of molecular diffusivity	7 8
4.2.2. 4.3.	Biogenic isoprene emissions  Concentrations and Measurements of gaseous pollutants	
4.3.1. 4.3.2.	Ozone Nitrogen Dioxide	10
4.3.3.	Ammonia	
4.3.4.	Sulphur Dioxide	
4.4.	Concentrations and Measurements of Particulate Matter	
4.4.1.	PM 2.5	
4.4.2.	Nitrate	
4.4.3.	Sulphate	
4.4.4.	Ammonium	
4.4.5. 4.4.6.	Sodium Organic Carbon	
4.4.7.	Elementary Carbon	
4.4.8.	PM10	
4.4.9.	Mineral Dust	
4.5.	Deposition	
4.5.1.	NHx Deposition	
4.5.2.	NOy Deposition	51
4.5.3.	SOx Deposition	53
4.6.	Statistics	55
5.	Conclusions and recommendations	56
6.	References	56
7.	Appendix	57
8.	Signature	66

# 1. Changes

#### 1.1.1. Functional Changes

- Implementation of the 3-tiered approach for deposition based on the levels:
  - o climate zone
  - o land use type
  - o vegetation type
- updated land use maps
  - o v2.3: EEA200, Corine2000, world water bodies 2011, corine2018
  - o v3.0: Corine2018, ESA2015
- extension of LOTOS-EUROS land use classifications
- improved translations between Corine2018, ESA2015 to the LOTOS-EUROS land use classifications
- harmonization of molecular diffusion parameter used in the calculation of the dry-deposition velocities of gas molecules
- switch to select chemistry scheme CB7. Note that CB4 is still the default

## 1.1.2. Technical Changes

- Limit outflow to max 90% to avoid empty cells.
- Removed deprecated boundary grids.
- Removed duplicate values in data variables list, added check on duplicates.
- Use double precision arrays to convert from real to date; required for particular boundary condition files.
- Write "le.copy.jb" file to run directory rather than source directory.
- Introduced data variables "zenith" and "coszen" to replace the arrays in dims
- Updated UTOPyA and other scripts.
- Included implementation to use less memory for reading emissions
- Option to read OH fields from previous run, used for methane- and sulphur-only runs.
- Added settings for CAMS-REG-ANT v7\_0 emissions.
- Restructured time profile definition into cases "static" and "selection".
- support change in sst[k] filenames in ECMWF meteo archive.
- Removed deprecated and unused files, parameters and macro's

## 1.1.3. Bug Fixes

• Fixed a unit conversion in reading emission data from the *data* structure.

Impact-score=potentially high.

If the *data* filetype structure for reading emissions defined in the file lotos-euros-emissions.rc is: le.emis.*your-emission-name*.filetype : data in combination with the unit 'Mg/year' or 'tonnes/year'

the unit conversion in le\_emis\_data.f90 did not go correctly. It led to zero emissions.

Fixed bug in obtaining target units in "Variables\_Calc\_Total"

Impact-score=zero.

Instead of an argument "check\_units", the code could should have used an argument "units" to obtain the target units. This part of the code was not used anyway, and would have automatically lead to an error if it was used.

• bugfix that "coszen" of previous hour was used to compute stability class.

TNO Public 3/67

Impact-score=low. Only around sun-rise and sun-set differences are seen, but these are not very large.

Fixed bug in array bounds when interpolation target is outside non-cartesian grid.

Impact-score=low

This ensures that a range of source cells is limitted to the allowed range, otherwise an out-of-bounds error might occur when mapping input data to the model grid.

• Bug-fix to use correct iihour\_local at year-switch in le\_emis\_tno\_base.F90

Impact-score=low

For the first hour of the year a time profile values was selected out of the array bounds. This never seemed to have cause a significant problem.

Output of biogenic emissions changed from emis\_bio to emis-bio.

Impact-score=low

The name changed to facilitate automatic break-up of filenames in different parts in postprocessing.

# 2. Detailing of functional changes

In LOTOS-EUROS v3.0, we introduce the three-tiered land use approach and CB7 as the main functional improvements to the model. Both developments are described in detail in the LOTOS-EUROS Reference Guide v3.0. [1] Along with the implementation of the three-tiered approach which, in principle, does not lead to any changes of the model results, there are several updates and improvements that do affect the model results.

First of all, the underlying land use (lu) maps are updated in the open-source versions of LOTOS EUROS v2.3 and v3.0 (Appendix, Table 5). In v2.3, the maps EEA200, Corine2000, world water bodies 2011, and CORINE2018 were used: in v3.0 it is CORINE2018 and ESA2015. In the modeled domain of this report, the main differences between v2.3 and v3.0 are outside the CORINE domain which include Belarus, Ukraine, and parts of west Russia, and north of Africa. In Ukraine, Belarus and west Russia, a large fraction of arable land (ara) and grassland (grs) is now forest (both coniferous and broadleaf). This change has a large impact on the deposition of various compounds as forests are known to promote deposition through e.g. Ra. In the north of Africa, parts of forest fraction is now assigned to grassland. This change has again impact on the Ra. The change of forest lu-fraction is shown in Figure 84. Second, the LOTOS-EUROS lu-classes are extended with the semi-natural land (sem) class (see Table 6 in the Appendix) which is assigned to e.g. natural grassland, transitional woodland shrub, and inland marches (see Table 7 in the Appendix). As an example, the dry deposition parameters of this new class are listed for the temperate climate and default vegetation in table A1 in the LOTOS-EUROS Reference Guide v3.0.000. All other parameters can be found in the deposition parameter file (base/000/data/ deposition-parameters.nc). In addition, the two forest classes coniferous (cnf) and deciduous (dec) forest are replaced/extended by coniferous evergreen (fce), coniferous deciduous (fcd), and broadleaved evergreen (fbe), and broadleaved deciduous (fbd) forest. In the default version of LOTOS-EUROS, the broadleaf forest is deciduous and the coniferous forest is evergreen, meaning that there is no lu-fraction assigned to fbe and fcd. Therefore, the extensions of the forest classes have no effect on simulation results. Lastly, the desert (dsr) class has been renamed into barren land (brn). Third, the translation between Corine2018<sup>1</sup> and ESA2015<sup>2</sup> to LOTOS-EUROS lu-classes has been improved as shown in Table 7. The differences with the largest expected impact are:

) TNO Public 4/67

<sup>&</sup>lt;sup>1</sup> https://land.copernicus.eu/en/products/corine-land-cover/clc2018

<sup>&</sup>lt;sup>2</sup> https://www.esa.int/ESA\_Multimedia/Images/2018/09/2015\_global\_land\_cover\_map

- The Moors and heathland and Sclerophyllous vegetation class changed from other (oth) into sem.
- The Transitional woodland-shrub changes from forest (dec+cnf) into sem. Forests promote deposition as it has large surface area from its branches and leaves impacting the stomatal pathways via Rb and Rc (eq. 5.8 in Ref [1]) and the branches causes the air to mix well leading to a low aerodynamic resistence Ra. Therefore, this change is expected to have a large impact on the deposition of various species.
- The Sparsely vegetated areas class changes from dsr into sem. A similar argument as before, seminatural land contains more vegetation compared to the desert leading to a low aerodynamic resistence Ra. Therefore, the sem class has larger deposition velocities compared to the dsr class.
- The mixed forest is now fully assigned to 'Broadleaved deciduous forest' (fbd). Areas with the largest coverage of mixed forest are in the mountainous region in the Alps, eastern Europe and Scandinavia. The coniferous parts of these mixed forests contains mostly larks, which behave as deciduous trees in terms of deposition.

For the CORINE classes, the land use classes with significant lu-fraction are shown in Figure 82 and Figure 83.

Forth, in the Mediterranean climate zone, the vegetation parameters of vpdmin, vpdmax, Tmin, Topt, Tmax where vpd is the vapor pressure deficit, T the temperature, min the minimum, max the maximum and opt the optimum are adjusted according to the vegetation of the Mediterranean climate. [5] Previously, these vegetation parameters were accessible via the mediterranean flag; now in v3.0 these vegetation parameters are the default.

Lastly, as the molecular diffusivity is a molecular property and to keep to the physical parameters in the model consistent, the definition of the molecular diffusivity has been harmonized in various parts of the calculation of dry-deposition rates. [3] In v2.3, for the calculation of the Rb and Rc, different values of the molecular diffusivity were used (Table 1). In v3.0, we select the value corresponding to Diffc-Rc, as the impact of changing Diffc-Rc was smaller compared to the impact of Diffc-Rb. Note that the effect of the molecular diffusivity on the deposition rate is for most species insignificant, except for fast-depositing species such as NH3 for which the increased diffusivity (Diffc-Rb<Diffc-Rc) can lead to increased depositions.

Table 1 The molecular diffusivity parameters Diffc-Rb and Diffc-Rc were used in v2.3.. In v3.0, only the values of Diffc-Rc were used. Units are in  $[m^2/s]$ 

	O3	NH3	NO	NO2	SO2	CO
Diffc-Rb	0.144e-4	0.191e-4	0.199e-4	0.136e-4	0.112e-4	0.176e-4
Diffc-Rc	0.130e-4	0.210e-4	0.160e-4	0.130e-4	0.110e-4	0.160e-4

The other main functional change in LOTOS-EUROS v3.0 is the introduction of Carbon Bond 7 (CB7) as an optional new chemistry scheme. CB7 includes extended chemical reactions and it enables more detailed simulation of chemical conversions important for the formation of secondary organic aerosols. Please see section 4.2 of the LOTOS-EUROS Reference Guide v3.0 and chapter 14 of the User Guide v3.0 for more details. [1,2] At the moment, CB7 is available under the disclaimer that it has not reached the same level of consolidation in the model as CB4, and we are happy to receive feedback from users. This report focusses on the effect of the changes due to the updates and fixes from v2.3 to v3.0 using the CB4 chemical scheme. The report of the impact of CB7 versus CB4 and the three-tiered land use approach is available upon request. The practical changes, i.e. selecting the updated lu-map and corresponding deposition parameter file in the three-tiered approach or selecting CB4, is described in detail in the LOTOS-EUROS User Guide v3.0.

TNO Public 5/67

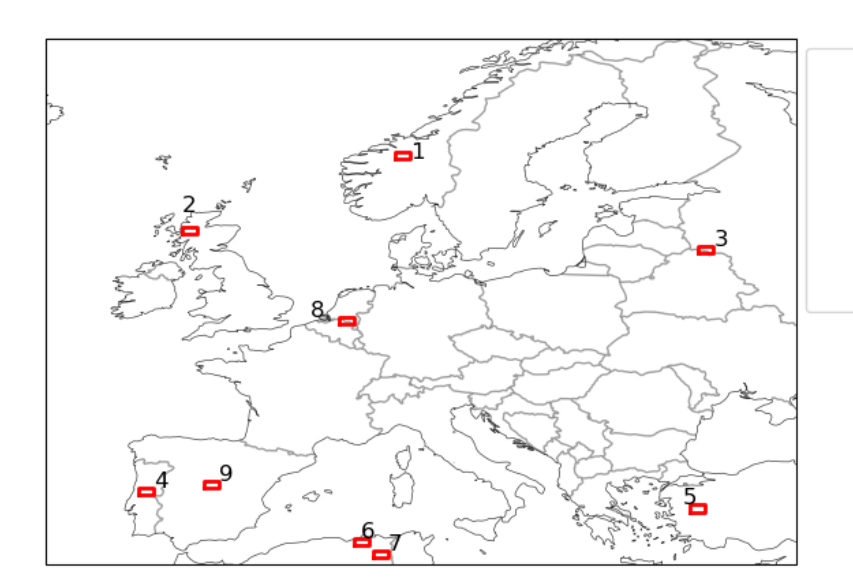
# 3. Evaluation Approach

#### Simulation details

The impact of the functional changes were tested by LOTOS-EUROS simulations over 2018 with a spin-up period of 10 days on the MACC domain (W15-E35; N35-N70, 0.5x0.25° resolution). This includes CAMS\_v2.2REF2 emission with condensables. Biogenic emissions using tree-specific emission factors, soil-NOx emissions, sea salt emissions, desert dust, road resuspension and agricultural dust emissions and GFAS wildfire emissions (from MACC) were used. Note that due to the lu-fraction changes, the biogenic emissions are not the same in the two versions. Climatological boundaries from EMEP, Isaacson and Logan are used together with 3-hourly results from the CAMS-nrt product. This basically implies that for the most important tracers, the CAMS-nrt product is used. Additionally, timeprofiles from TEMPO v3.2 are used. These profiles have a detailed profile specified per country and sector.

### Analysis of deposition velocities

The changes in the observed concentrations are partly explained by the changes in deposition velocity as the deposition flux is a multiplication of deposition velocity and the concentrations (see e.g. Eqn. 5.1 in the LOTOS-EUROS Reference Guide v3.0). To inspect the changes in deposition velocity as function of the lu-classes in detail, a day in the winter (5<sup>th</sup> of January 2018) and summer (5<sup>th</sup> of June 2018) were simulated while printing all deposition velocities as function of all species listed in the results and lu-class to file. The locations shown in Figure 1 were selected for further inspection based on their large change of concentrations between v2.3 and v3.0. All domains are lengths 1<sup>o</sup> longitude and 0.5<sup>o</sup> latitude. In the appendix, the lu-class changes and recategorizations are shown the bar plots in Figure 85 to Figure 89.



- 1 Norway (9.03E,62.35N)
- 2 Scotland (-5.17E,57.33N)
- 3 Russia-Belarus-border (29.24E,56.09N)
- 4 Portugal (-8.10E,39.98N)
- 5 Turkey (28.70E,38.87N)
- 6 Algeria (6.26E,36.62N)
- 7 Algeria2 (7.56E,35.80N) 8 the-Netherlands (5.34E.51.33N)
- 9 Madrid (-3.69E,40.43N)

Figure 1 The locations where the land use fractions and deposition velocities are inspected in the winter and summer. Red blocks indicate the sampled domain, the numbering lists the name/location with their coordinates.

#### Measurement stations

The simulated concentrations are compared to the measurement stations listed in Table 2 which' location is shown in Figure 2. These measurement stations are chosen as they are spread over the domain, not in elevated areas and are located areas with (relatively) homogeneous land use classes.

TNO Public 6/67

HR0011A

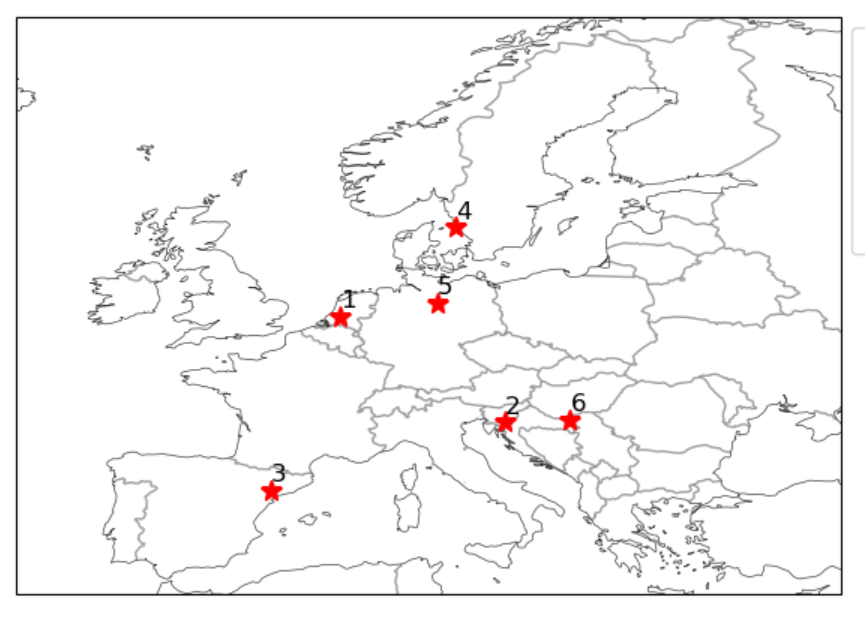
	Station Code	Name	Country	Lon [ºE]	Lat [ <sup>0</sup> N]	Altitude [m]
1	NL0644R	Cabauw Wielsekade	The Netherlands	4.92	51.97	1
2	S10008R	Iskrba	Slovenia	14.87	45.57	520
3	ES0014R	Els Torms	Spain	0.72	41.40	470
4	SE0014R	Råö	Sweden	11.91	57.39	5
5	DF0002R	Waldhof	Germany	10.76	52.80	74

Croatia

18.83

45.70

Table 2 Measurement stations' station code, name, country, longitude, latitude and altitude.



Kopacki Rit

measurement stations:

0

- 1. NL0644R (4.92E,51.97N)
- 2. SI0008R (14.87E,45.57N)
- 3. ES0014R (0.72E,41.40N)
- 4. SE0014R (11.91E,57.39N)
- 5. DE0002R (10.76E,52.80N)
- 6. HR0011A (18.83E,45.70N)

Figure 2 Locations of the measurement stations indicated by the red stars and numbered 1 to 6. The legend shows their coordinates.

# 4. Results and Discussion

Here, we present the effects of the changes due to the updates and fixes from v2.3 to v3.0. First, the change due to the harmonization of the molecular diffusivity is evaluated in section 4.1. Then in section 4.2, the changes in biogenic emissions due to the lu-fraction and classification changes are inspected. In section 4.3, the concentrations of the gaseous pollutants ozone, nitrogen dioxide, ammonia, sulphur dioxide are discussed compared to ground measurements from EBAS<sup>3</sup> and EEA<sup>4</sup>. In section 4.4, the concentrations of particulate matter are discussed. For PM2.5, the concentrations of nitrate, ammonium, sulphate, organic carbon, elementary carbon and sodium are discussed and for pm10, the discussion also includes mineral dust. In section 4.6, the averaged statistics, namely the root mean squared error (RMSE), the coefficient of determination (R2), and the normalized mean bias (NMB), over the measurement stations are presented from EBAS and EEA measurement stations.

TNO Public 7/67

<sup>&</sup>lt;sup>3</sup> https://www.eea.europa.eu/en/datahub

<sup>&</sup>lt;sup>4</sup> https://ebas.nilu.no

# 4.1. Harmonization of molecular diffusivity

The effect of the molecular diffusivity on the deposition velocity is shown in Figure 3. The data is taken on 2018-06-05 of The Netherlands (grid cell at 5.34E; 51.33N) on the coniferous (evergreen) forest as the coniferous forest is known to have large deposition rates and thus will show most effects. Observed from the figures, only for ammonia (NH3), the update of the molecular diffusivity has an impact leading to increased dry-deposition fluxes. Therefore, only at domains with large lu-fractions of forest, the effect may be observed. Elsewhere, the harmonization of the molecular diffusivity has no significant impact.

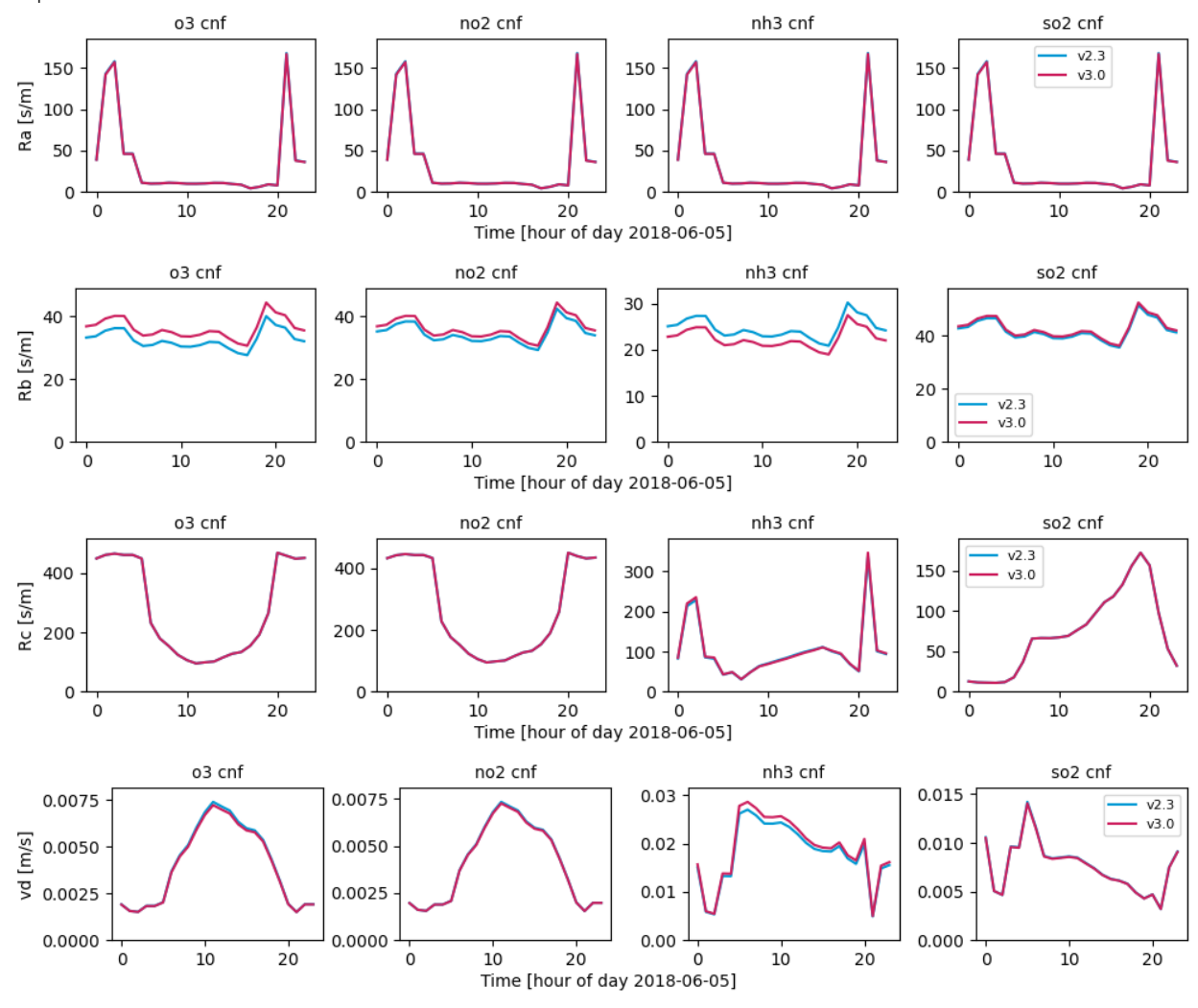


Figure 3 The Ra, Rb, Rc and the deposition velocity of ozone, nitrogen dioxide, ammonia, and sulphur dioxide on the coniferous (evergreen) forest class at (5.34E; 51.33N), i.e., location 8 in Figure 1, on 05-06-2018. For v2.3, the coniferous forest class is called cnf, for v3.0 it is tmp\_fce\_def.

# 4.2. Biogenic emissions

The land use fractions and classifications impact the biogenic emissions in LOTOS-EUROS as it used the land use fraction map to, for example, determine tree-specific emissions, sea salt emissions, and desert dust. Therefore, the updated land use map led to changed biogenic emissions in the model. In this section, we list the compounds that are significantly impacted by the update, namely: NO, and isoprene.

TNO Public 8/67

## 4.2.1. Biogenic NO emissions

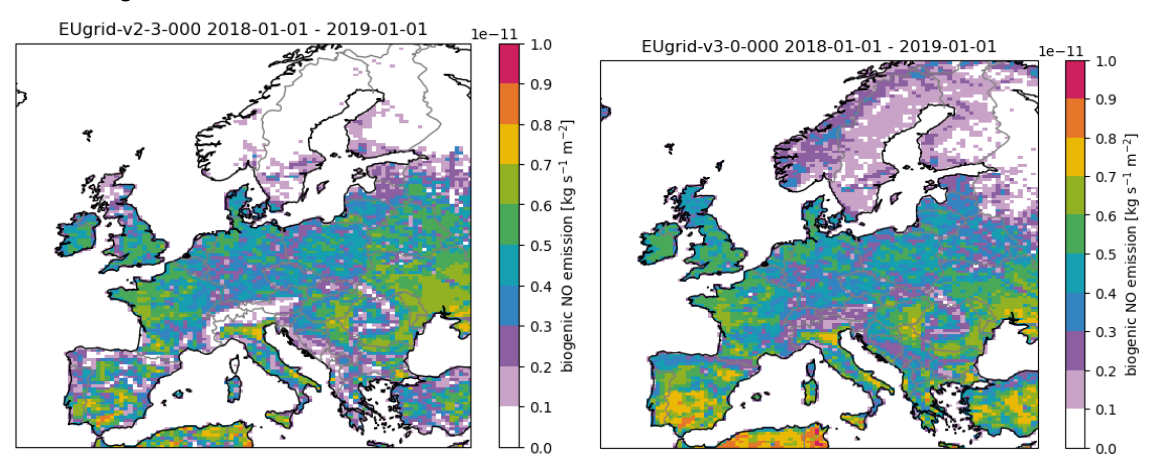


Figure 4: Biogenic NO emissions

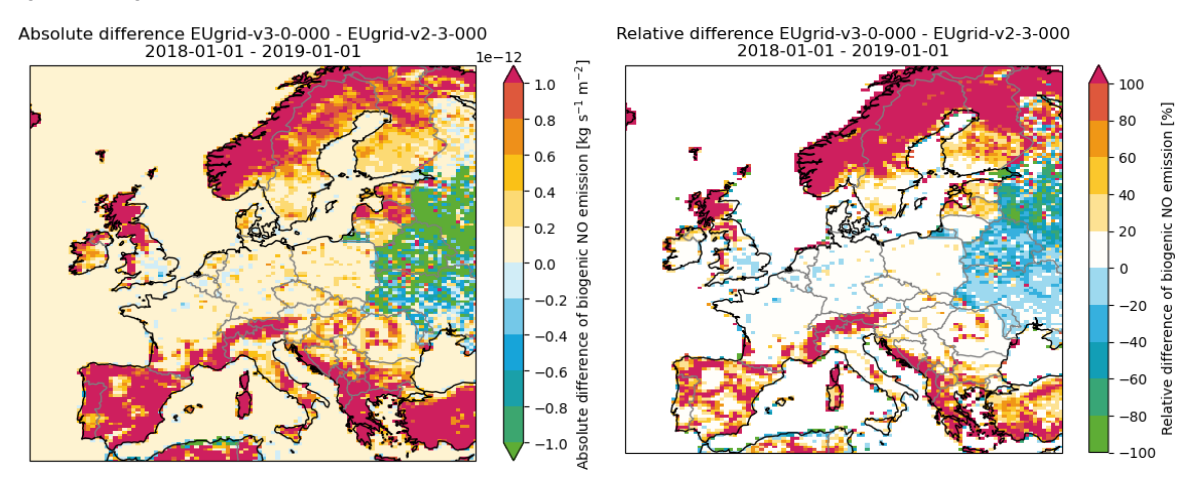


Figure 5: Absolute and relative difference of biogenic NO emissions.

Biogenic nitrogen monoxide (NO) emissions are caused by natural soil microbial processes and in the model controlled by the three lu-dependent parameters A\_bio\_no, temp\_coeff\_no and base\_coeff\_no listed in the deposition parameter file. The changes in lu-classes and fractions clearly have a large effect on the biogenic emissions of NO as shown in Figure 4 and Figure 5. In Scandinavia, Scotland, southern Europe including Spain, Greece, Turkey, and parts of the Alps, and north Africa show a large increase of biogenic NO emissions of >10<sup>-12</sup> kg s<sup>-1</sup>m<sup>-2</sup> or ~+100%. The LOTOS-EUROS lu-classes changed largely over these regions (as shown in Figure 82 and Figure 83) leading to an increased semi-natural class instead of lu-classes: *oth, grs+wai, dec+cnf and dsr.* The following CORINE2018 classes are responsible for the increased biogenic NO emissions (als shown in Figure 82 and Figure 83):

- 1. moors and heathland (oth --> sem),
- 2. peat bogs (grs +wai --> sem),
- 3. transitional woodland shrub (dec+cnf --> sem),
- 4. natural grassland (oth --> grs),
- 5. sparsely vegetated areas (dsr --> sem)

where in brackets the old to new LOTOS-EUROS classification change is indicated.

In contrast, Belarus, Ukraine, and west of Russia show a large decrease of biogenic NO emissions of <10<sup>-12</sup> kg s<sup>-1</sup> m<sup>-2</sup> or 0 to -100%. The land use classes changed over these regions with the introduction of ESA2015. The main changes responsible for the decrease of biogenic NO emissions the change of the

) TNO Public 9/67

classes *ara*, *crp*, and *cnf* into the class of *dec*. Specifically, the landuse class change of ara and crp class into dec is responsible for the decreased biogenic NO emission.

Nitrogen monoxide in the atmosphere reacts with ozone and nitrogen dioxide in a cyclic manner, influenced by UV light and volatile organic compounds (VOCs). During the day, the following reactions involving NO, O3 and NO2 are fast:

Reaction 1:  $NO + O_3 \rightarrow NO_2 + O_2$ 

Reaction 2:  $NO_2 + O_2 + M + h\nu \rightarrow NO + O_3 + M$ 

where M may be a VOC and hv is radiation. [4] These two chemical reactions are cyclic as the products of reaction 1 are the reactants of reaction 2 and vice versa. Hence, changing the concentration of a single reactant will lead to a shift of concentration of the other compounds.

# 4.2.2. Biogenic isoprene emissions

Biogenic tree-specific emissions include isoprene and terpene (not shown here) which are only minorly impacted by the lu-changes. Only in Ireland a decrease of isoprene is observed of -1.0 kg s<sup>-1</sup>m<sup>-2</sup> or ~-80%.

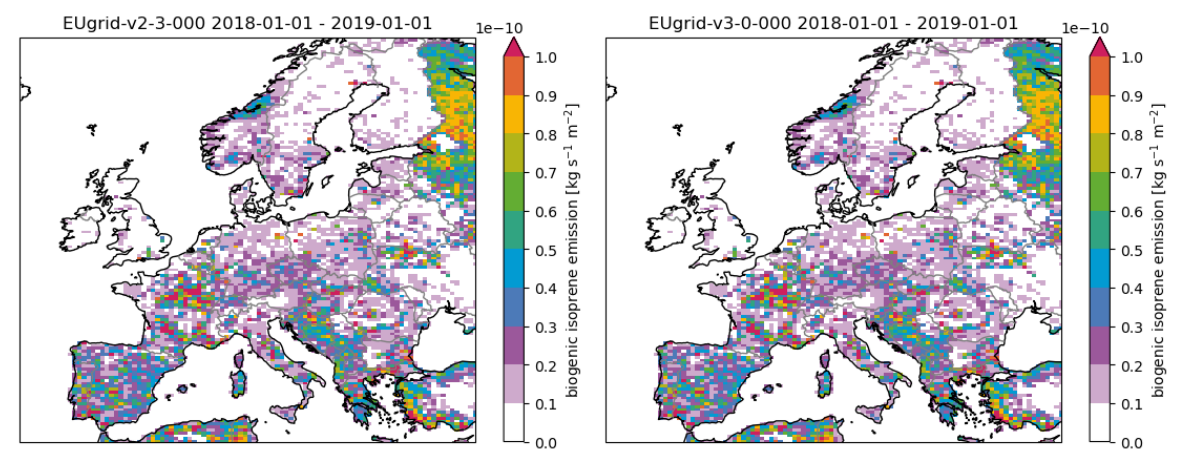


Figure 6: Biogenic isoprene emissions

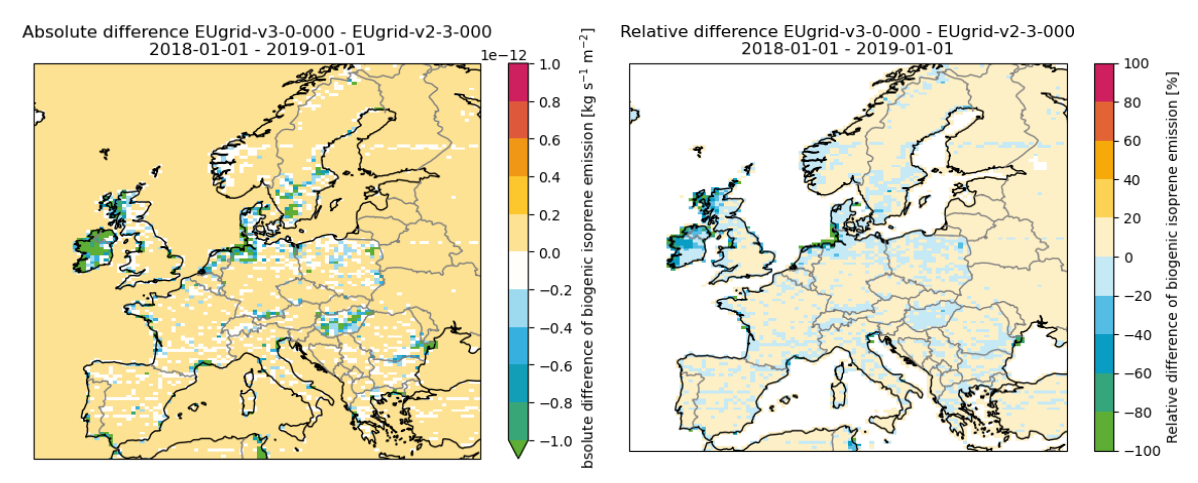


Figure 7: Absolute and relative difference of biogenic isoprene emissions.

TNO Public 10/67

# 4.3. Concentrations and Measurements of gaseous pollutants

In this section the concentration maps of the species ozone, nitrogen dioxide, ammonia, and sulphur dioxide are discussed in 4.3.1 to 4.3.4, respectively.

# 4.3.1. Ozone

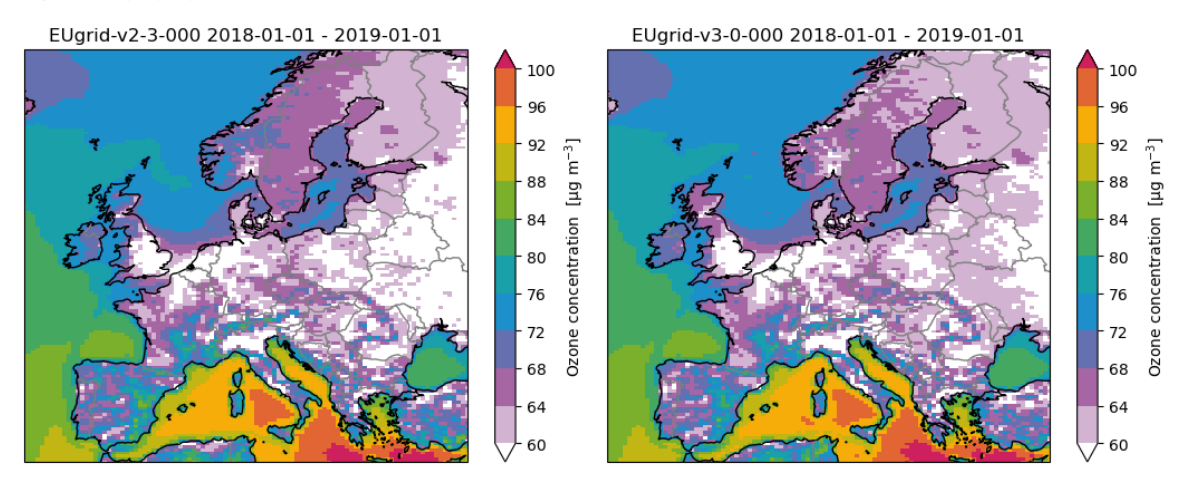


Figure 8: Concentration of ozone in air.

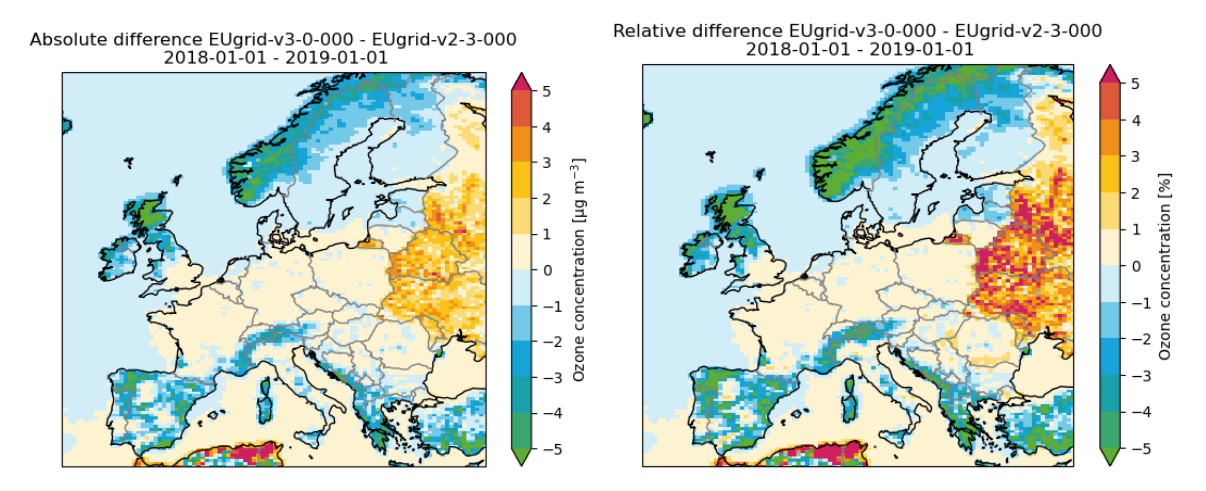


Figure 9: Absolute and relative difference of ozone concentration in air.

TNO Public 11/67

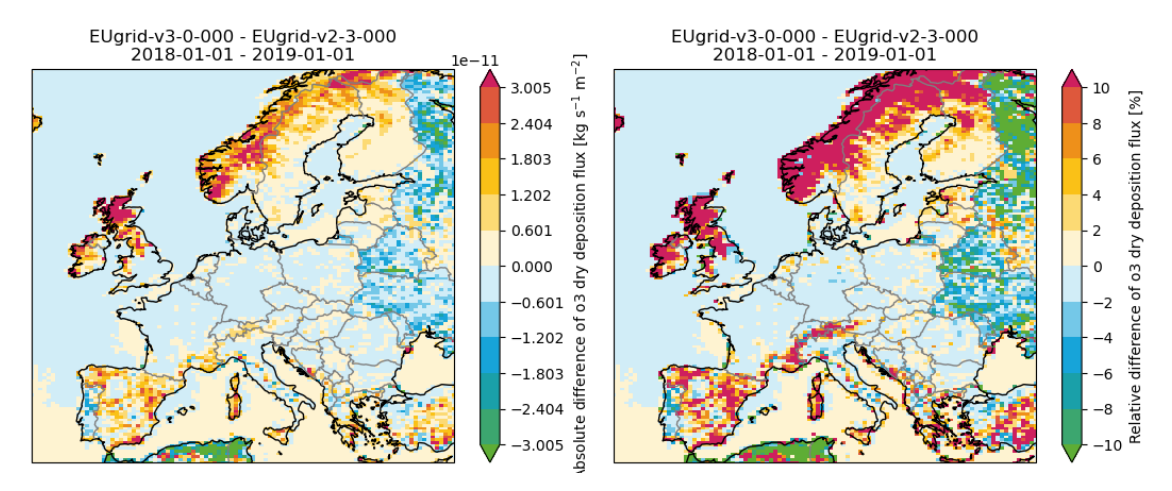


Figure 10: Absolute and relative difference of ozone dry deposition flux.

Shown in Figure 8 and Figure 9 are the ozone concentrations and (relative) differences between version v2.3.000 and v3.0.000. The ozone concentrations show a decrease in the south of Europe, Scotland, and Norway up to 4-5  $\mu$ g/m³ (~-5%). In eastern Europe, namely Belarus, Ukraine and west of Russia an increase of 1-2  $\mu$ g/m³ (~5%), and in the north of Algeria and Tunisia an increase of >5  $\mu$ g/m³ (~3-5%) is shown. Through central Europe, such as in The Netherlands, Germany, France, and Poland no significant changes are observed.

Comparing the trends in absolute difference concentration in Figure 9 with the absolute difference of biogenic NO emission in Figure 5, we observe the same trends but reversed. As written by Reaction 1, increased NO concentrations lead to decreased O3 concentrations as Reaction 1 shifts to the right hand side, and vice versa. Hence, the majority of the observed ozone concentration change is assigned to the effect of biogenic NO emissions.

In addition, the ozone dry deposition is impacted by the land use changes as shown in Figure 10. Here, we highlight the locations with significant changes:

- decreased dry deposition is observed in:
  - o North Africa (Algeria): A large fraction of arable land (0.72 out of 0.80) is now assigned to grassland which shows lower deposition velocities, specifically during the day in the summer.
- increased dry deposition is observed in:
  - In Scotland, the former classifications in oth, dsr and wai are now sem. The largest lufraction are found in "semi-natural vegetation heaths" (tmp\_sem\_hth) and "semi-natural vegetation herbacious" (tmp\_sem\_hrb). The dry deposition velocity is larger for the seminatural class compared to the old oth, drs and wai class.
  - o Similar in Norway, the vegetation types Moors and heathland (oth) and Sparsely vegetated areas (dsr) which cover approximately 0.40 of the lu-fraction changes into sem. This land use change causes the ozone deposition velocity to increase in the summer, but remains equal in the winter.
  - o In vegetation parameters in the mediterranean climate have been adapted. In parts of Spain and Turkey, we observe more dry deposition of ozone even though the concentrations are lower.

#### Ozone Measurements

The averaged statistics over the EBAS and EEA measurement stations are listed in Table 3 and Table 4. in the Appendix and the temporal mean per station are shown in the Figure 11 and Figure 12. The averaged statistics of the EBAS measurements, for ozone concentrations change from 18,51  $\mu$ g/m³ to 18,45  $\mu$ g/m³ (RMSE), 0,51 to 0,52 (R2), and 0.05 to 0.04 (NMB). The 8-hour averaged ozone

TNO Public 12/67

concentrations (MDA8) change from 14,02  $\mu$ g/m³ to 13,66  $\mu$ g/m³ (RMSE), 0,58 to 0,59 (R2), and 0,06 to 0,05 (MNB). The EEA measurements stations show a similar minor change in averaged statistics. The simulation results compared to the measurements stations listed in Table 2 are shown in the Figure 13 to Figure 18. The stations NL0644R, SE0014R, SI0008R, and DE0002R all lie in regions that are little affected by the updates. Hence, little difference between v2.3 and v3.0 is observed in the diurnal plots, scatter plots and time traces. Only, ES0014R, located in Spain, shows a difference, albeit mostly only during the night, showing mainly lower concentration in the evening and early in the morning. The measurement station HR0011A, located in Croatia, shows a shift in the morning and the evening to an earlier hour.

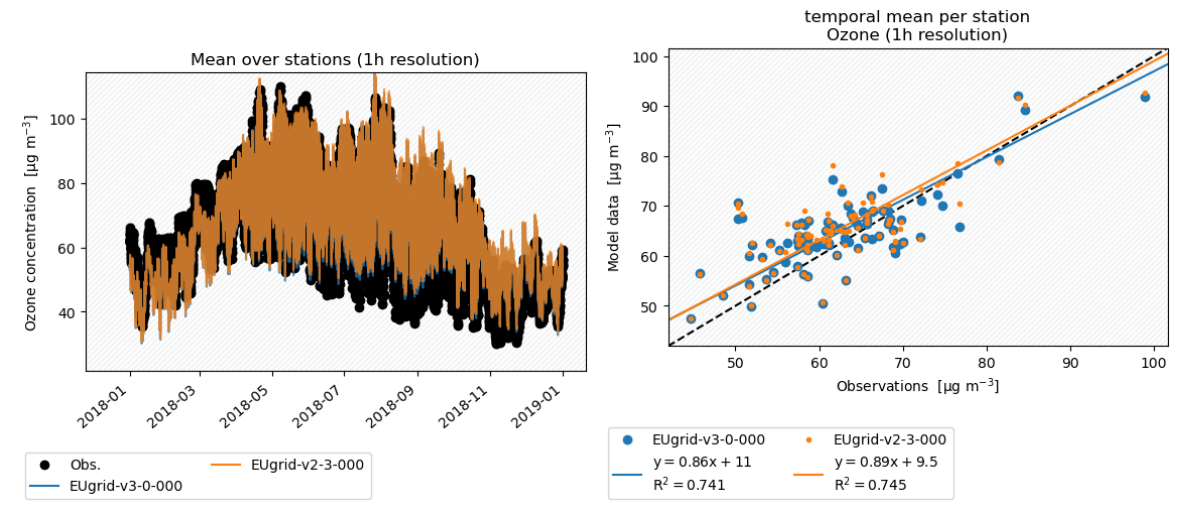


Figure 11: Line plots of ozone for mean of EBAS stations.

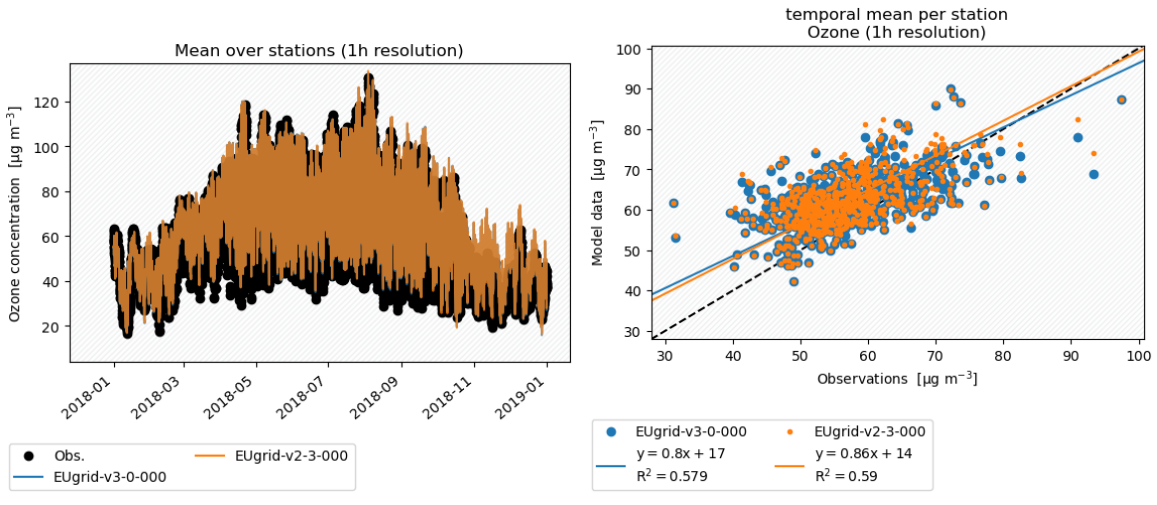


Figure 12: Line plots of ozone for mean of EEA stations

) TNO Public 13/67

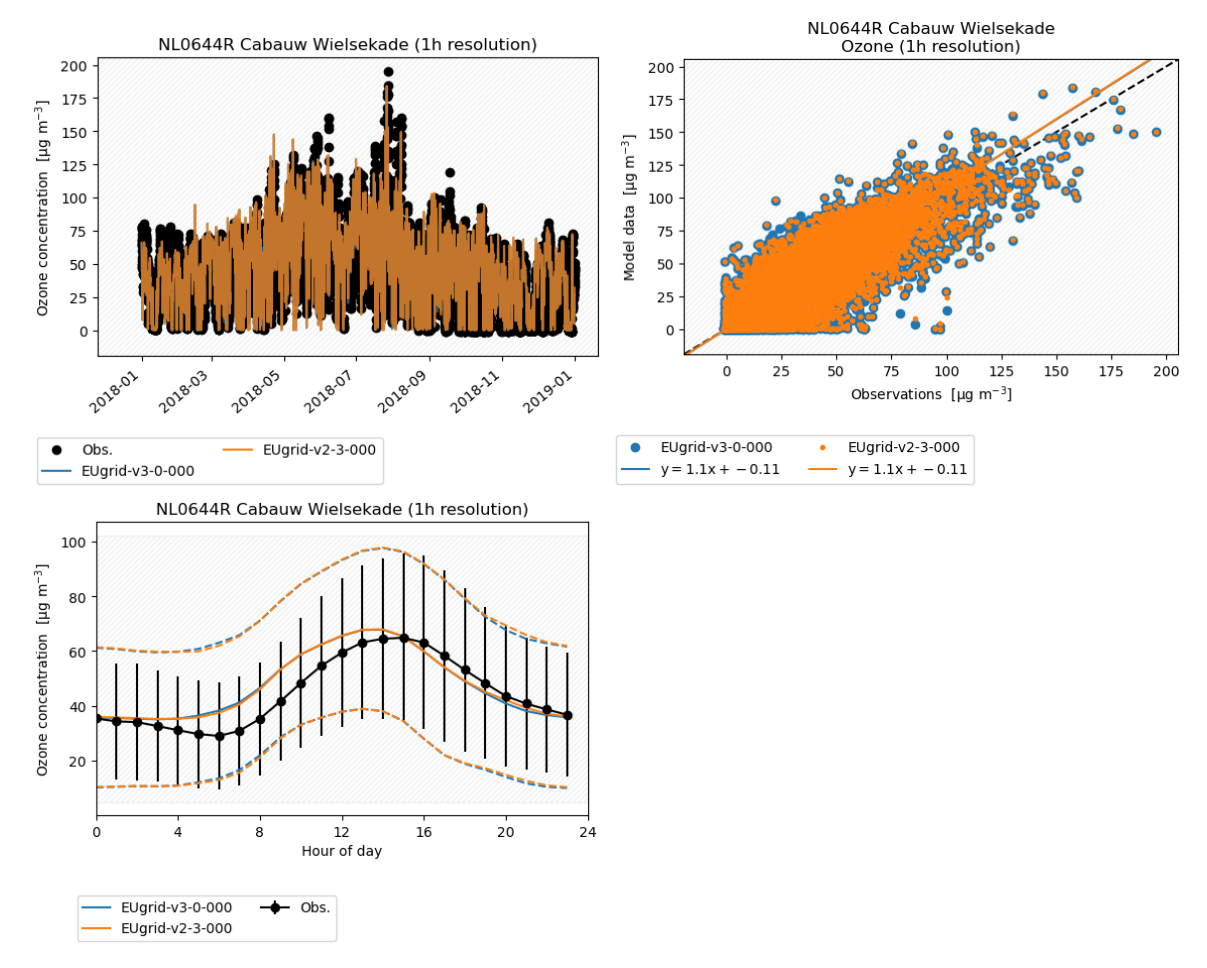


Figure 13: Line plots of ozone for station NL0644R.

TNO Public 14/67

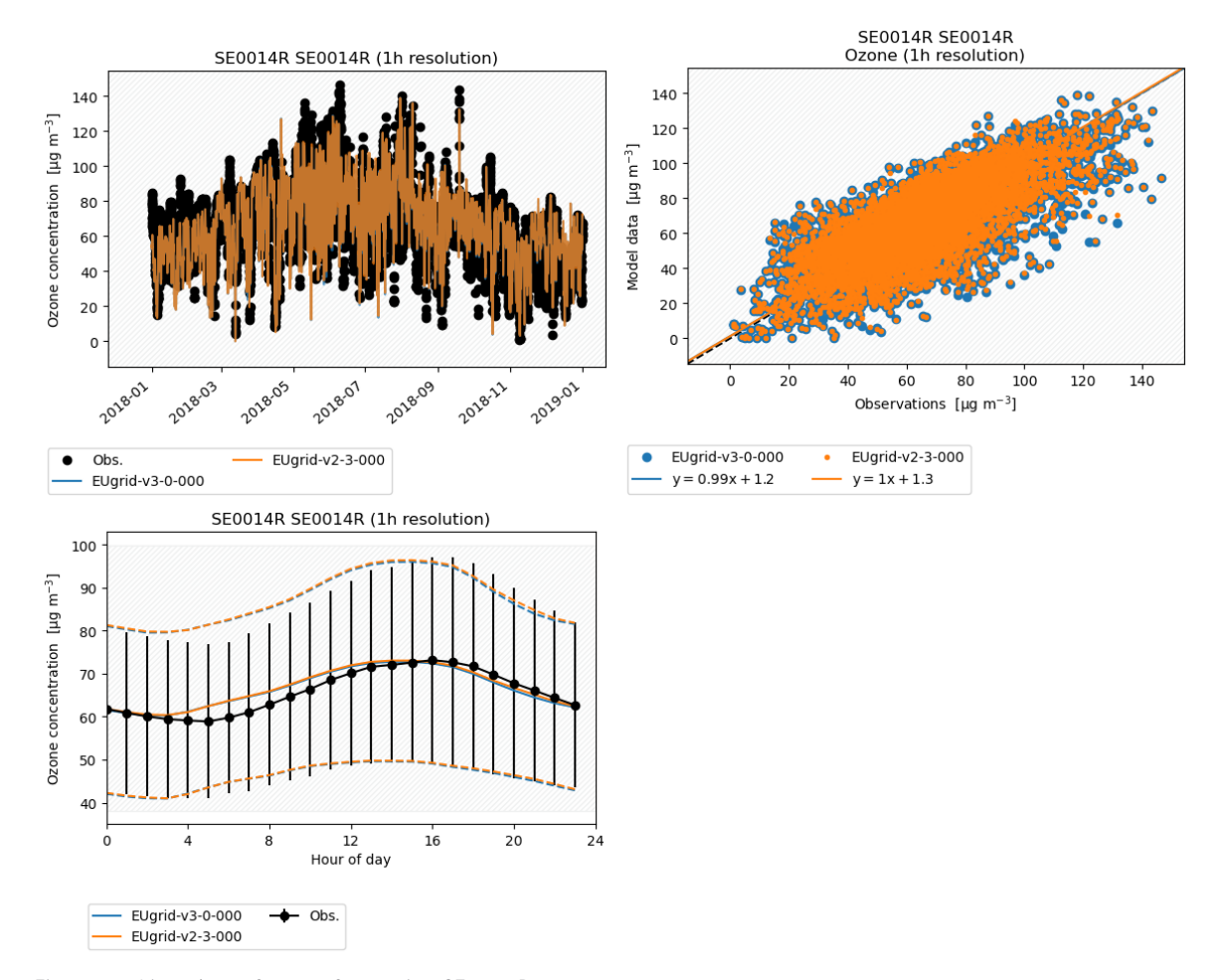


Figure 14: Line plots of ozone for station SE0014R.

TNO Public 15/67

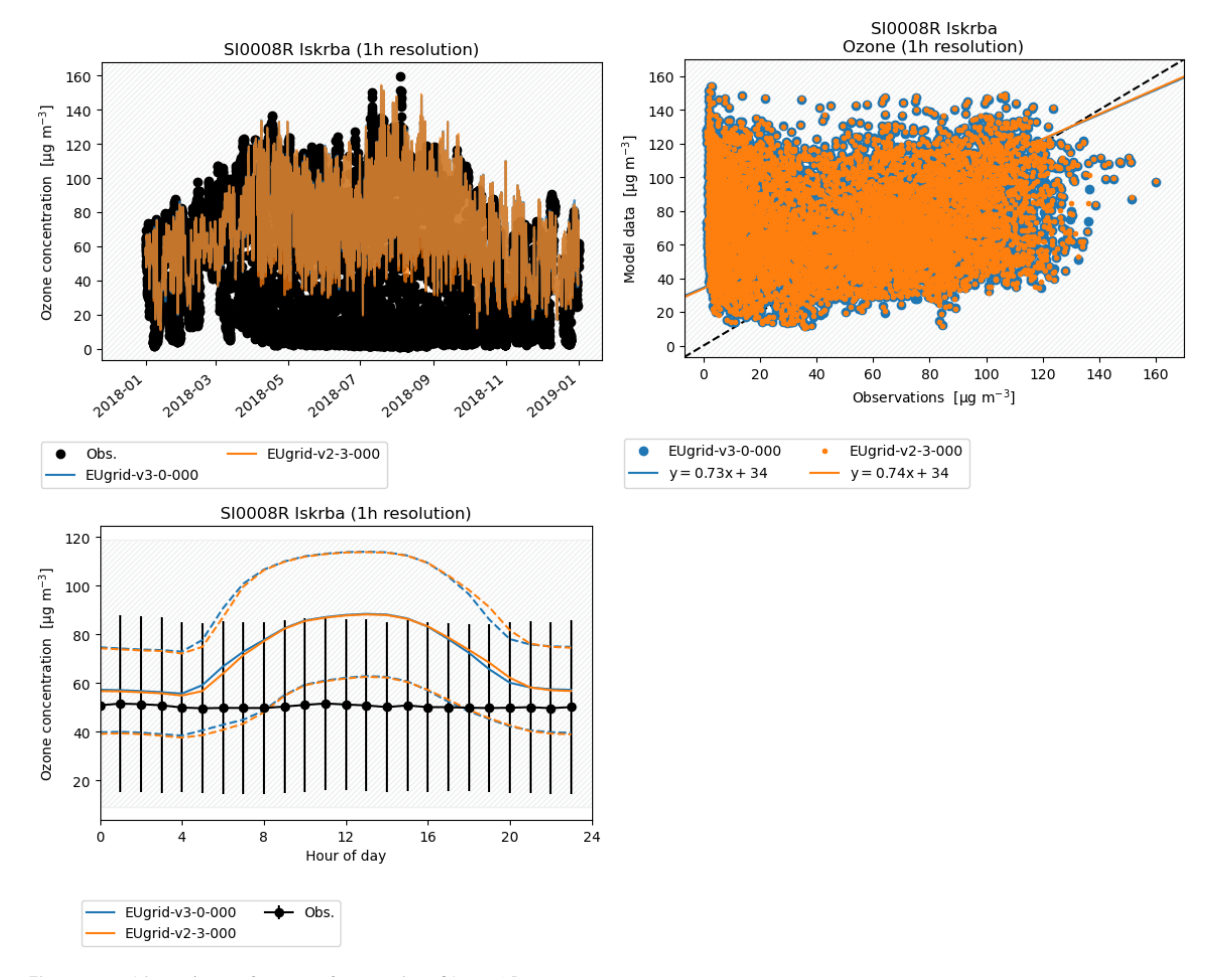


Figure 15: Line plots of ozone for station SI0008R.

TNO Public 16/67

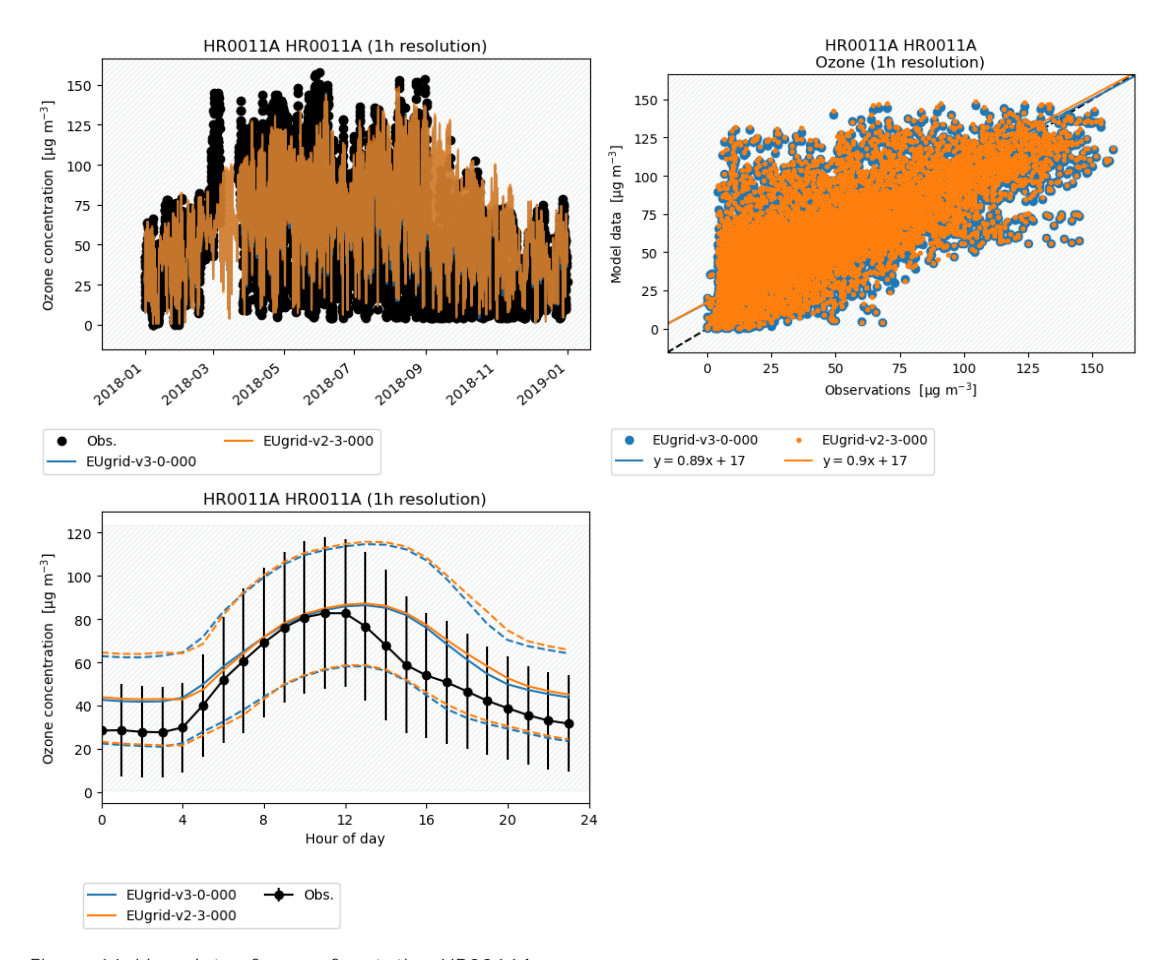


Figure 16: Line plots of ozone for station HR0011A.

TNO Public

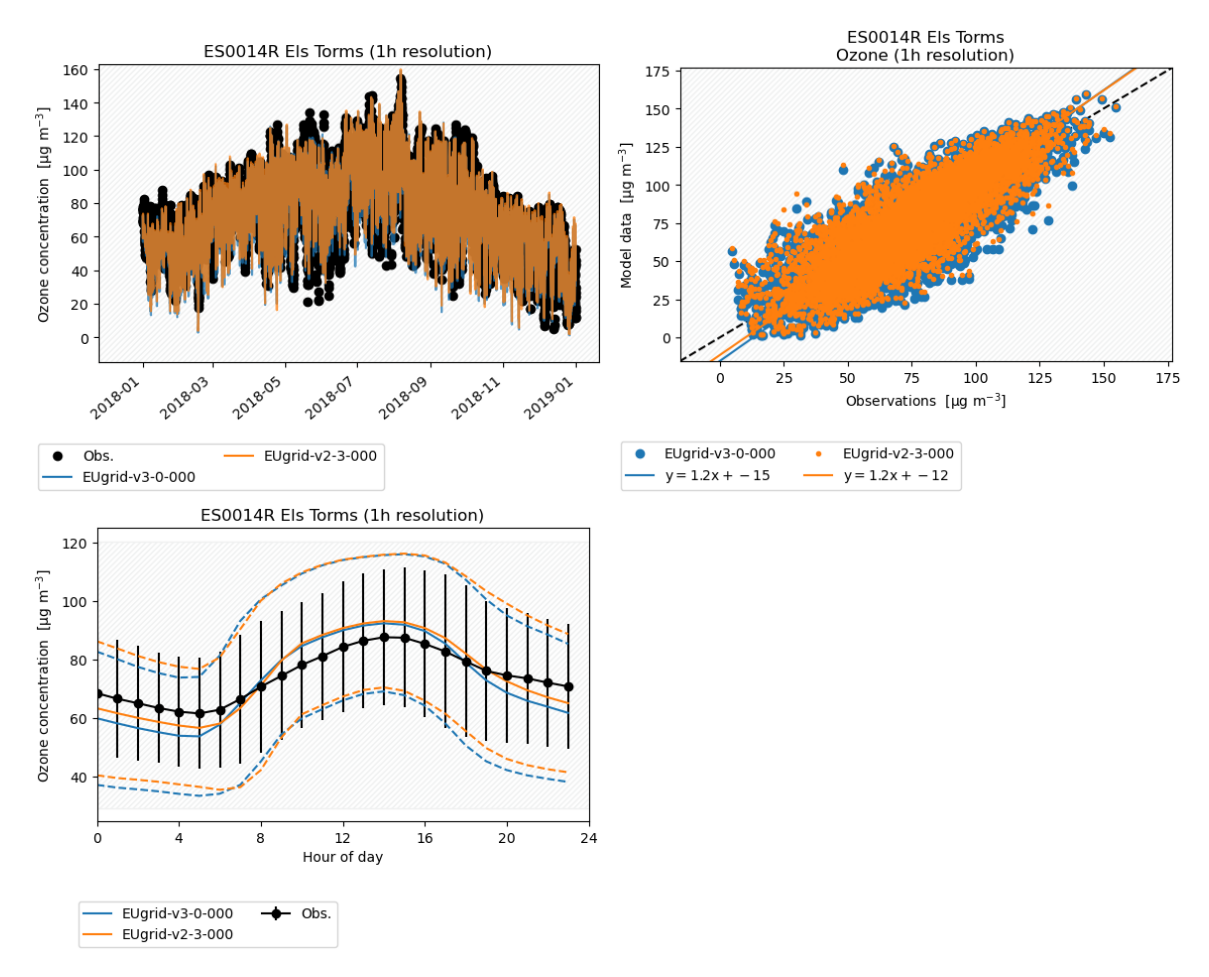


Figure 17: Line plots of ozone for station ES0014R.

TNO Public 18/67

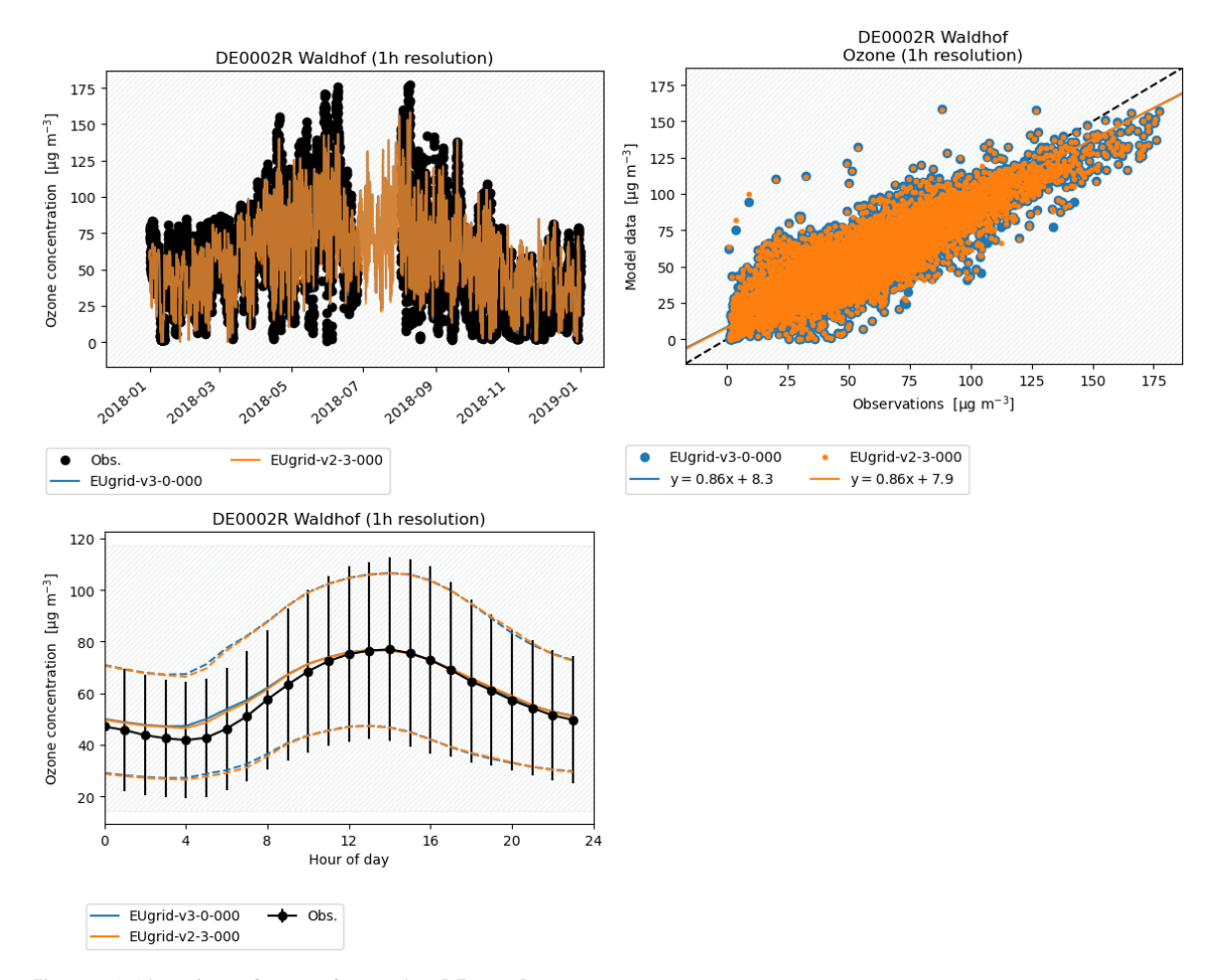


Figure 18: Line plots of ozone for station DE0002R.

TNO Public

# 4.3.2. Nitrogen Dioxide

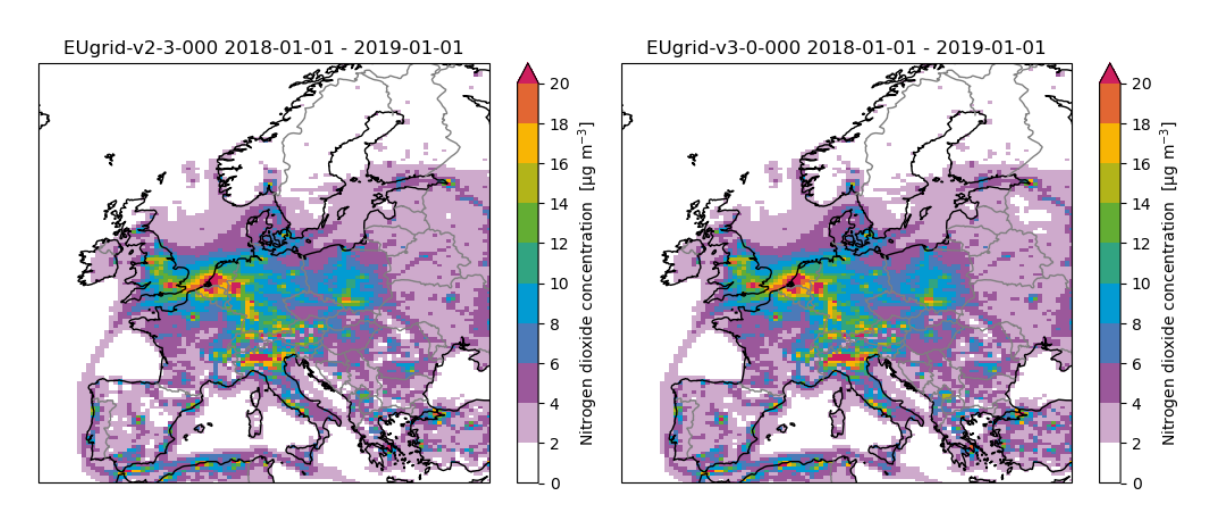


Figure 19: Concentration of nitrogen dioxide in air.

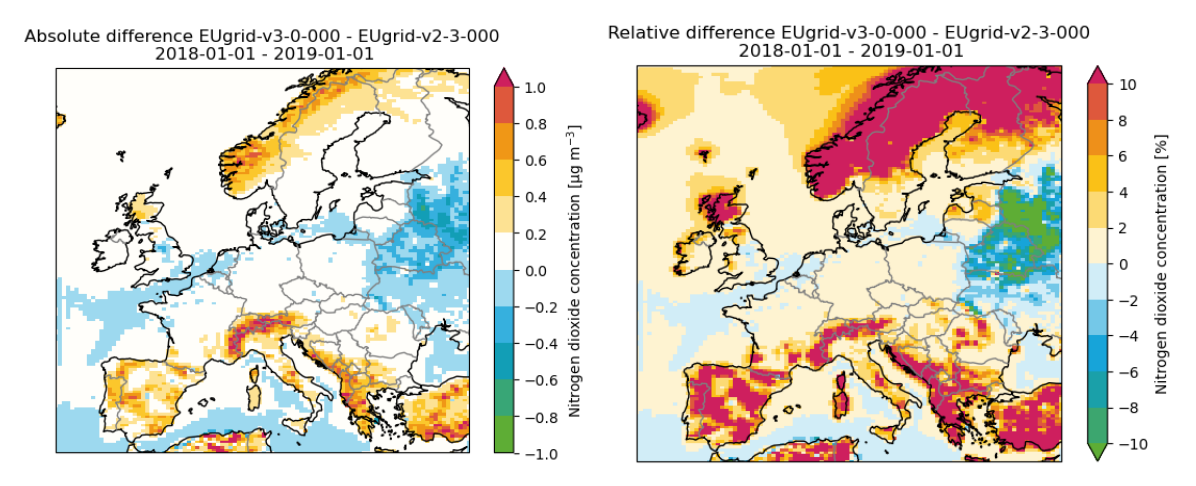


Figure 20: Absolute and relative difference of nitrogen dioxide concentration in air.

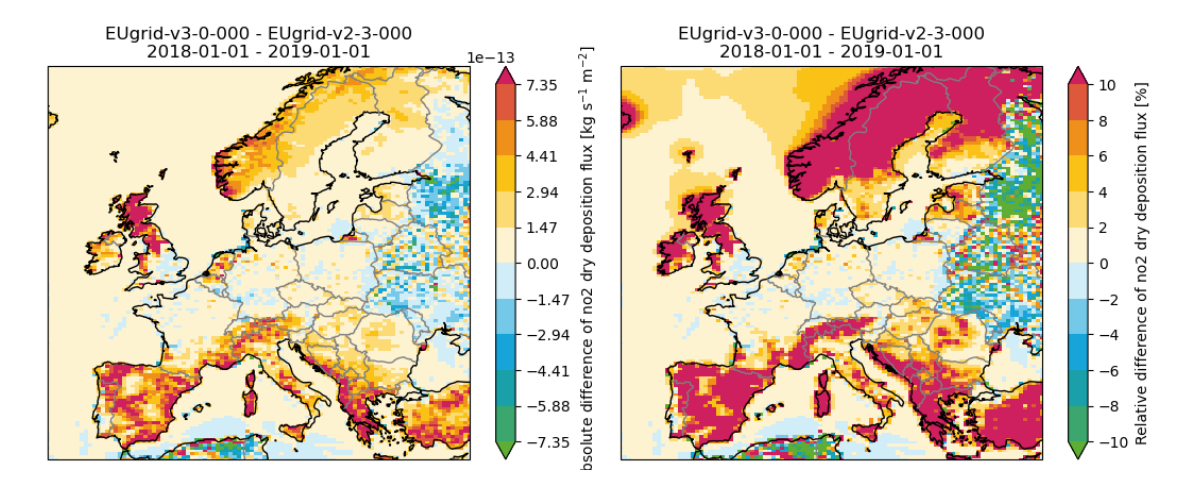


Figure 21: Absolute and relative difference of nitrogen dioxide dry deposition flux.

TNO Public 20/67

Shown in Figure 19 and Figure 20 are the nitrogen dioxide concentrations and (relative) differences between version v2.3.000 and v3.0.000. Nitrogen dioxide concentrations increase mainly over the north (Scandinavia, Scotland 0.6  $\mu g/m^3$  (>10%) ) and south of Europe (Spain, Alps, Greece, Turkey, and N. Afrika 0.6  $\mu g/m^3$  (>10%)), while a decrease of NO $_2$  up to around 0.6  $\mu g/m^3$  (<10%) is observed in east Europe / Russia. In central Europe, e.g. The Netherlands, Germany, Poland, and France, the NO $_2$  concentrations are not impacted.

Similar as for ozone, when comparing the trends in absolute difference  $NO_2$  concentration in Figure 20 with the absolute difference of biogenic NO emission in Figure 5, we observe the same trends as the regions with increased (relative) NO concentrations coincide with the increased NO2 concentrations. As written by Reaction 1, increased NO concentrations lead to increased  $NO_2$  concentrations as Reaction 1 shifts to the right hand side. Hence, the majority of the observed  $NO_2$  concentration change is assigned to the effect of biogenic NO emissions.

The change in concentrations due to biogenic NO emissions directly translates into increased dry deposition fluxes shown in Figure 21. When comparing the relative change in concentration and dry deposition, most regions coincide as the change in concentration directly leads to a similar relative change in deposition. Except in northern Africa where less  $NO_2$  dry deposition and higher  $NO_2$  concentrations are observed. In the location Algeria2, a large fraction of the forest (both dec and cnf) are reallocated to grassland which leads to significantly lower dry deposition velocities resulting in less dry deposition flux.

The averaged statistics over the EBAS and EEA measurement station are listed in Table 3 and Table 4 in the Appendix and the temporal mean per station are shown in Figure 22 and Figure 23. The averaged nitrogen dioxide statistics between hourly EBAS measurements and LOTOS-EUROS, change from 5,74  $\mu$ g/m³ to 5,79  $\mu$ g/m³ (RMSE), 0,34 to 0,33 (R2), and 0,17 to 0,20 (NMB) and the statistics derived between the daily measurements and simulations change from 3,43  $\mu$ g/m³ to 3,54  $\mu$ g/m³ (RMSE) to 0,35 to 0,33 (R2), and 0,47 to 0,69 (NMB). The comparison to EEA measurements stations shows a similar minor change in averaged statistics.

The simulation results compared to the measurements stations listed in Table 2 are shown in the Figure 24 to Figure 27. All the stations lie in regions that are little affected by the changes. The diurnal profile of the station Els Torms shows increased NO $_2$  concentrations during evening and early in the morning. For nitrogen dioxide, a clear difference between the concentrations at the EBAS and EEA stations is observed. The EEA stations lie in urban area's showing concentrations up to 40  $\mu$ g/m³ which LOTOS-EUROS systematically underestimates with a R² of 0.675. The EBAS stations are mostly located in rural and remote areas showing concentrations up to 18  $\mu$ g/m³ which LOTOS-EUROS overestimates but with a R² of 0.934.

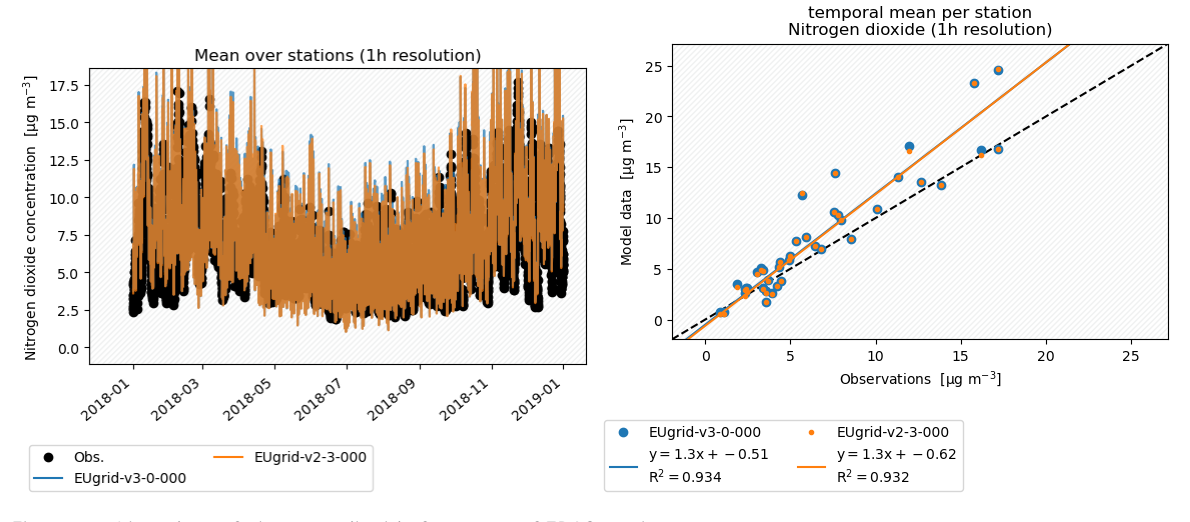


Figure 22: Line plots of nitrogen\_dioxide for mean of EBAS stations.

TNO Public 21/67

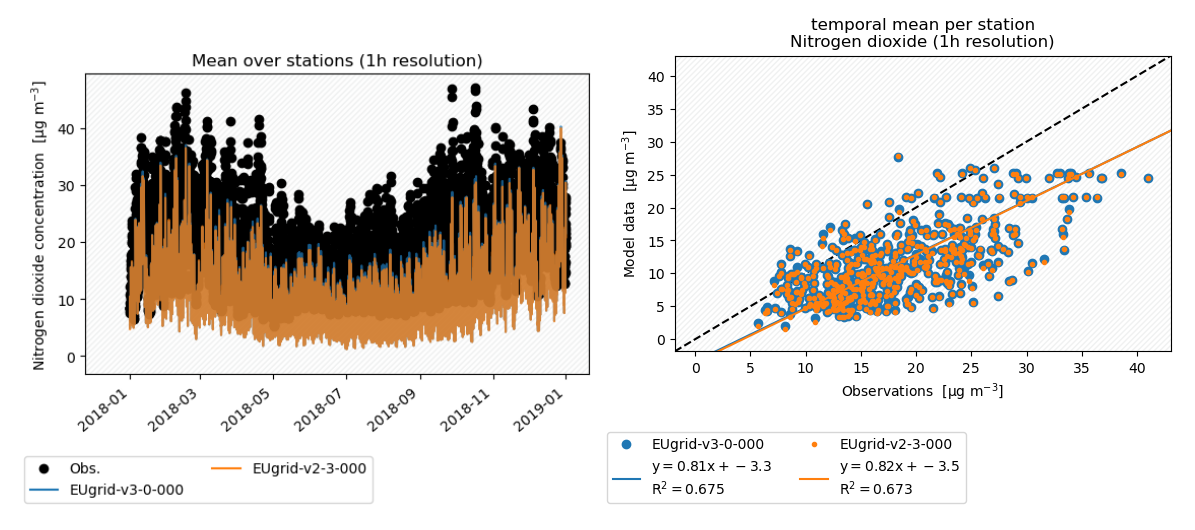


Figure 23: Line plots of nitrogen\_dioxide for mean of EEA stations.

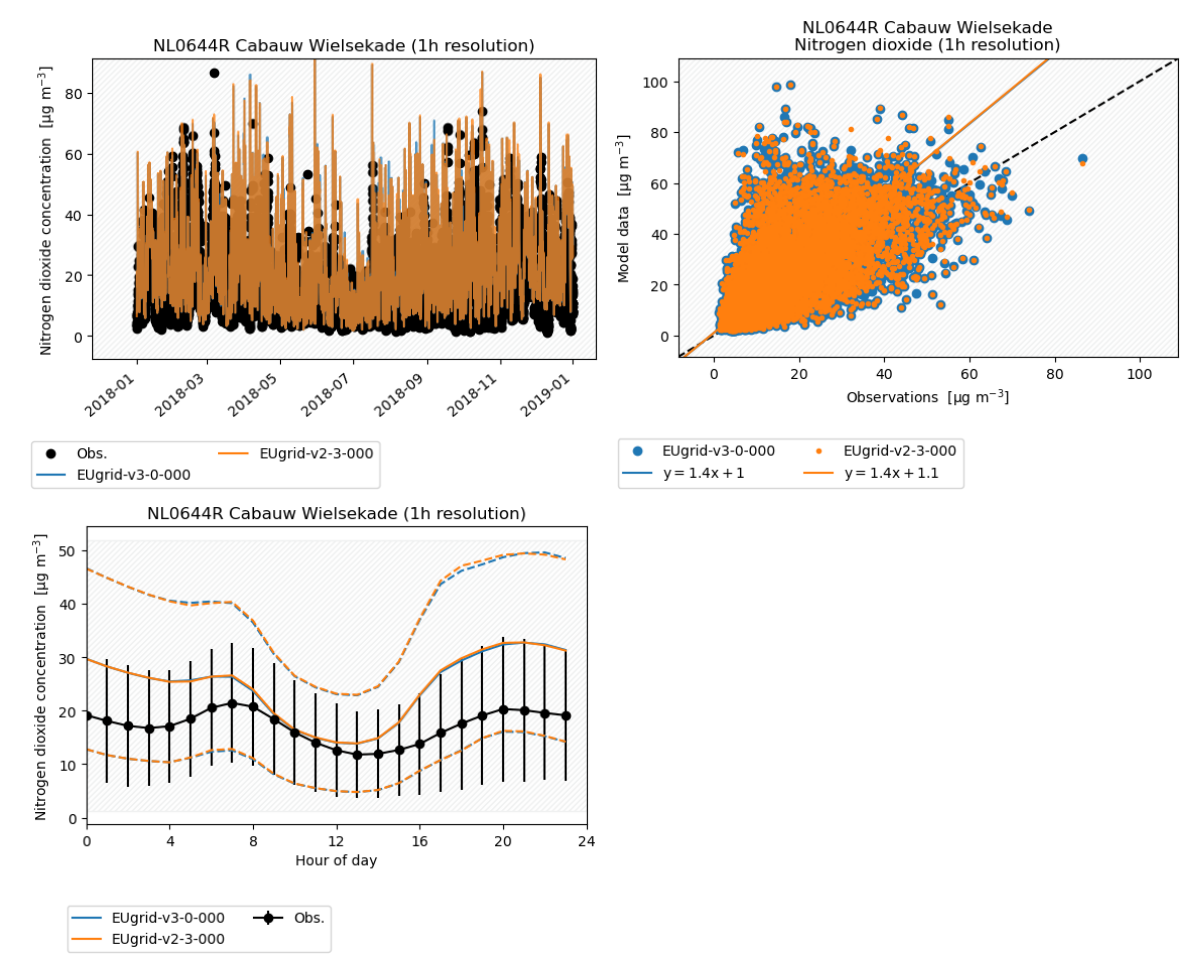


Figure 24: Line plots of nitrogen\_dioxide for station NLO644R.

TNO Public 22/67

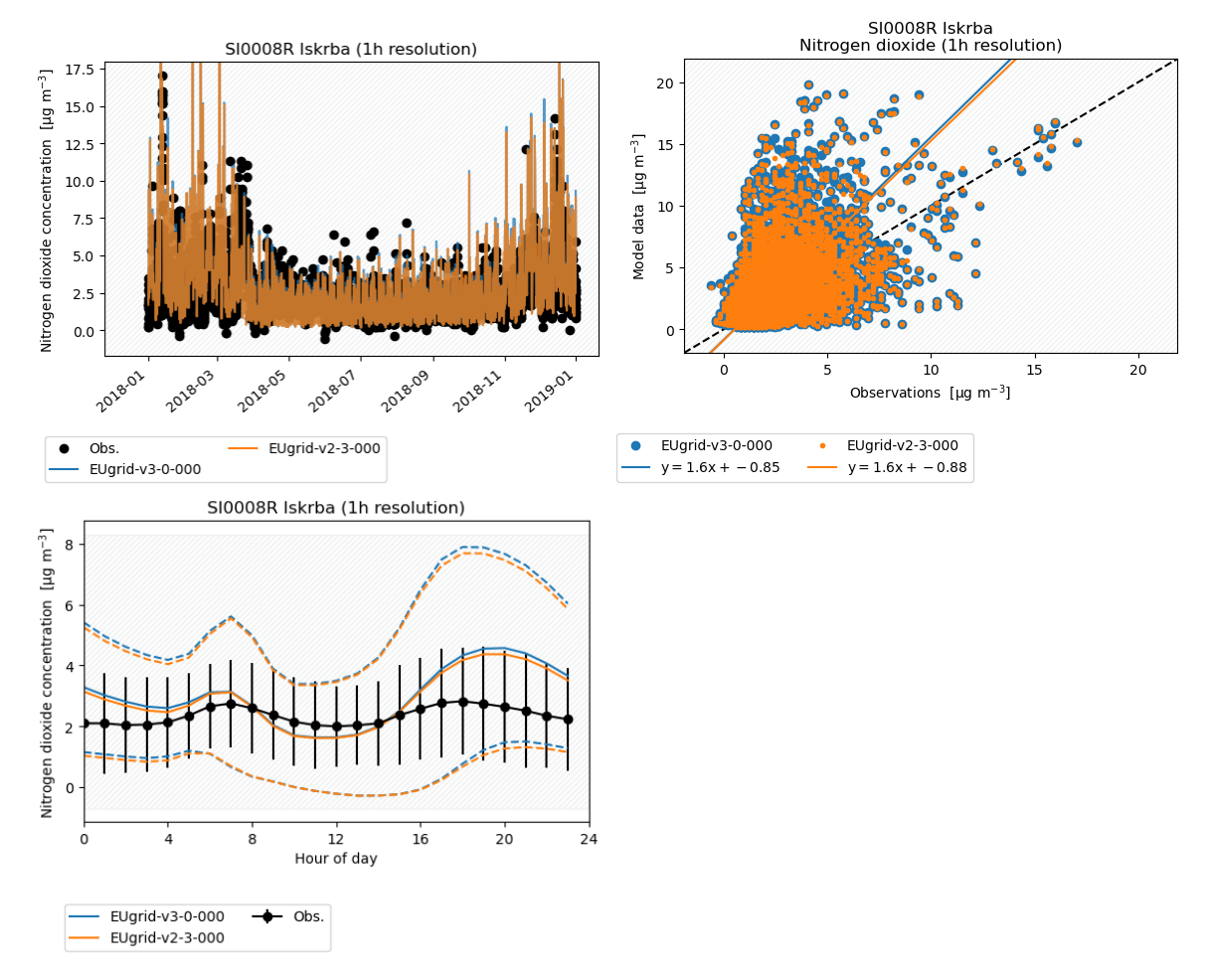


Figure 25: Line plots of nitrogen\_dioxide for station SI0008R.

TNO Public 23/67

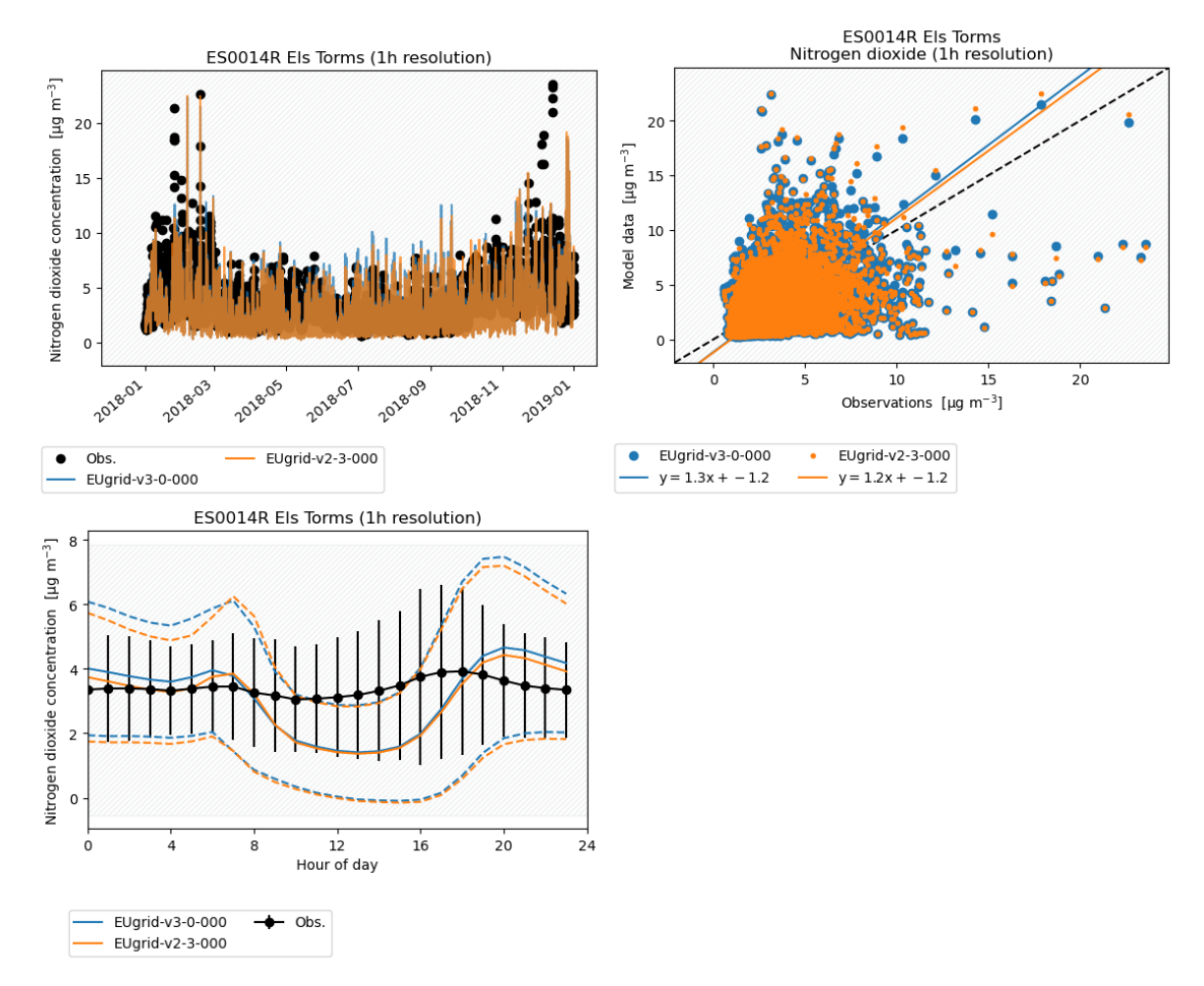


Figure 26: Line plots of nitrogen\_dioxide for station ES0014R.

TNO Public 24/67

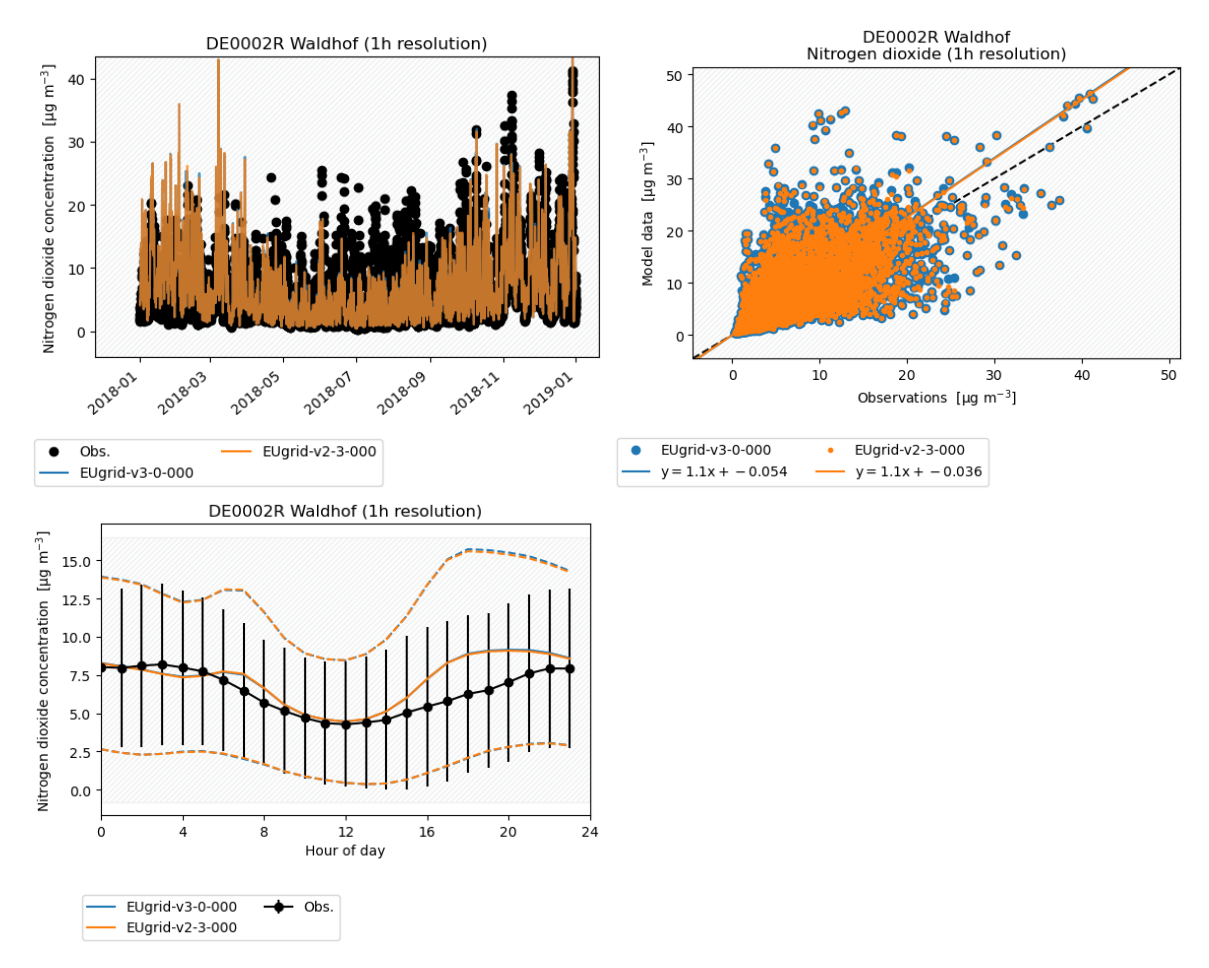


Figure 27: Line plots of nitrogen\_dioxide for station DE0002R.

TNO Public 25/67

# 4.3.3. Ammonia

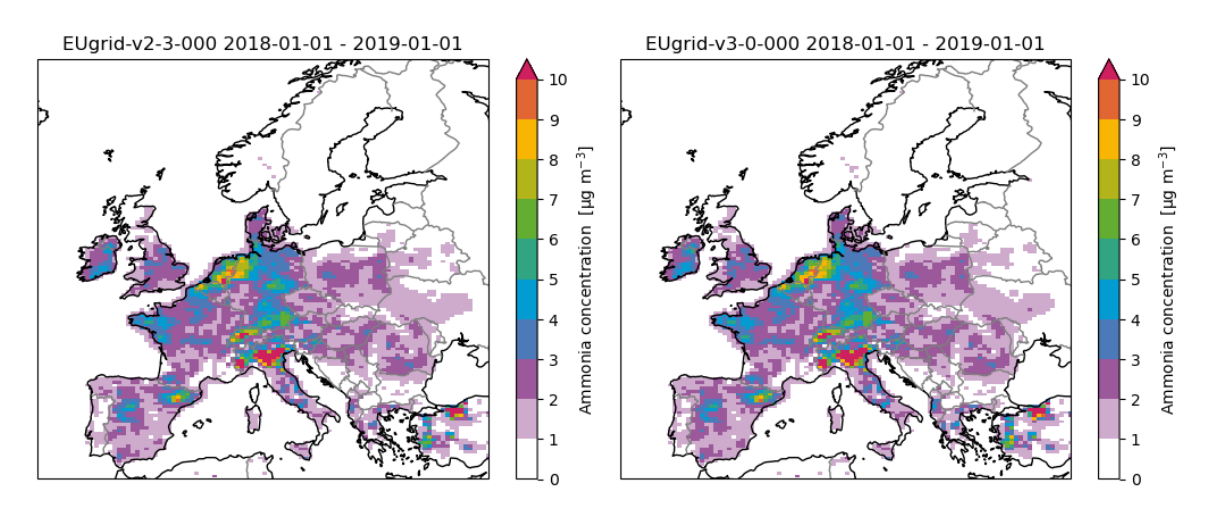


Figure 28: Concentration of ammonia in air.

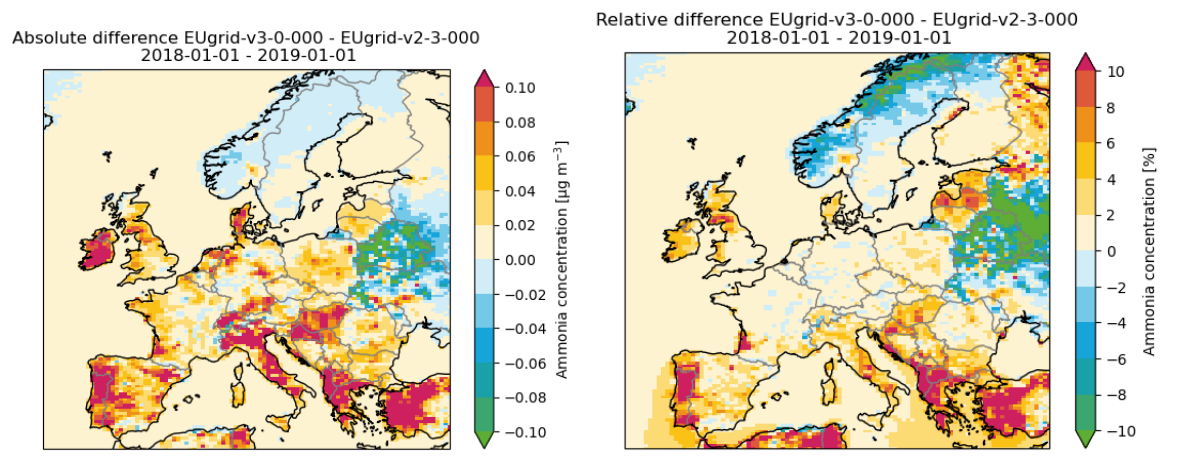


Figure 29: Absolute and relative difference of ammonia concentration in air.

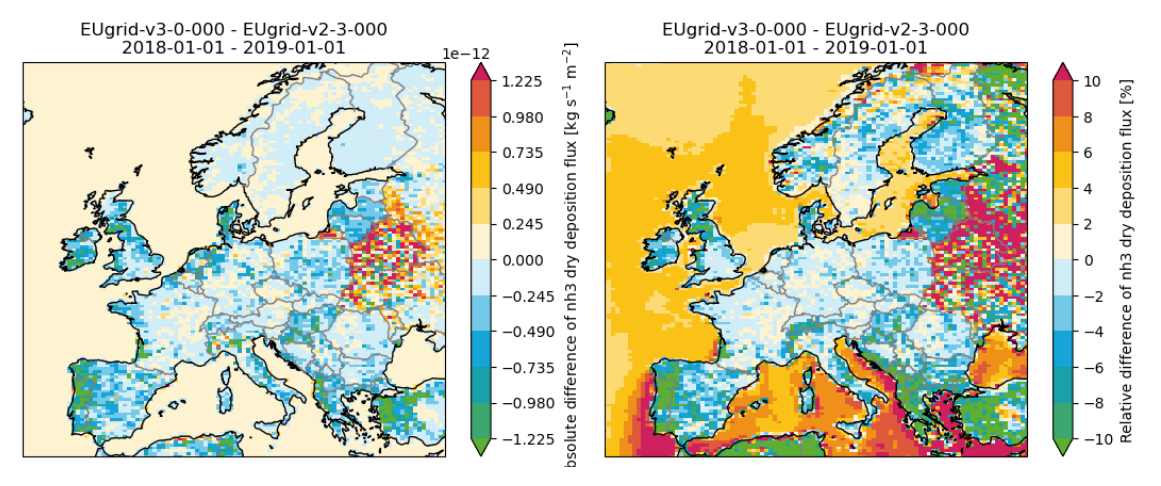


Figure 30: Absolute and relative difference of ammonia dry deposition flux.

TNO Public 26/67

Shown in Figure 28 and Figure 29 are the ammonia concentrations and (relative) differences between version v2.3.000 and v3.0.000. In central Europe, little to no change in concentration is observed i.e. [-0.1, 0.1]  $\mu g/m^3$  or [-2.0, 2.0]%. However, in Turkey, Portugal, and the border between Belarus and Russia, larger (relative) differences are observed. In Figure 30, the absolute and relative difference in dry deposition are shown. In the regions where the concentrations are changed, the dry deposition shows a reversed effect. Therefore, the changes in concentration on ammonia is largely attributed to the change in dry deposition velocities.

- In Portugal an increase of  $\sim 0.2 \, \mu g/m^3$  ( $\sim 10\%$ ) ammonia concentration is observed. In this region, the Transitional woodland-shrub class, previously assigned to cnf and dec forest, is now assigned to sem. The sem lu-class shows lower NH3 deposition velocities compared to the forest classes resulting in higher ammonia concentrations. Therefore, the reallocation of the lu-fractions are the cause of the ammonia concentration increase.
- In Turkey, the dec and cnf forest land use fractions have decreased and the grs, crp and oth have increased. Forests typically lead to more deposition. So in Turkey, the decrease of deposition is the cause of the observed increased ammonia concentrations of 0.1 µg/m³ (~10%).
- In Norway, a decrease of -0.02 µg/m³ or ~5-10% in ammonia concentrations is partly explained by the changes in land use classes, i.e. the change of the *Moors and heathland* (oth) and *Sparsely vegetated areas* (dsr) to sem. The sem lu-class has an increased NH3 deposition velocity, specifically during the summer, leading to decreased concentrations of ammonia. At the same time, NH<sub>3</sub> is converted into ammonium in the presence of HNO<sub>3</sub> which is derived from NO<sub>2</sub> (see section 4.4). Thus, increased NO<sub>2</sub> concentrations in Scandinavia (Figure 20) will lead to decreased NH<sub>3</sub> concentrations.
- In Russia/east Europe, a decrease of  $\sim 0.1 \, \mu g/m^3$  ( $\sim 10\%$ ) on ammonia levels is observed, which can be attributed to the change in lu-class from from ara and crp to forest, i.e. fce and fbd.

The averaged statistics over the EBAS measurement stations are listed in Table 3 in the Appendix. The averaged ammonia statistics of the hourly LOTOS-EUROS versus EBAS measurements, change from 4,23 to 4,24 (RMSE), 0,11 to 0,11 (R2), and 0.00 to 0.01 (NMB), and for the daily EBAS measurements all statistics remain equal. The statistics show practically no change, as expected from the change in concentrations and the locations of the measurement stations.

TNO Public 27/67

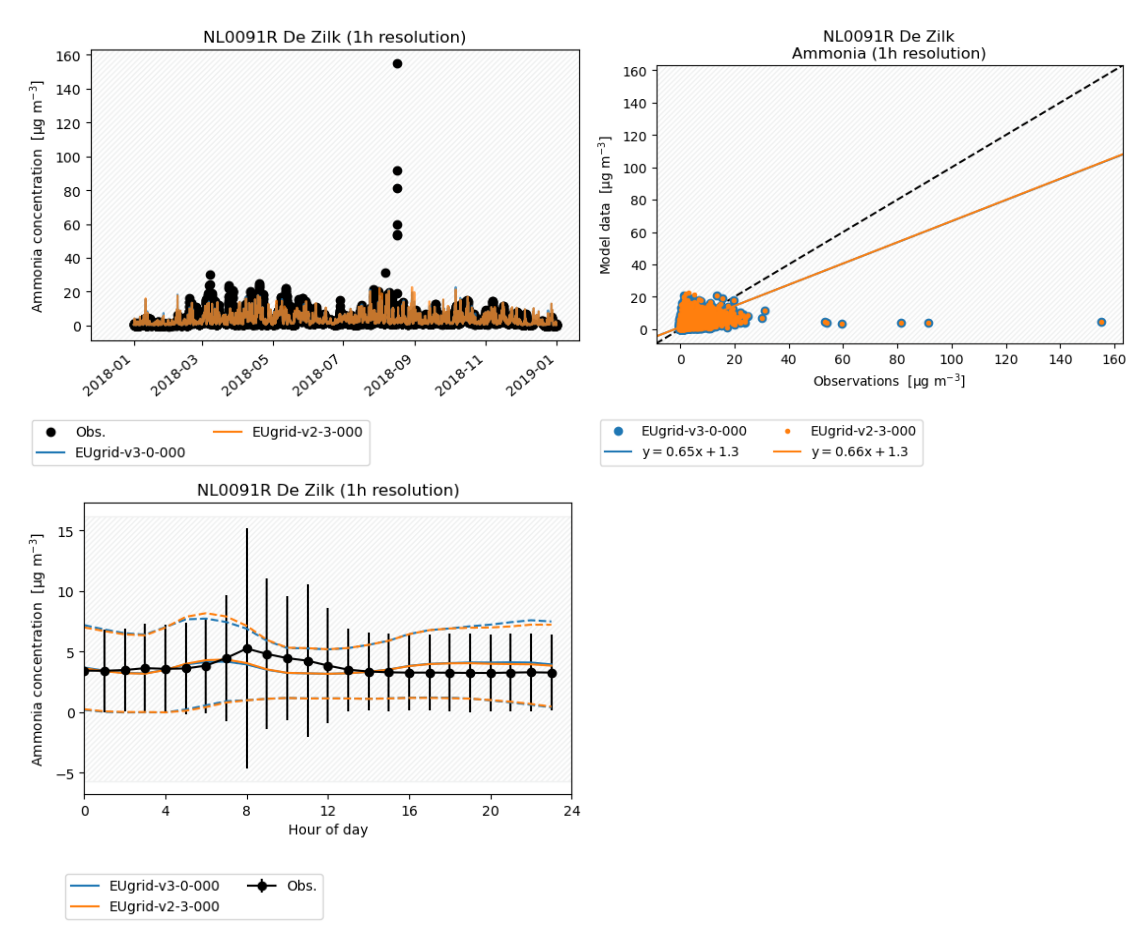
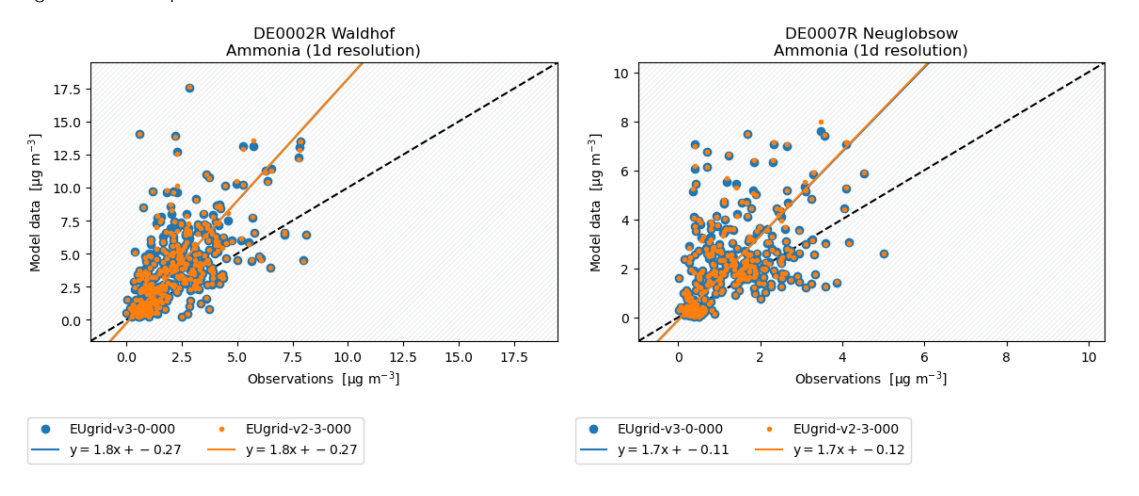


Figure 31: Line plots of ammonia for station NL0091R.



TNO Public 28/67

# 4.3.4. Sulphur Dioxide

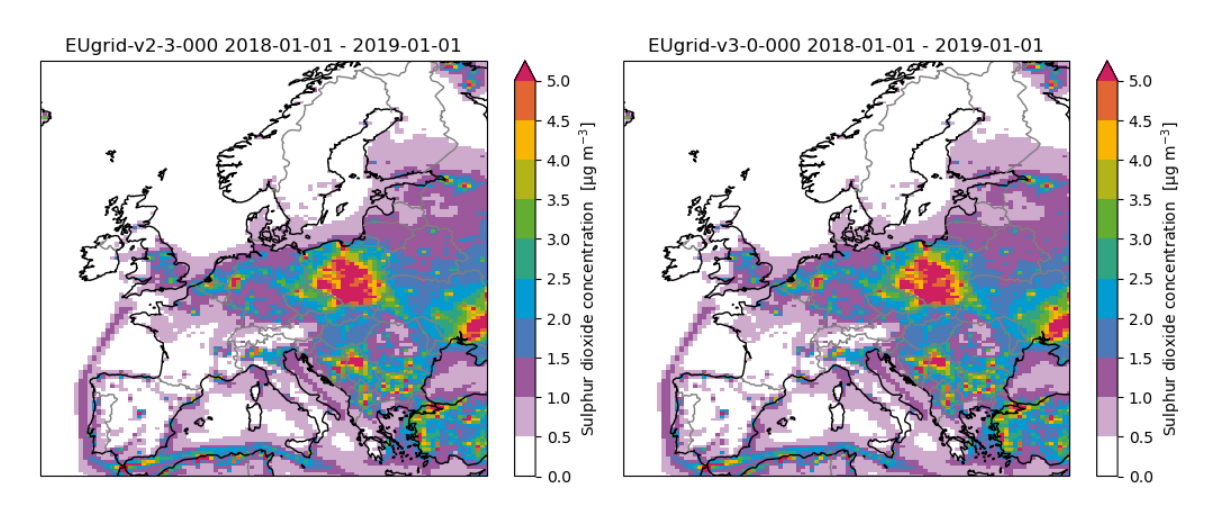


Figure 32: Concentration of sulphur\_dioxide in air.

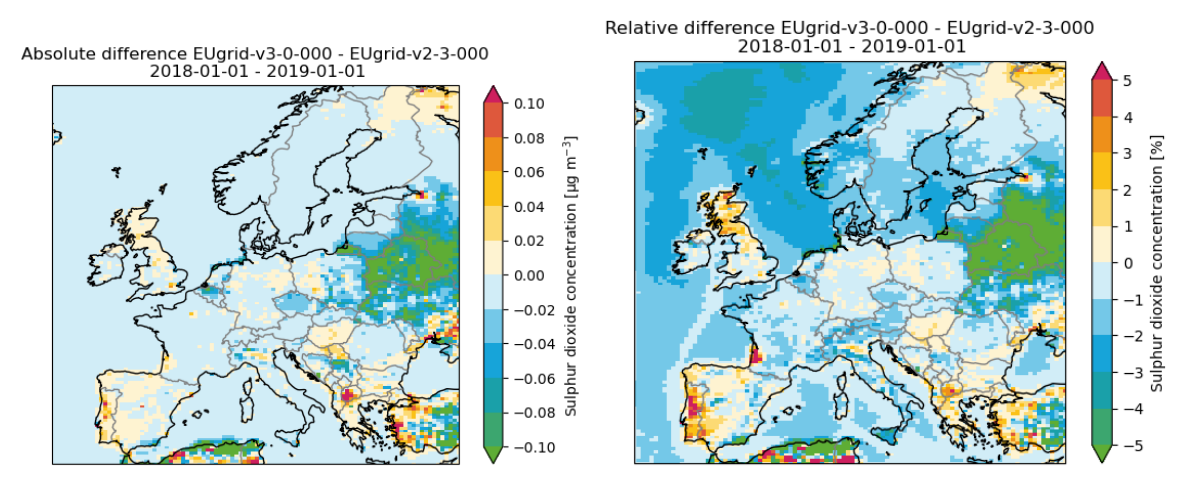


Figure 33: Absolute and relative difference of sulphur dioxide concentration in air.

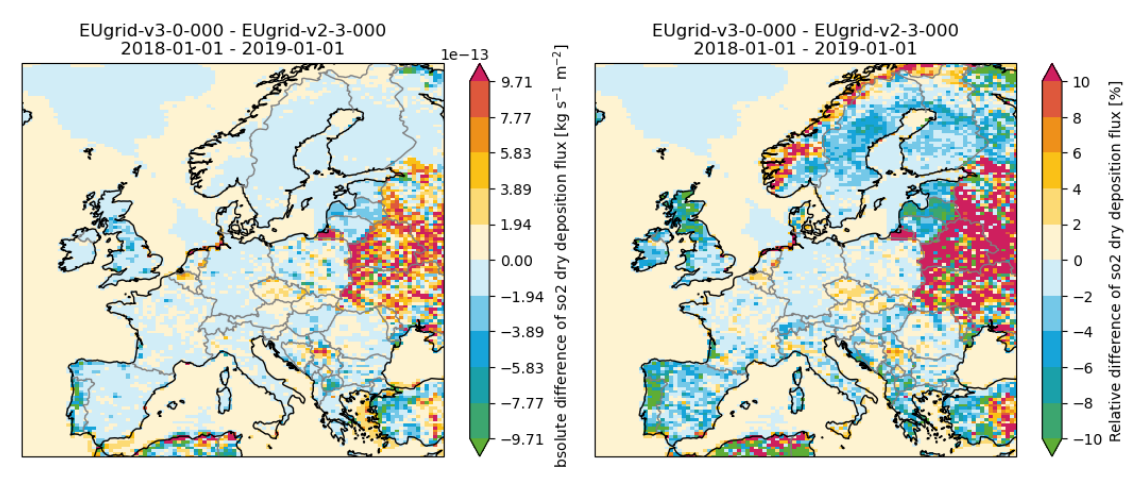


Figure 34: Absolute and relative difference of sulphur dioxide dry deposition flux.

TNO Public 29/67

An overall decrease of  $SO_2$  concentration of approximately 0-0.04  $\mu g/m^3$  (~0 to -2%) is observed over most of the domain which is assigned to the chemical conversion into sulphate as discussed in section 4.4.3.

Larger relative concentration differences are primarily observed in Russia/Eastern Europe and north Africa, with significant differences of approximately 0.10  $\mu$ g/m³ (~5%). In these regions, we observe an increase of SO<sub>2</sub> dry deposition flux up to 1e-12 kg s<sup>-1</sup> m<sup>-2</sup> or ~10% shown in Figure 34. In Russia/Eastern Europe, particularly along the Russia-Belarus border, the slight concentration decrease is attributed to the changed dry deposition velocity coming from the land-use from arable land (ara) and cropland (crp) to forest types such as fce and fbd. In northern Algeria, large areas of arable land (ara) have transitioned to grassland (grs), which exhibits a slightly higher deposition velocity in winter. As the SO<sub>2</sub> concentrations in North Africa are generally low, this change appears highly pronounced in the relative difference plot.

In parts of Portugal, France, Greece and Turkey increased  $SO_2$  concentration levels of >5% are observed. In the areas, the transitional woodland shrub landuse category (dec+cnf -> sem, shown in Figure 82) leads to ~10% lower deposition fluxes as shown in Figure 34.

In Norway, the sparsely vegetated areas (dsr -> sem, shown in Figure 82) leads to increased  $SO_2$  deposition velocities of 1e-12 kg s<sup>-1</sup> m<sup>-2</sup> or 8-10%. Seminatural lands have greater dry deposition velocities as the turbulence of air caused by the vegetation branches lowers air resistances compared to deserts.

The averaged statistics over the EBAS and EEA measurement station are listed in Table 3 and Table 4 in the Appendix and the temporal mean over the stations are shown in Figure 35 and Figure 36. The hourly averaged sulphur dioxide concentrations [ $\mu g/m^3$ ] statistics derived from EBAS measurements and LOTOS-EUROS simulations, change from 2,05  $\mu g/m^3$  to 2,04  $\mu g/m^3$  (RMSE), 0,19 to 0,19 (R2), and 2,23 to 2,21 (NMB), while the daily measurements change from 1,11 to 1,11 (RMSE), 0,10 to 0,10 (R2), and 1,67 to 1,68 (NMB). The EEA statistics also show very minor differences.

The simulation results compared to the measurements station ES0014R (Els Torms), listed in Table 2, is shown in Figure 37. Els Torms lies in a region where little change is observed, as confirmed by the diurnal and scatter plot.

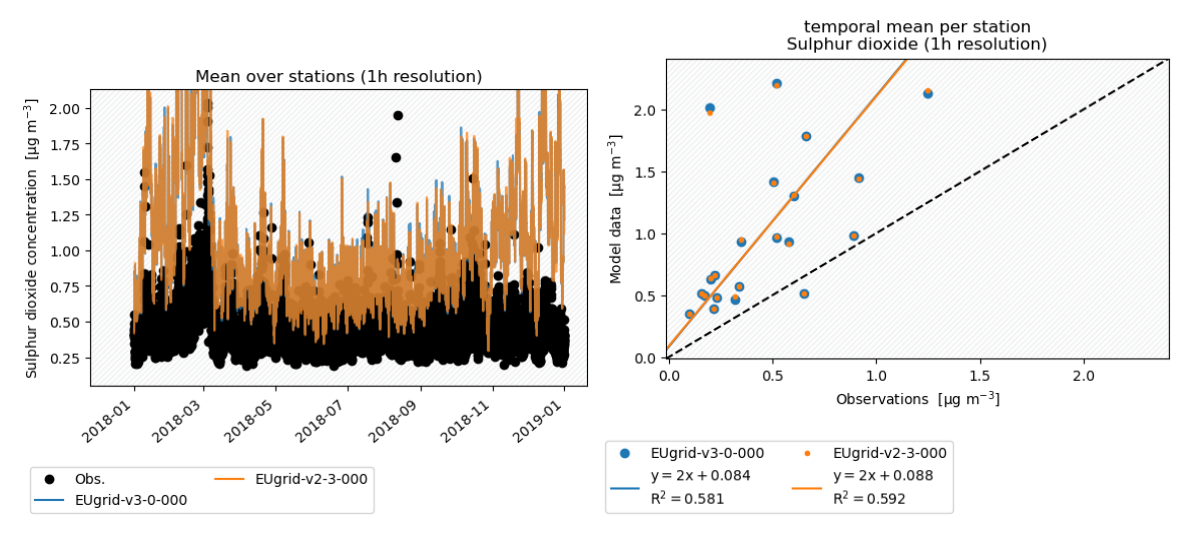


Figure 35: Line plots of sulphur\_dioxide for mean of EBAS stations.

TNO Public 30/67

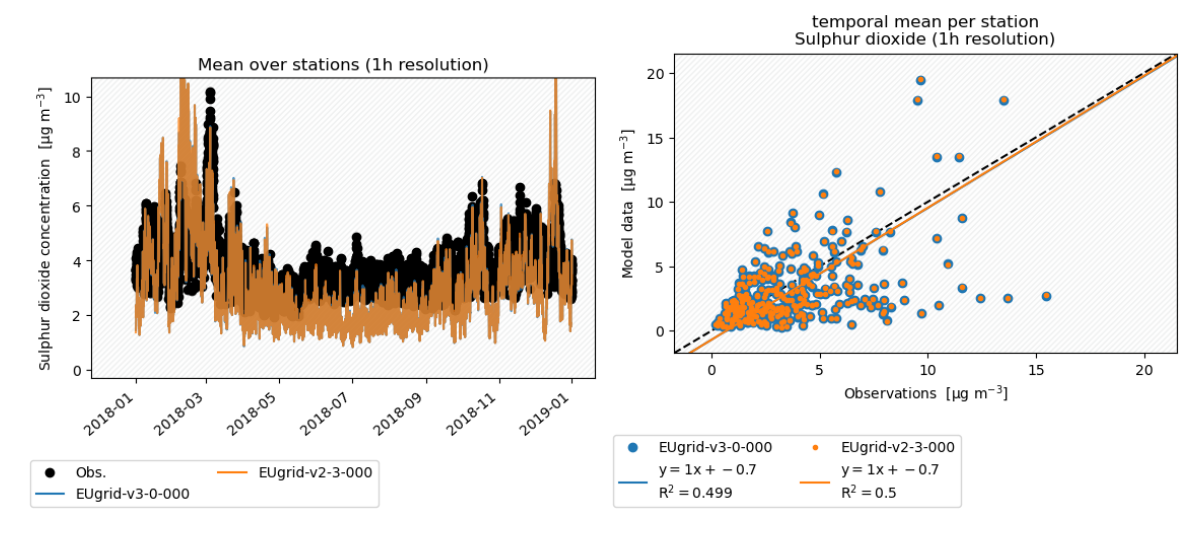


Figure 36: Line plots of sulphur\_dioxide for mean of EEA stations.

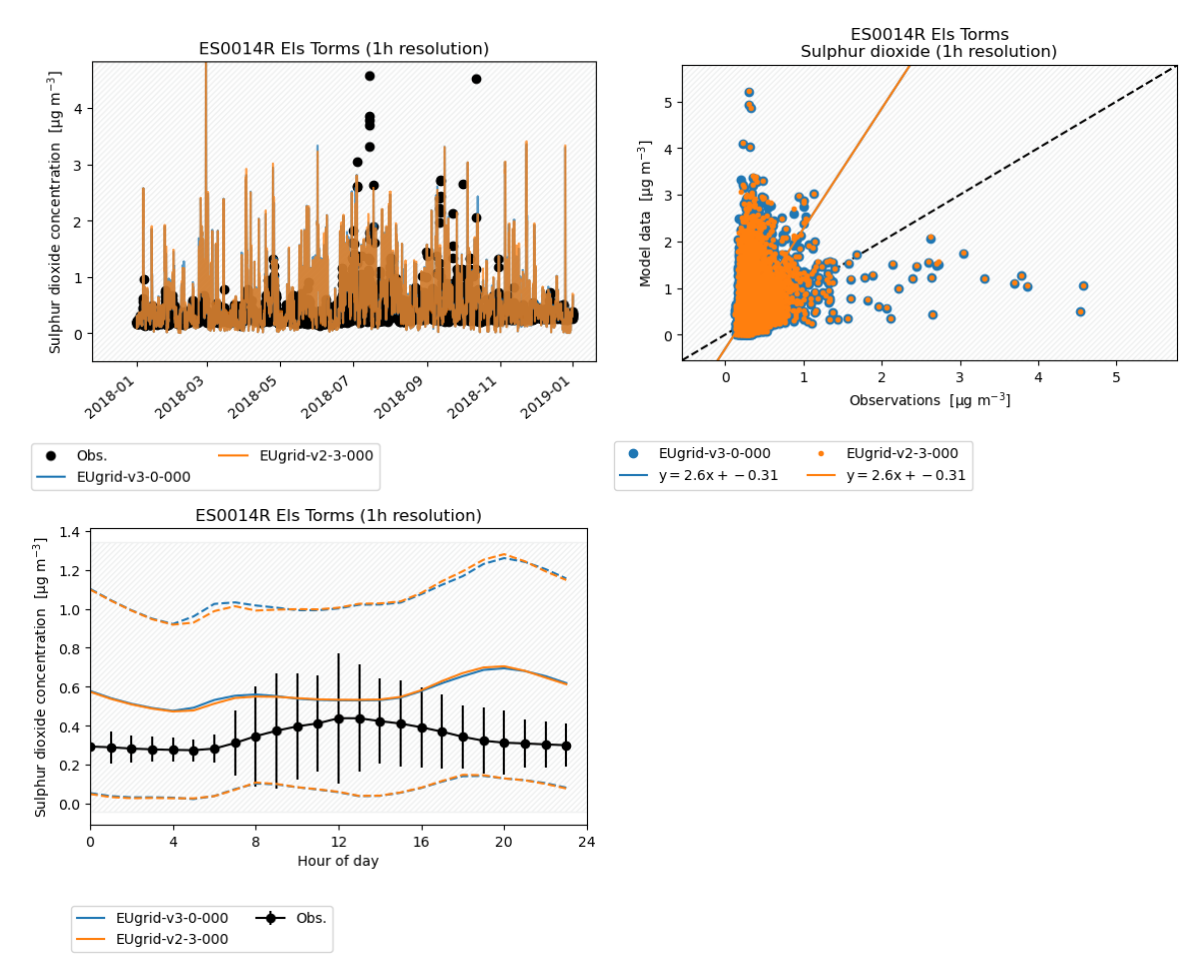


Figure 37: Line plots of sulphur\_dioxide for station ES0014R.

TNO Public 31/67

### 4.4. Concentrations and Measurements of Particulate Matter

In this section, the concentrations of particulate matter is described. First the concentrations of PM 2.5, that is particulate matter up to 2,5  $\mu m$  in size, is discussed including concentrations ammonium, nitrate, sulphate, sodium, organic carbon, and elementary carbon in PM2.5 in sections 4.4.2 to 4.4.7, respectively. Then in section 4.4.8-4.4.9, PM 10, that is particulate matter up to 10  $\mu m$  in size, is discussed including mineral dust.

#### 4.4.1. PM 2.5

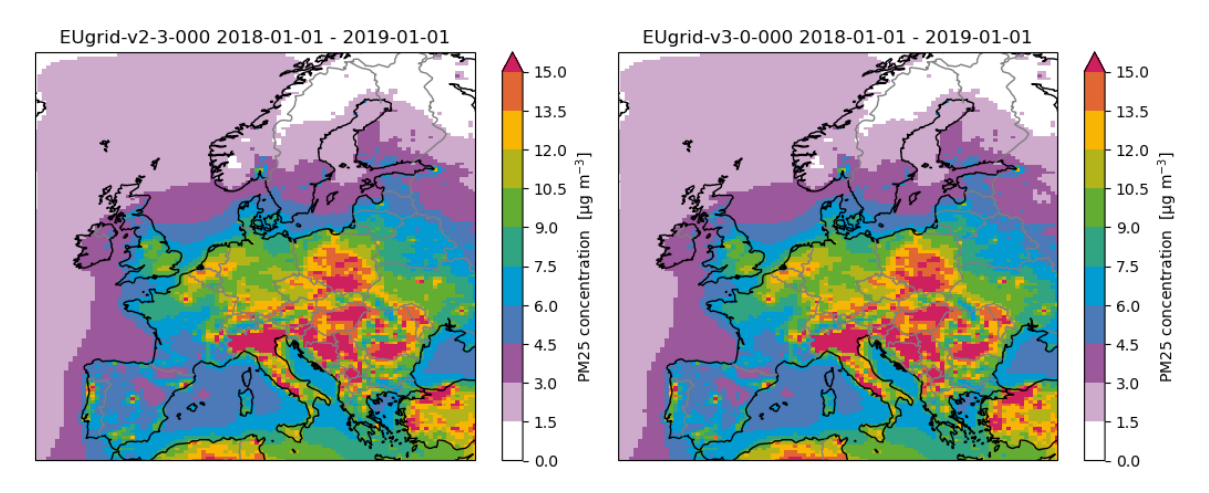


Figure 38: Concentration of pm25\_mass in pm25.

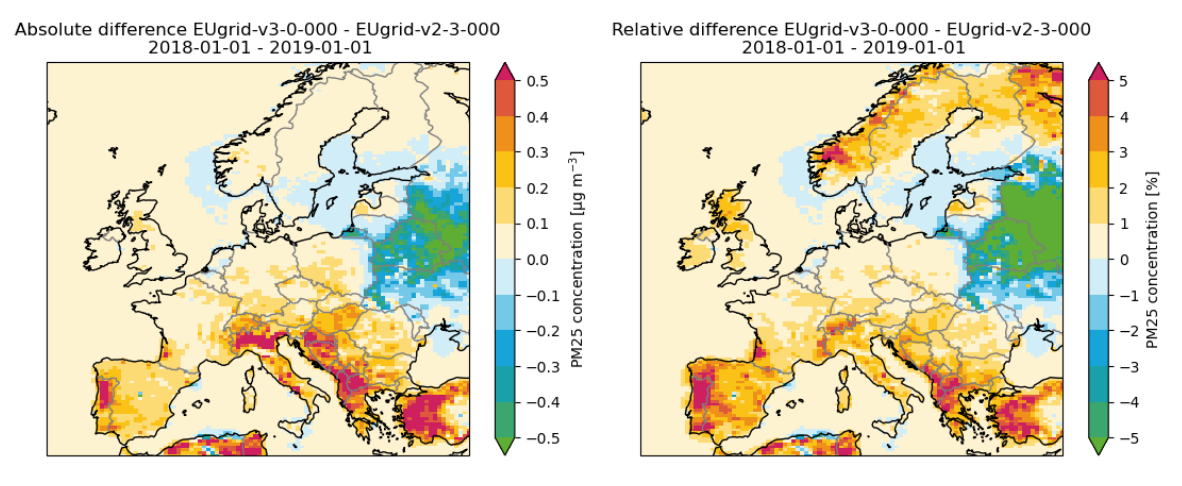


Figure 39: Absolute and relative difference of PM2.5 concentration in air.

The PM2.5 concentration increases mainly in the south of the domain, in parts of Italy, Albania, north Macedonia, Portugal, Turkey, Tunisia, and Norway up to 0.5  $\mu$ g/m³ or +5%. The increase in mainly determined by ammonium and nitrate, to a lesser extent by sulphate and organic carbon. Sodium and elementary carbon have only very minor effect.

In Belarus/Russia, dry deposition of many species is increased leading to a significant reduction of PM2.5 up to -0.5  $\mu$ g/m³ or -5%. Also here, sodium and elementary carbon play a small role compared to the other species.

TNO Public 32/67

The statistics of mean of all stations stays practically equal shown Figure 40. A similar behavior is observed for the EEA measurement stations in Figure 41. The PM2.5 concentrations that remain unchanged at the measurement stations are also shown by the Figure 42 to Figure 46.

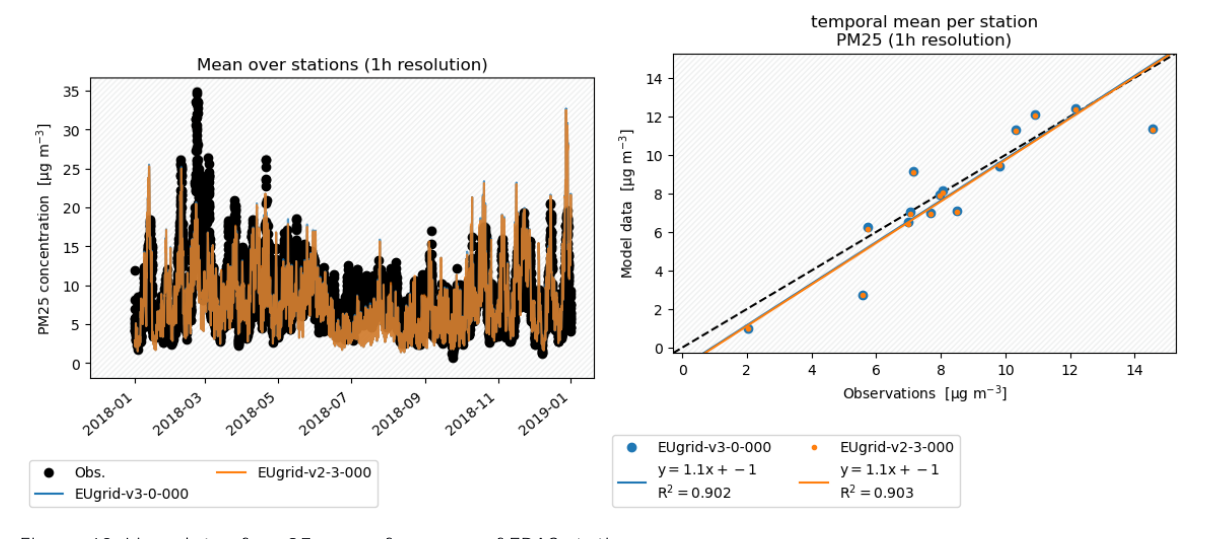


Figure 40: Line plots of pm25\_mass for mean of EBAS stations.

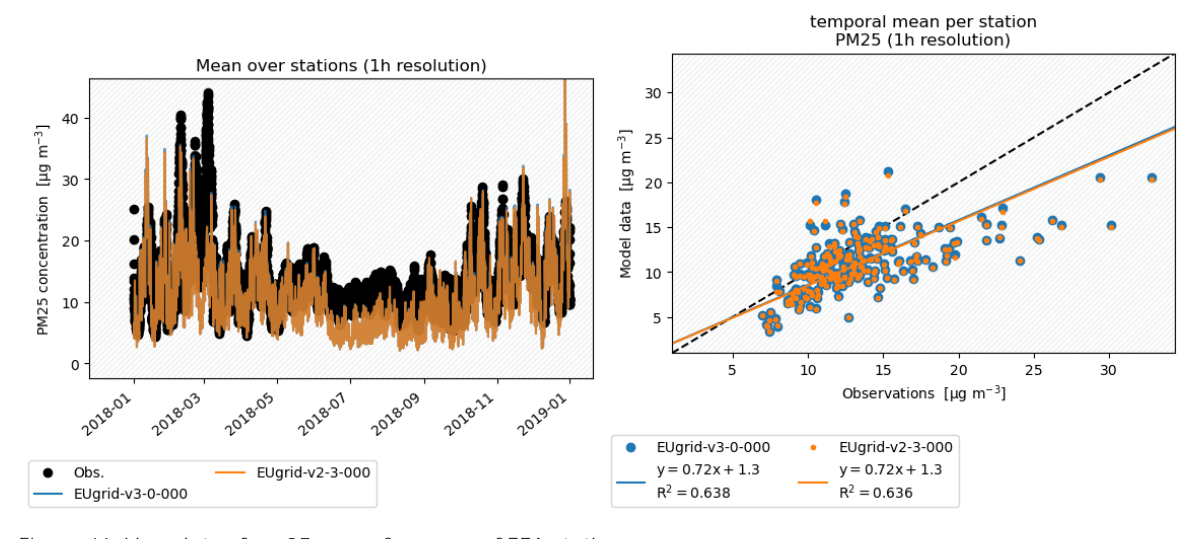


Figure 41: Line plots of pm25\_mass for mean of EEA stations.

TNO Public 33/67

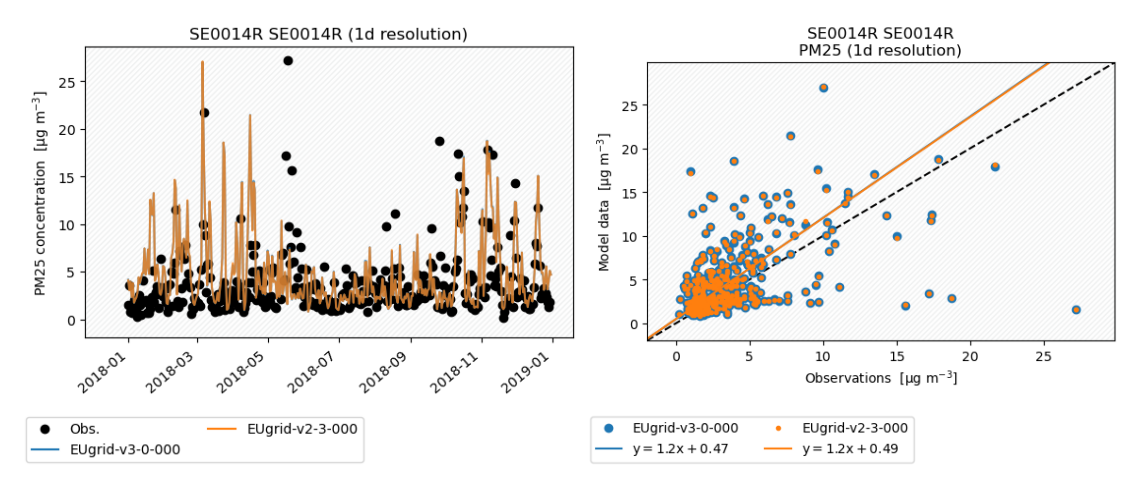


Figure 42: Line plots of pm25\_mass for station SE0014R.

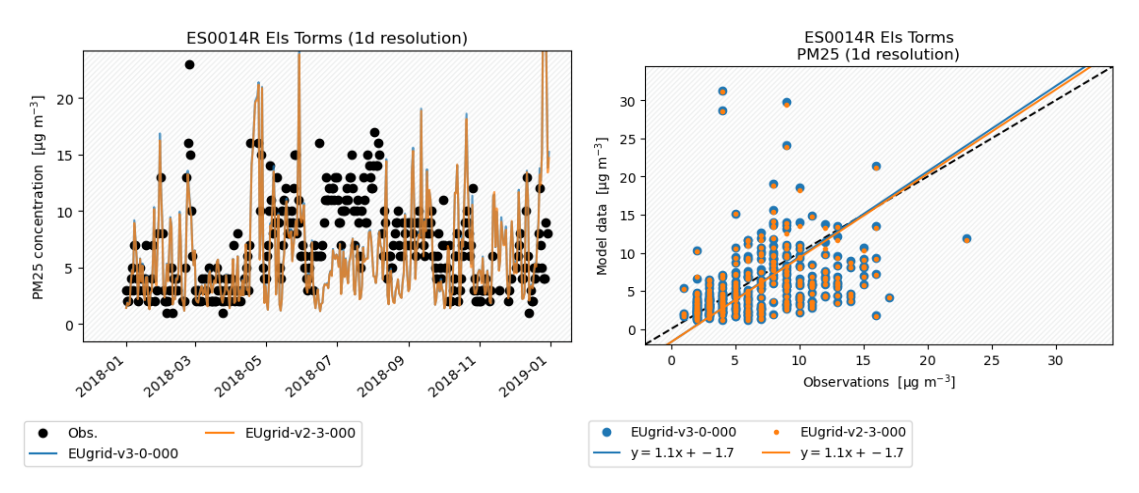


Figure 43: Line plots of pm25\_mass for station ES0014R.

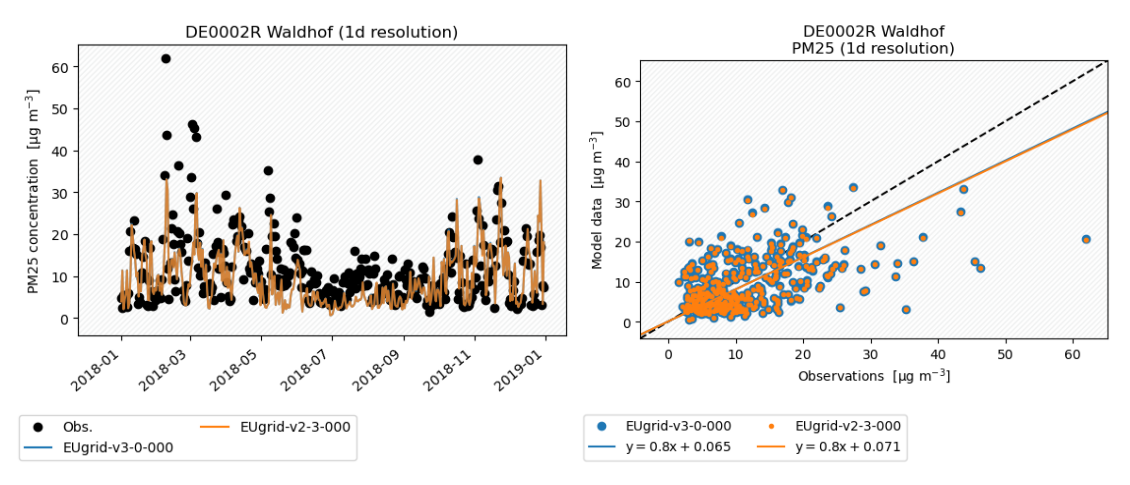


Figure 44: Line plots of pm25\_mass for station DE002R.

TNO Public 34/67

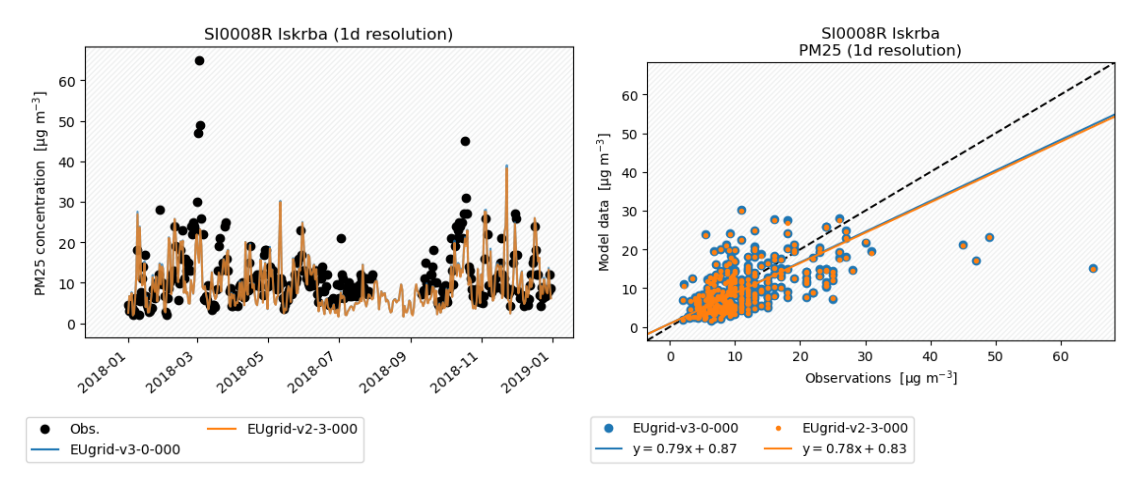


Figure 45: Line plots of pm25\_mass for station SI008R.

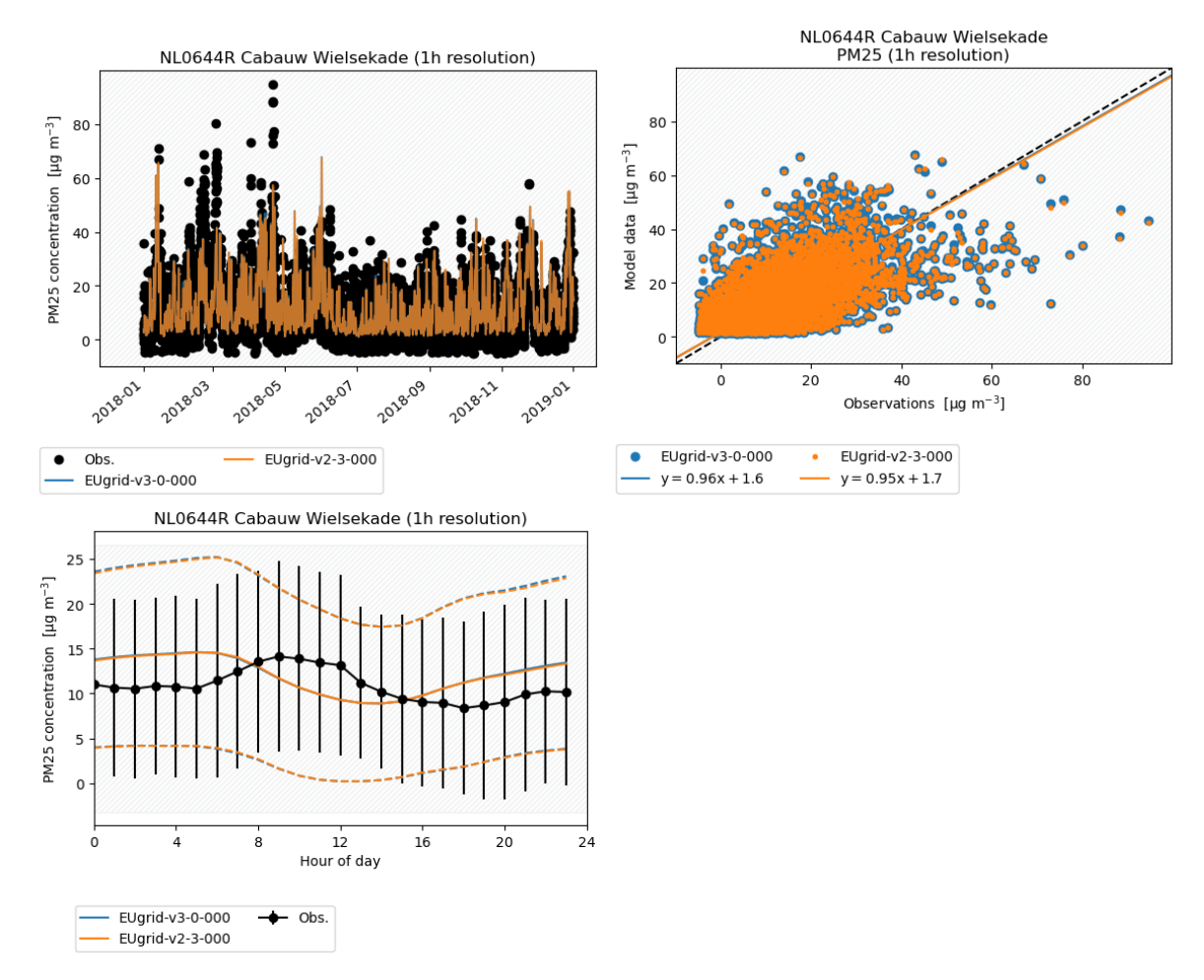


Figure 46: Line plots of pm25\_mass for station NL0644R.

TNO Public 35/67

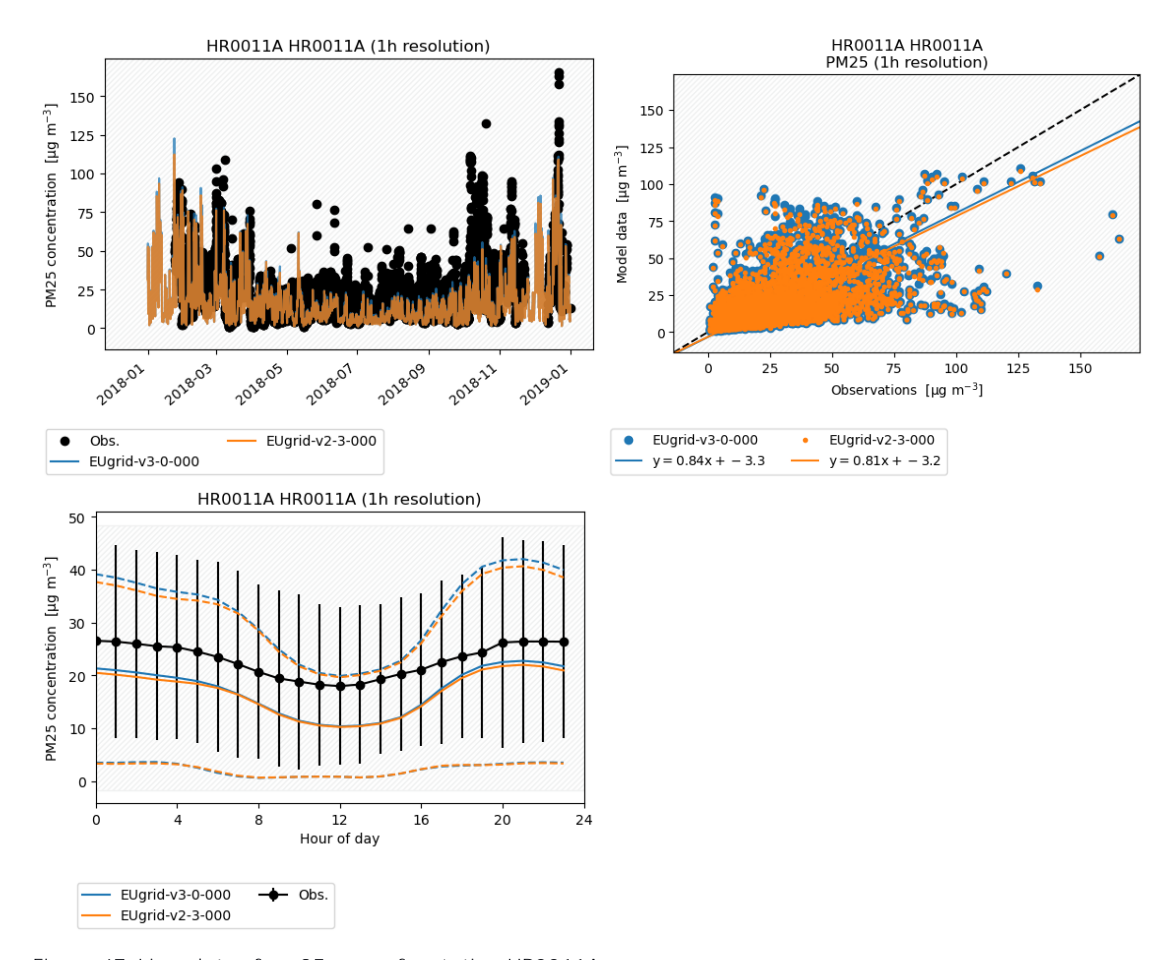


Figure 47: Line plots of pm25\_mass for station HR0011A.

TNO Public 36/67

#### 4.4.2. Nitrate

In the atmosphere,  $HNO_3$ , a derivative of nitrogen dioxide  $(NO_2)$ , reacts with ammonia  $(NH_3)$  to form nitrate  $(NO_3^-)$  and ammonium  $(NH_4^+)$  in the ratio  $NH_4^+:NO_3^-$ . Therefore, areas of concentration increase of nitrogen dioxide and ammonia illustrated in the concentration difference maps of Figure 20 and Figure 29, coincide with the concentration increases of nitrate and ammonium in Figure 49 and Figure 53, respectively. For example, the relative increase of nitrate in Norway, Spain, north Africa, Greece, Turkey, Portugal are driven by the increased  $NO_2$  concentrations. In addition, in Norway, the increased concentration of nitrate and ammonium explain the decreased concentration of ammonia in Figure 29.

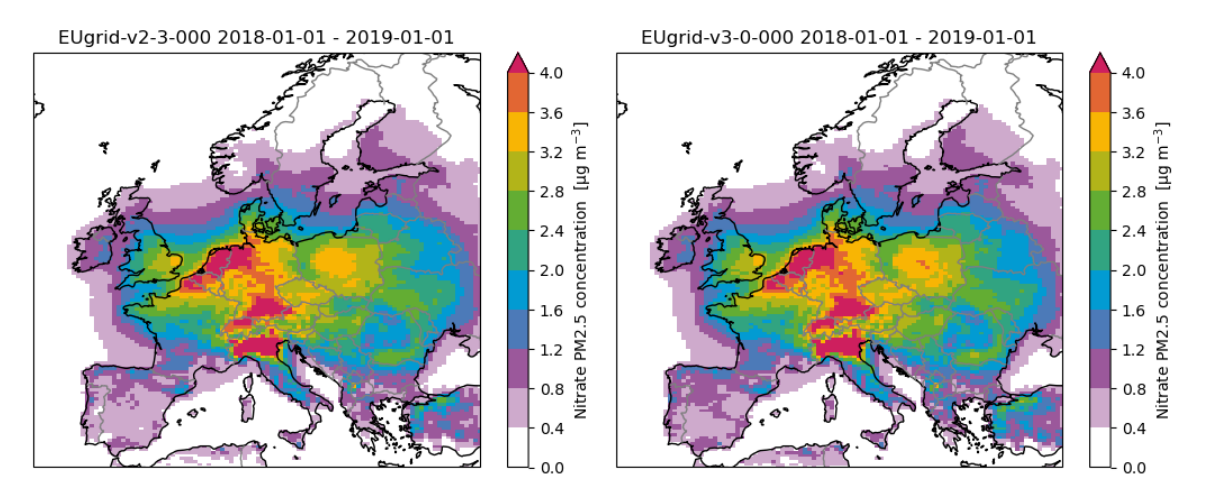


Figure 48: Concentration of nitrate in pm25.

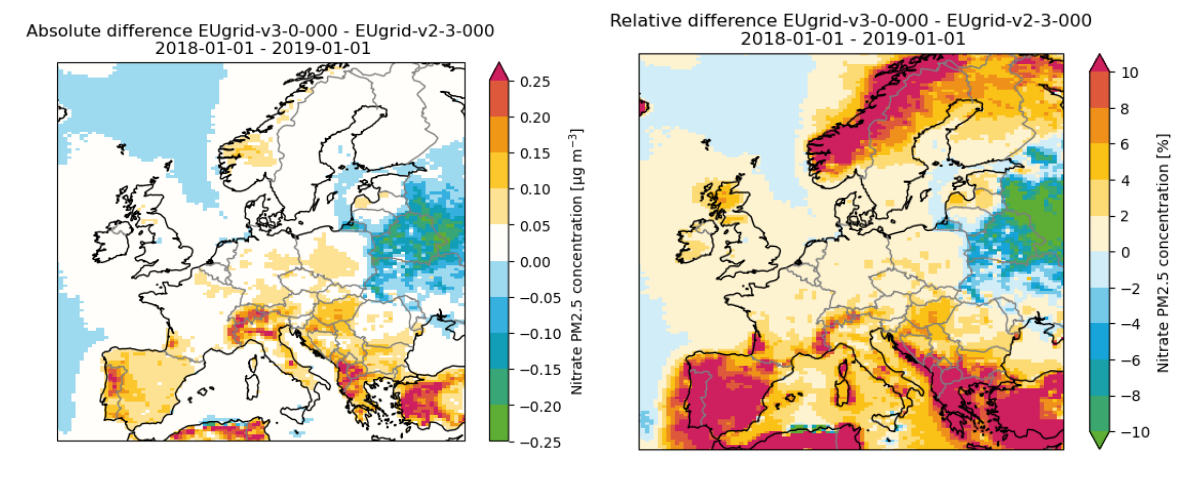


Figure 49: Absolute and relative difference of nitrate concentration in PM2.5.

TNO Public 37/67

## 4.4.3. Sulphate

In the atmosphere,  $H_2SO_4$ , a derivative of sulphur dioxide ( $SO_2$ ), reacts with ammonia ( $NH_3$ ) and thus competes with nitrate, to form sulphate ( $SO_4^{2-}$ ) and ammonium ( $NH_4^+$ ) in the ratio  $2NH_4^+$ :  $SO_4^{2-}$ . The pattern of the concentration difference of sulphate (Figure 51), coincides with the pattern in ammonia concentration differences in Figure 29. Therefore, the formation of sulphate, driven by the increased concentration of ammonia, leads to the overall decrease in concentration  $SO_2$  in the domain (Figure 33). In addition, the sulphate and ammonium concentration increase in France, Portugal and Turkey in Figure 51 and Figure 53, are caused by the CORINE lu-class transitional woodland-shrub which changed LOTOS-EUROS class from forest (deciduous and coniferous) to semi-natural shown in Figure 82. This luchange leads to less  $NH_3$  and  $SO_2$  dry depositions (see Figure 30 and Figure 34 for the dry deposition flux difference maps) which then leads to formation of ammonium and sulphate.

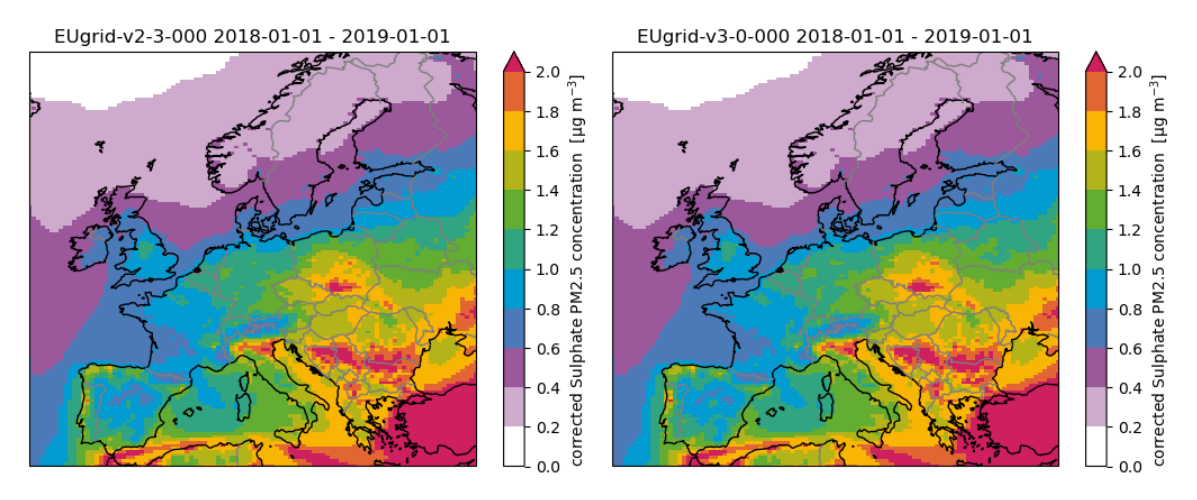


Figure 50: Concentration of sulphate in pm25.

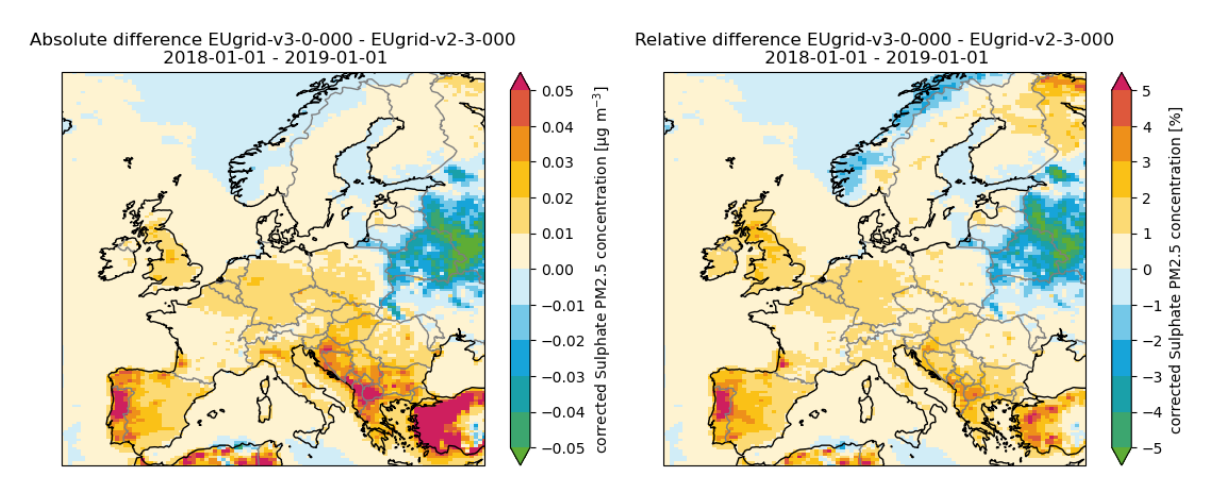


Figure 51: Absolute and relative difference of sulphate concentration in PM2.5.

TNO Public 38/67

### 4.4.4. Ammonium

The change in ammonium concentration is explained in sections 4.4.2 and 4.4.3, as ammonium is formed when  $NH_3$  reacts with  $HNO_3$  and  $H_2SO_4$ .

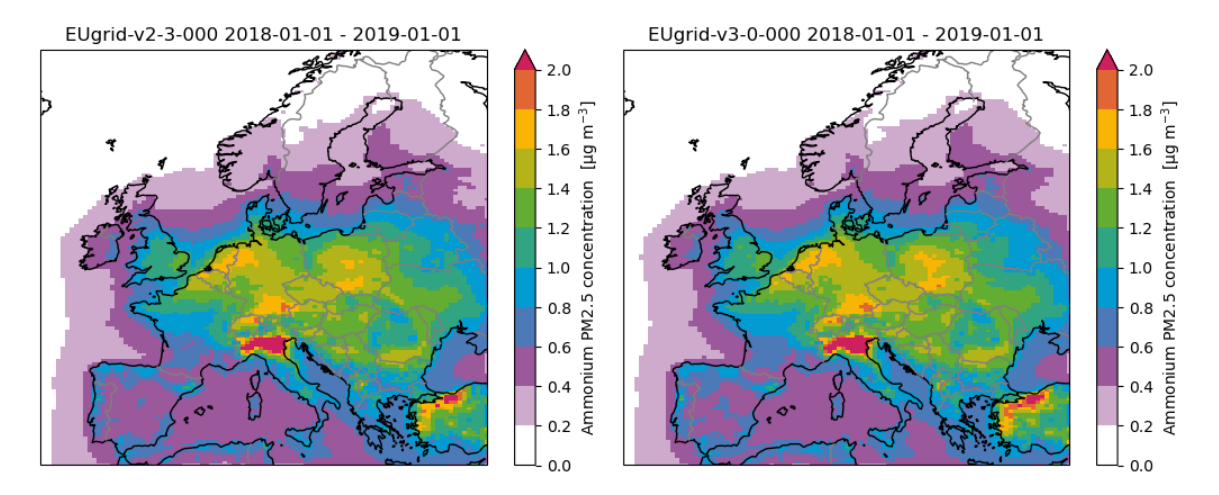


Figure 52: Concentration of ammonium in pm25.

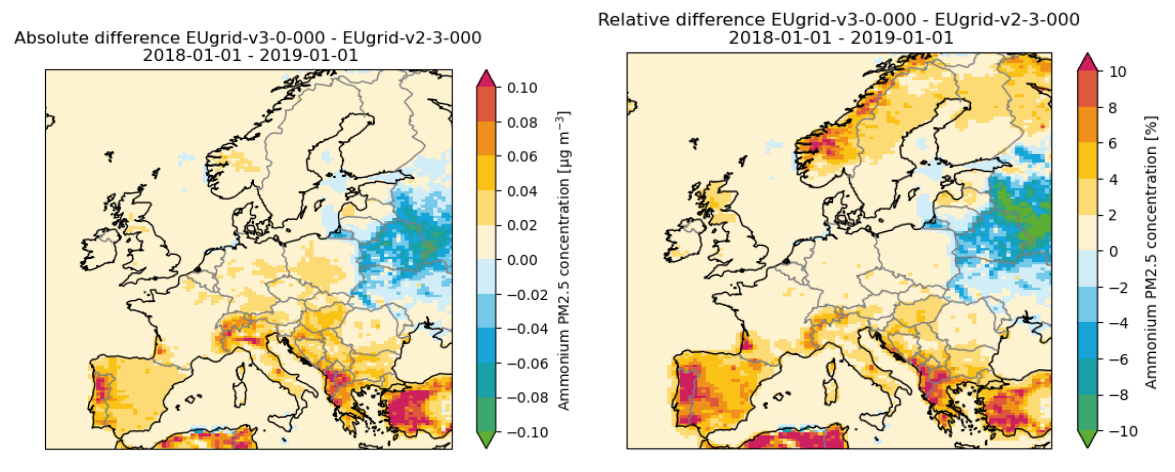


Figure 53: Absolute and relative difference of ammonium concentration in PM2.5.

) TNO Public 39/67

#### 4.4.5. Sodium

The changes in sodium in PM2.5 concentrations shown in Figure 55 originate from the changes of dry deposition, and changes of underlying land use maps as listed in Table 5.

The former change shows increased sodium concentrations in e.g. Portugal and Turkey as in these regions the forest fractions decrease (see Figure 87 and Figure 89). A similar pattern in the relative difference is observed for organic carbon and elementary carbon.

In addition, the changes of the underlying land use maps leads to a recategorization of certain water bodies in Russia, Ukraine, Belarus and Turkey as shown in Figure 56. In the three-tiered landuse approach the land use vegetation codes 'sea\_def', 'sea\_sds', 'sea\_shs', and 'sea\_tin' belong to the previous wat (seawater) class. The emission of seasalt increases the concentration sodium at lake Ladoga close to Sint Petersburg with 0.01  $\mu g/m^3$  or >5%.

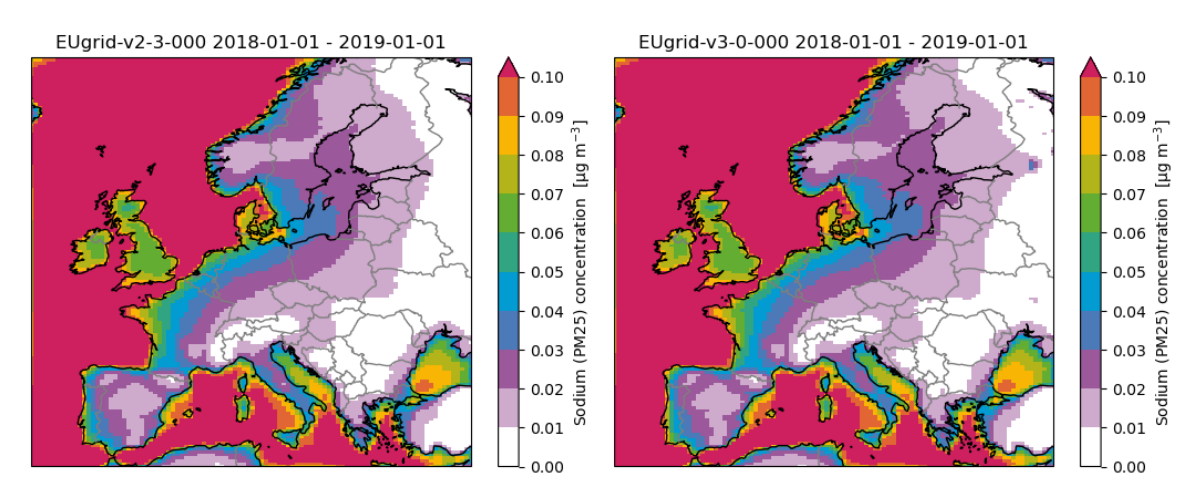


Figure 54: Concentration of sodium in pm25.

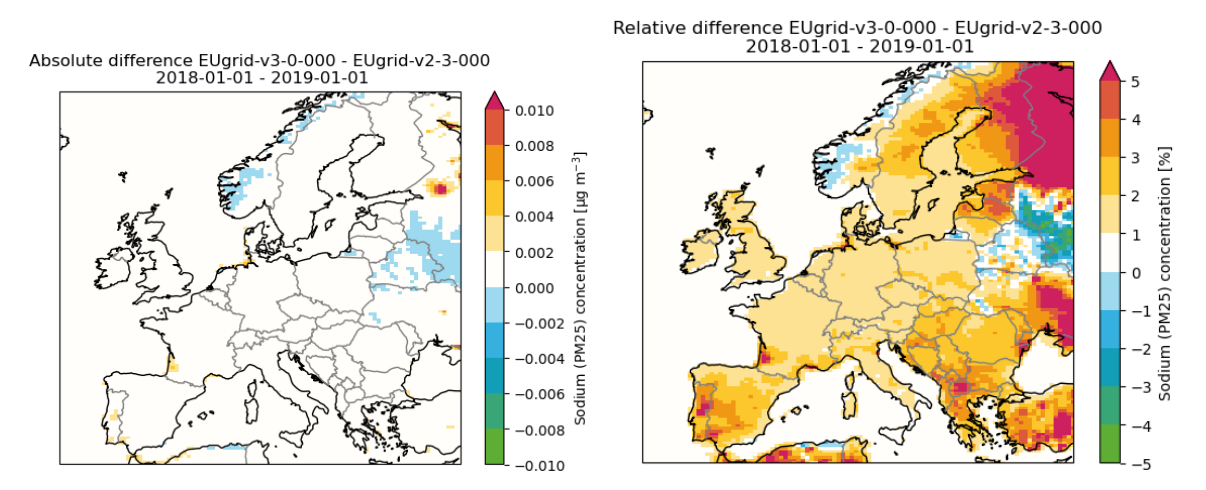


Figure 55: Absolute and relative difference of sodium concentration in PM2.5.

) TNO Public 40/67

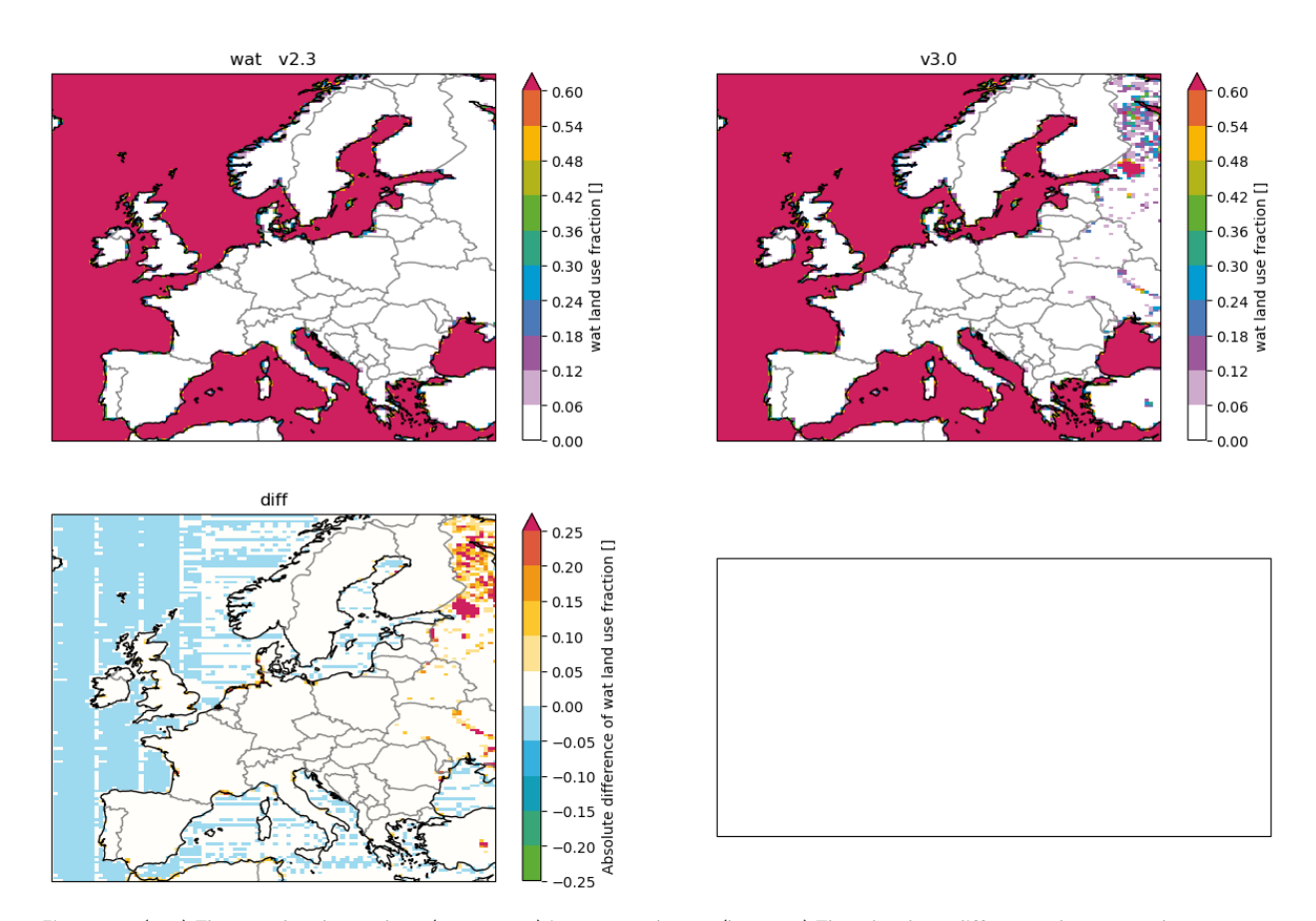


Figure 56 (top) The wat land use class (sea water) in v2.3 and v3.0. (bottom) The absolute difference between the watclass in v2.3 and v3.0. The relative difference is not shown as no valuable representation could be made when the lufractions are zero.

TNO Public 41/67

#### 4.4.6. Organic Carbon

The relative difference patterns of organic (OC) and elemental (EC) carbon in Figure 58 and Figure 60, respectively, are very similar. Both species are mainly influenced by dry deposition.

In Russia/Belarus, the OC and EC decreases up to -0.04 and -0.01  $\mu g/m^3$  or -5%, respectively. Similar as for other species such as NO2 and NH3, the reallocation of land use fractions from ara and crp to forest leads to increased depositions and thus decreased concentrations.

In increase of OC and EC in southern Europe (e.g. parts of France, Portugal, Turkey with +5% increase) and Scandinavia (Sweden and Finland with +2%), and Great Brittain (+2%) are caused by the CORINE luclass transitional woodland-shrub which changed LOTOS-EUROS class from forest (deciduous and coniferous) to semi-natural land shown in Figure 82. In this case, seminatural land deposits less than forests leading to increased concentrations of EC and OC.

The decreased concentrations of up to -2% in Norway is caused by the CORINE land use class Sparsely vegetated areas which changed from dsr into sem (see Figure 82 and Figure 83) which leads to increased deposition velocities. The effect of this land use class is also present in Turkey (-1%) and the Alpes (~0-1 %), but is less visible.

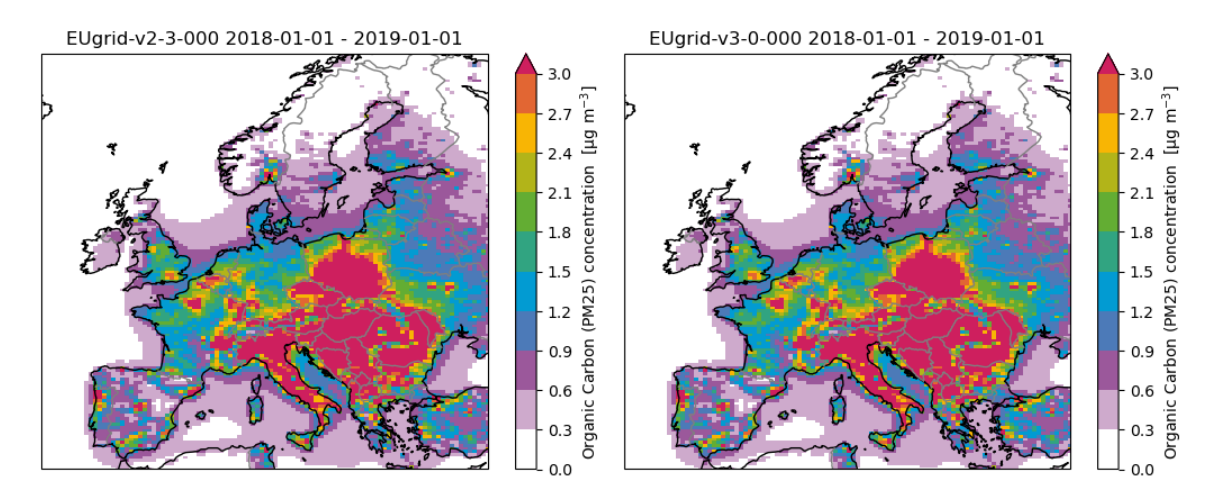


Figure 57: Concentration of organic\_carbon in pm25.

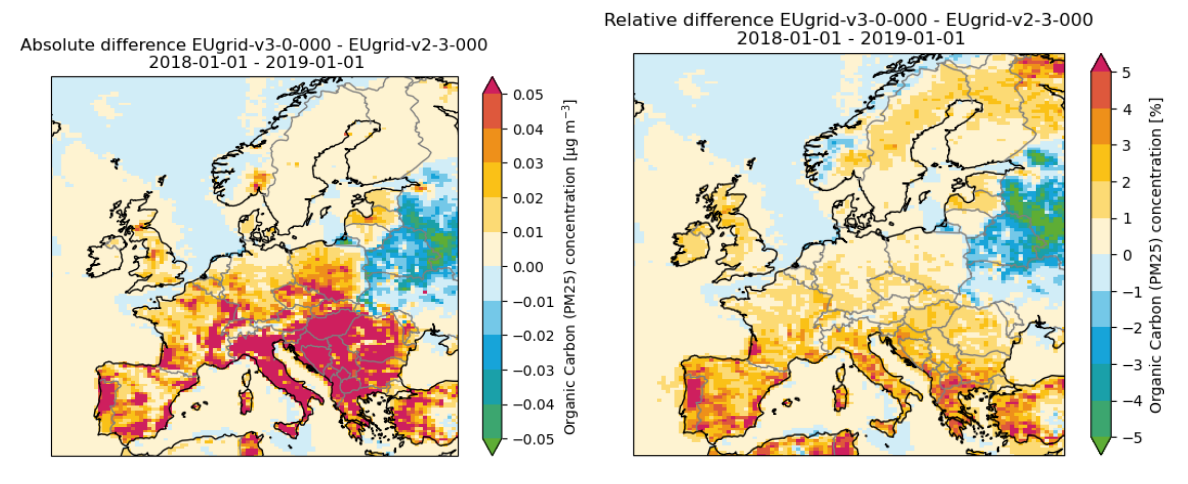


Figure 58: Absolute and relative difference of organic carbon concentration in PM2.5.

TNO Public 42/67

# 4.4.7. Elementary Carbon

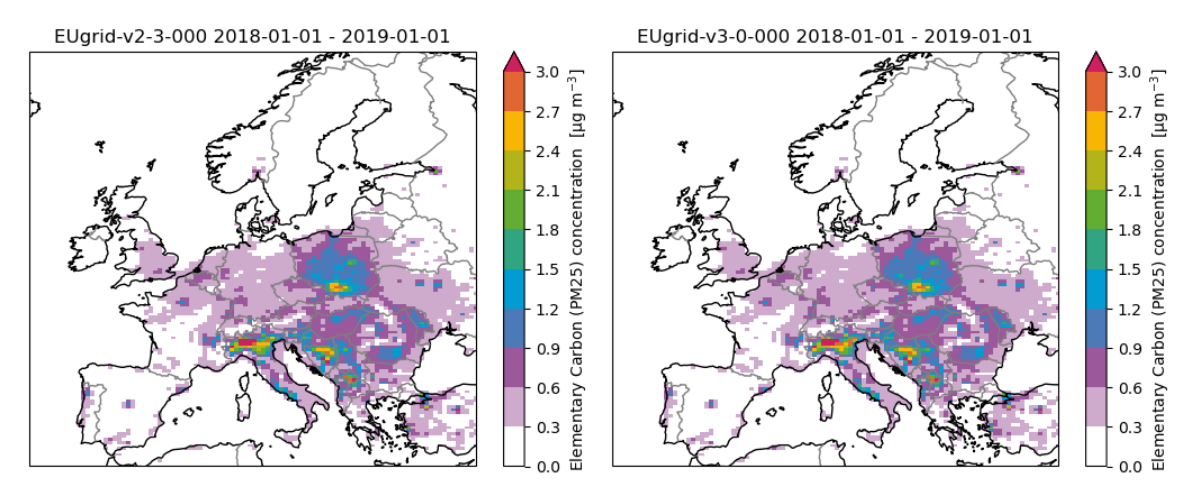


Figure 59: Concentration of elementary\_carbon in pm25.

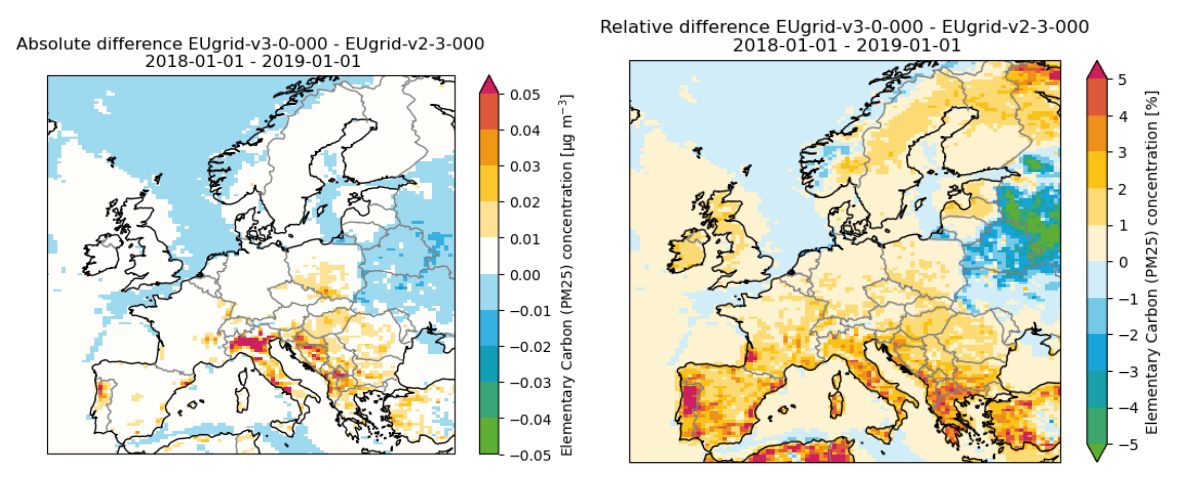


Figure 60: Absolute and relative difference of elementary carbon concentration in PM2.5.

) TNO Public 43/67

#### 4.4.8. PM10

The PM10 concentrations follow the general trends of PM2.5 (Figure 39), showing increase up to -1  $\mu$ g/m³ ~ 5% in Portugal, France, north Africa and parts of Turkey. While a decrease up to -1  $\mu$ g/m³ ~ 5% is shown over the Belarus/Russia. Thus, similar arguments discussed in sections 4.4.1 to 4.4.7 hold for PM10 too.

When comparing the relative difference maps in Figure 39 and Figure 62, the main differences are observed in the cities such as Paris and Madrid, along the Mediterranean coast of Spain and parts of The Netherlands and Belgium, and in Russia next to the border with Finland.

The mineral dust concentrations, shown in section 4.4.9, show a large overall decrease throughout Europe. Specifically, the cities Paris and Madrid show lower mineral dust. This is discussed in detail in section 4.4.9.

For PM10, the slight increases of concentrations are also visible at the measurement stations. The averaged statistics over the EBAS and EEA measurement station are listed in Table 3 and Table 4 in the Appendix and the temporal mean over the stations are shown in Figure 64 and Figure 64. In the latter Figure The averaged PM10 concentrations [ $\mu$ g/m³] statistics between hourly EBAS measurements and LOTOS-EUROS, change from 9.54 to 9.55 (RMSE), 0.19 to 0.19 (R2), and -0,14 to -0.13 (NMB). The daily EBAS and the EEA statistics also show very minor differences.

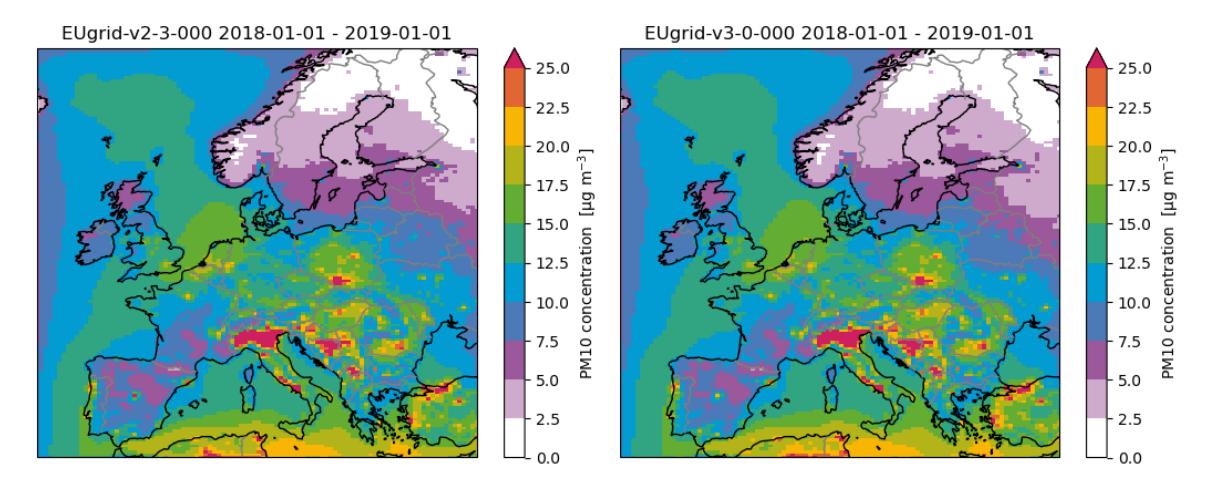


Figure 61: Concentration of pm10\_mass in pm10.

TNO Public 44/67

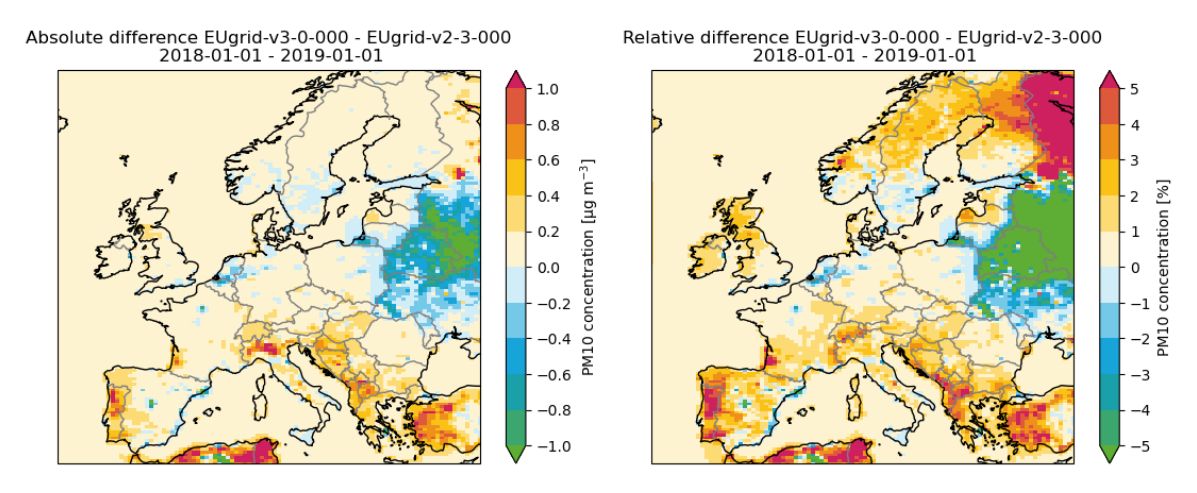


Figure 62: Absolute and relative difference of PM10 concentration in air.

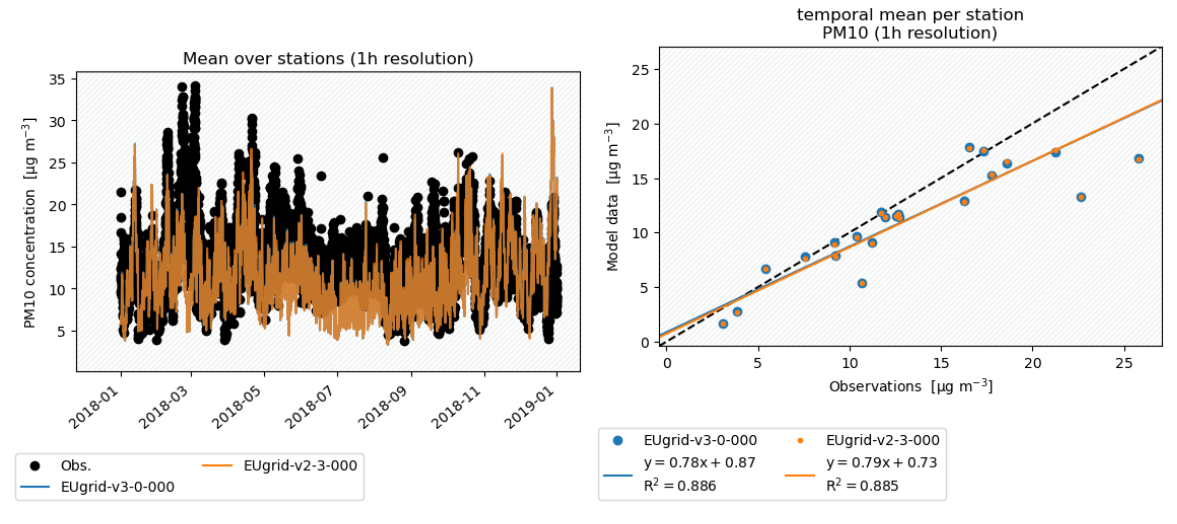


Figure 63: Line plots of pm10\_mass for mean of EBAS stations.

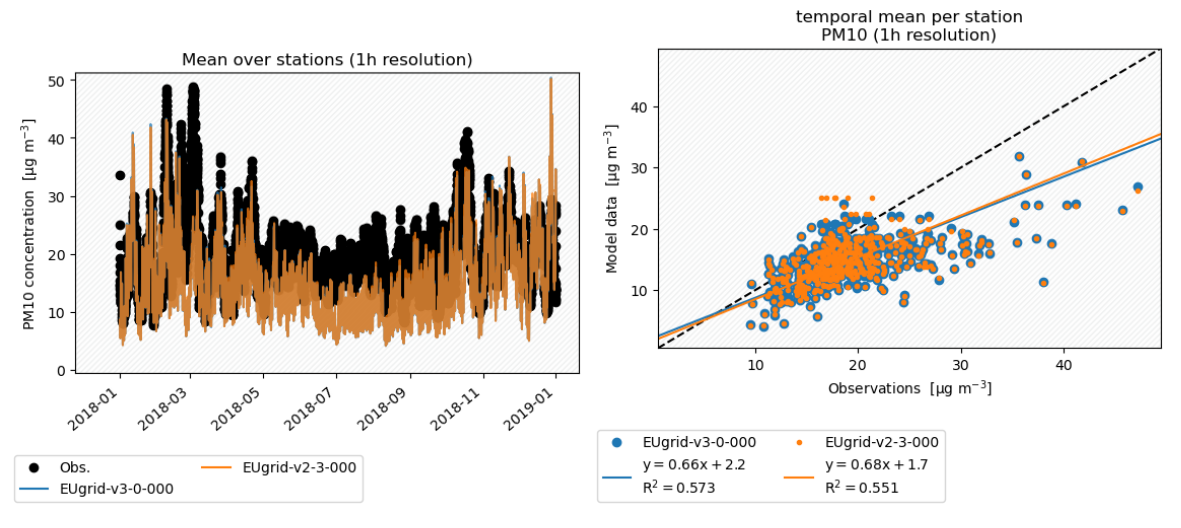


Figure 64: Line plots of pm10\_mass for mean of EEA stations.

) TNO Public 45/67

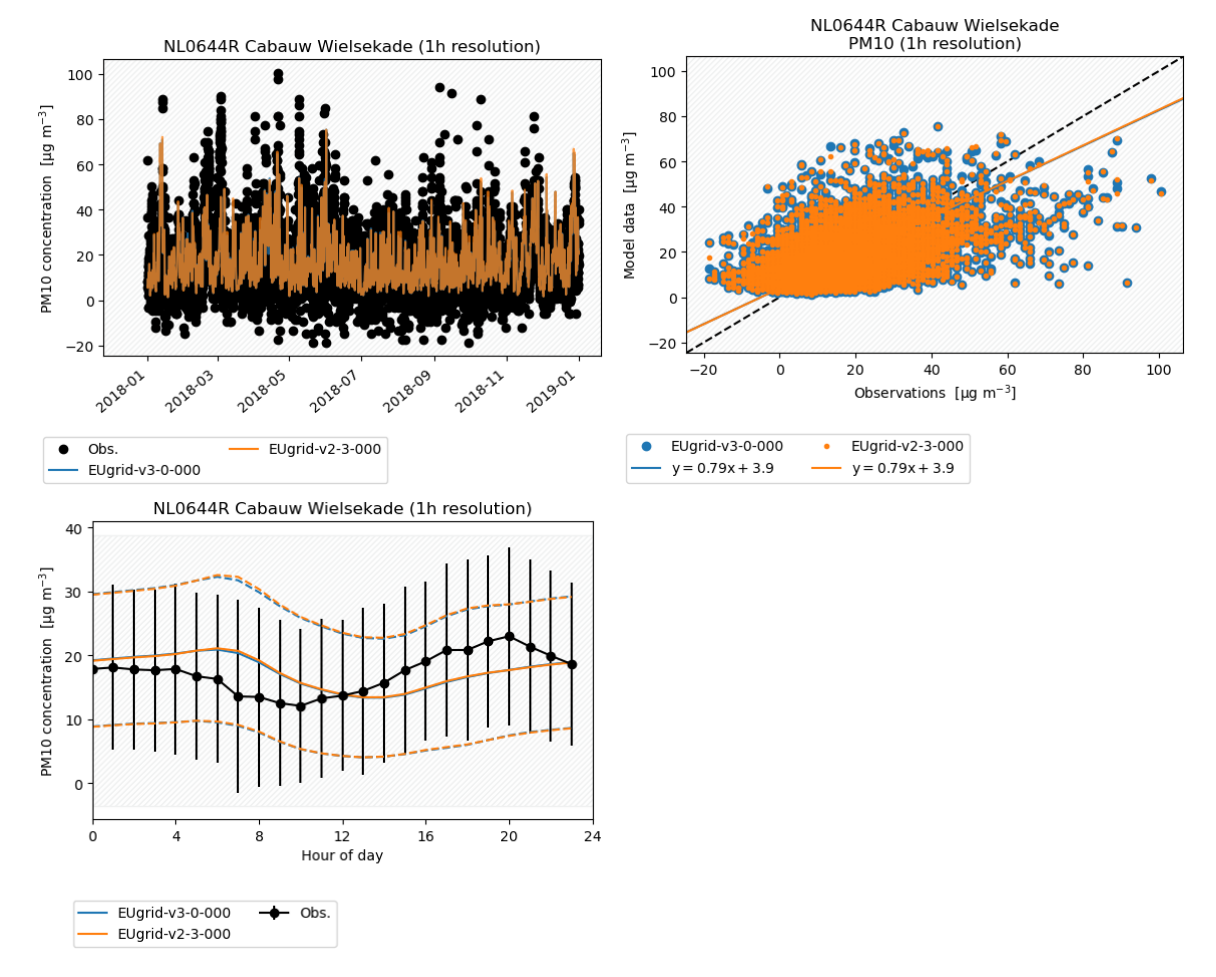


Figure 65: Line plots of pm10\_mass for station NL0644R.

TNO Public 46/67

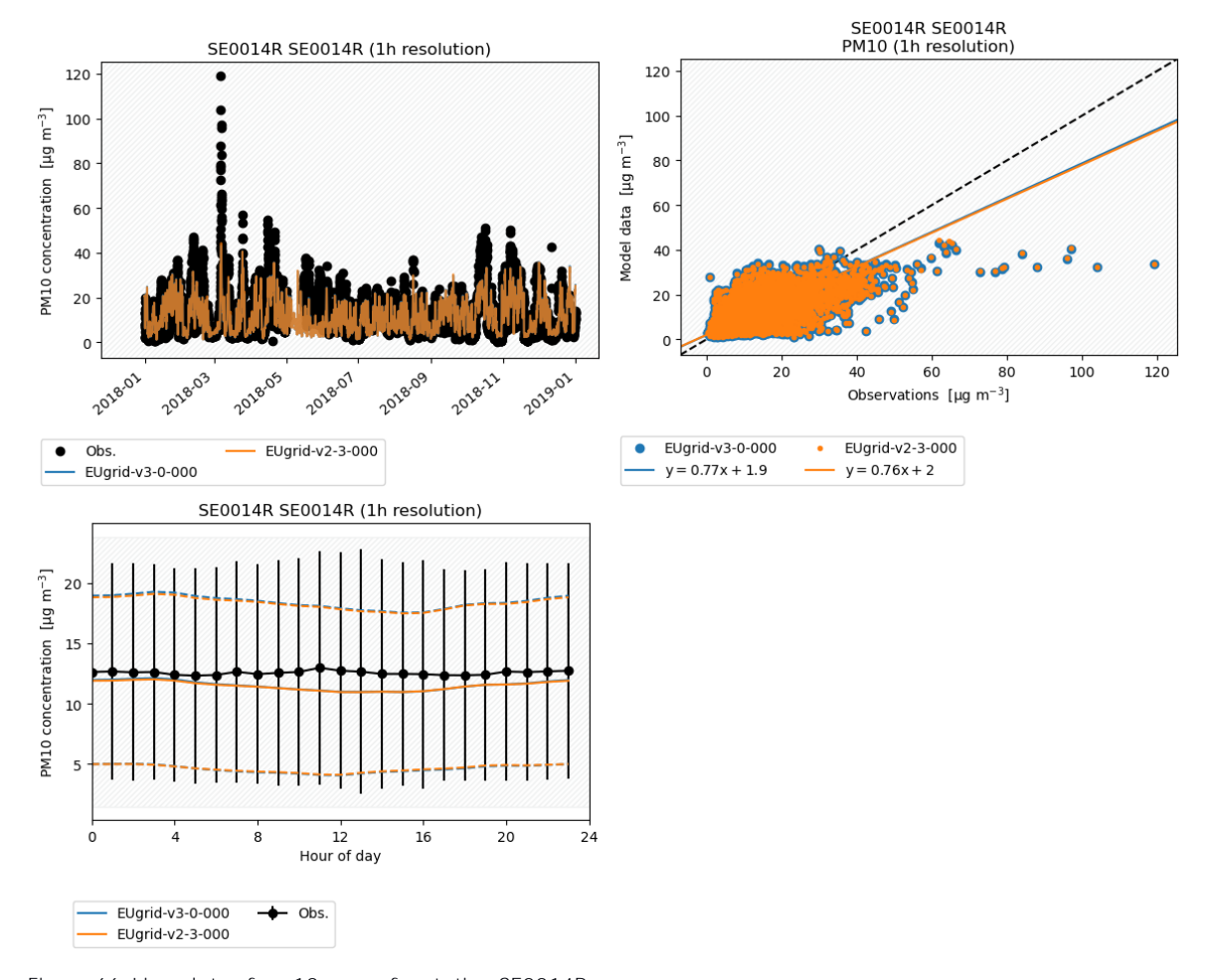


Figure 66: Line plots of pm10\_mass for station SE0014R.

TNO Public 47/67

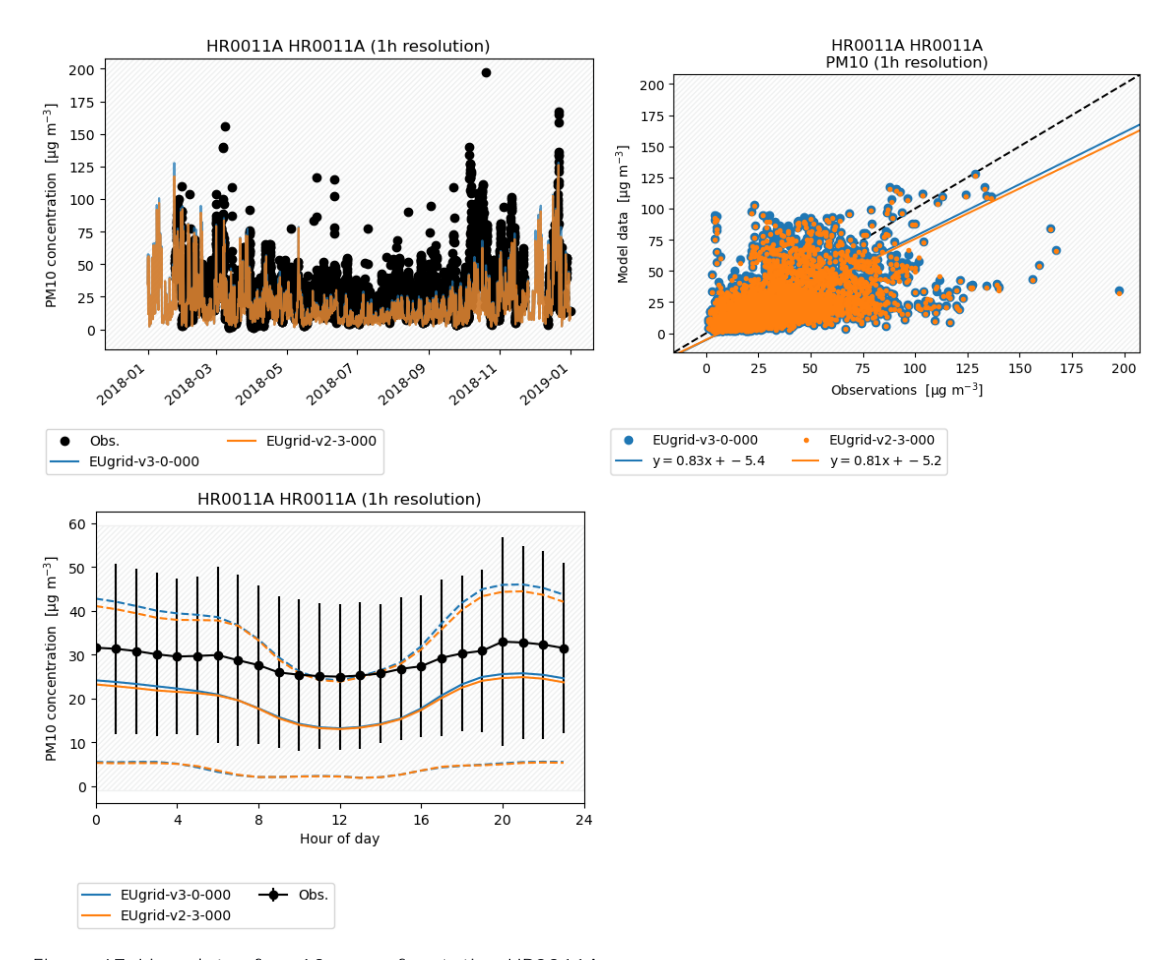


Figure 67: Line plots of pm10\_mass for station HR0011A.

TNO Public 48/67

#### 4.4.9. Mineral Dust

Most mineral dust comes from the Sahara and dry Northern African regions, evident by the concentration gradient from the south to the north of the domain in Figure 68. Its deposition (see equation 5.13 in the LOTOS-EUROS reference guide v3.0) is dependent on Ra, the aerodynamic resistance, which is dependent on e.g. the land use fractions of the whole cell, wind speed, the (vegetation) height, and friction velocity.

The land use class with a large vegetation height is the forest with a height of 20m. In Figure 84, we observe that there is decrease of forest fraction (relatively <-50%) in north of Africa, Turkey and parts of Portugal. In Turkey, a concentration increase of 0.2  $\mu$ g/m³ ~ 4% is observed and in north Africa (Algeria2), a concentration increase of 0.5  $\mu$ g/m³ ~ 5% is observed. In these region, fractions of coniferous and deciduous forest became grass land and seminatural land.

In Russia/Belarus, a concentration decrease of 0.5  $\mu$ g/m³ ~-10% is observed. In this region, Figure 84 shows a large increase of forest (relatively >50%) leading to lowered Ra, and thus more deposition of mineral dust and lower concentrations in PM10.

In cities such as Paris and Madrid the land use fraction of Green urban areas was in v2.3 assigned to grassland and in v3.0 to urban (Table 7). The urban class has a larger height h=10m compared to grassland with h=0.3m.

Over the full domain, a decrease of mineral dust is observed which is mostly assigned to the lu-class change of Land principally occupied by agriculture with significant areas of natural vegetation (Figure 83). Previously, this CORINE class was assigned to both arable land and cropland with a vegetation height of 1m and 2.5m, respectively. In v3.0, this class is fully assigned to crp with a height of 2.5m. Finally, because mineral dust is chemically inert, changes in its concentration can appear even in regions where land-use fractions remain unchanged, resulting in "halos" of elevated or reduced dust levels. These concentration halos are particularly evident along coastlines, extending from the coastline into the sea.

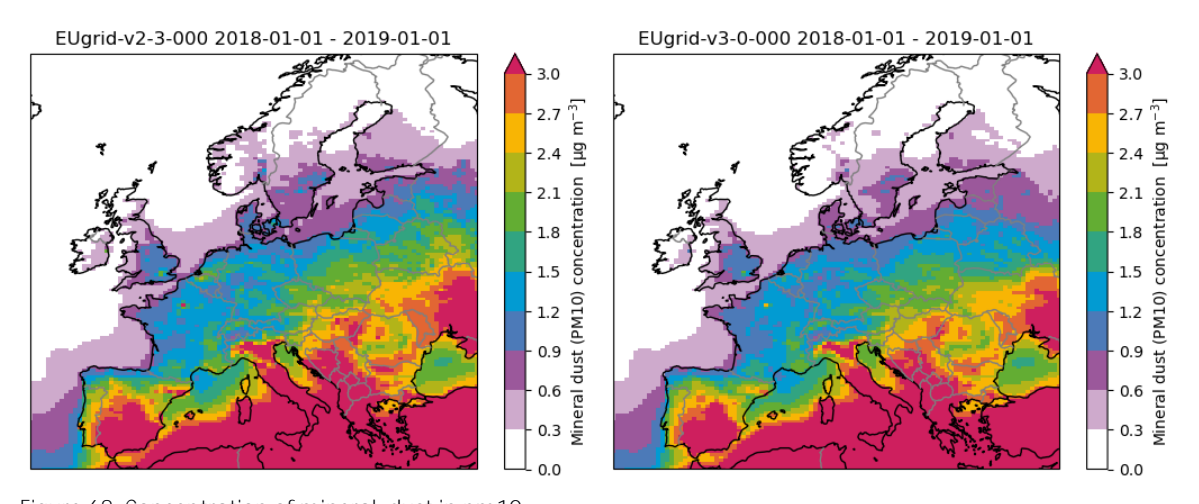


Figure 68: Concentration of mineral\_dust in pm10

) TNO Public 49/67

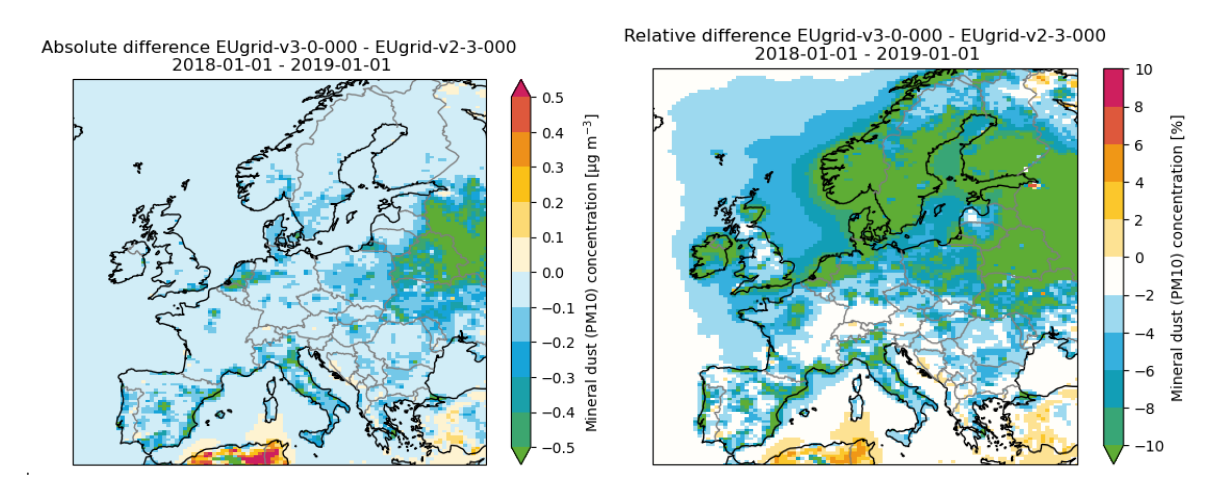


Figure 69: Absolute and relative difference of mineral dust concentration in PM10.

# 4.5. Deposition

## 4.5.1. NHx Deposition

The relative difference map of NHx deposition shows similar trends as observed for ammonia and ammonium in Figure 29 and Figure 53, respectively.

- In Norway, the increased concentration difference of ammonium compared to the decrease of ammonia was explained by the reactivity of NH3 with HNO<sub>3</sub> and H<sub>2</sub>SO<sub>4</sub>. For NHx dry deposition, we observe a mixed behavior in Norway.
- In Russia/Belarus, the increased forest fraction increases the dry deposition of NH3 and NH4a with 0.10 mg/m² ~10%.
- In parts of France, Portugal, Turkey and Albania, the transitional woodland-shrub class changing from forest to seminatural (Figure 82) leads to decreased NHx dry depositions of -0.10 mg/m<sup>2</sup> ~10%.

The wet deposition is strongly related to the concentrations of ammonia and ammonium (shown in sections 4.3.3 and 4.4.4, resp.).

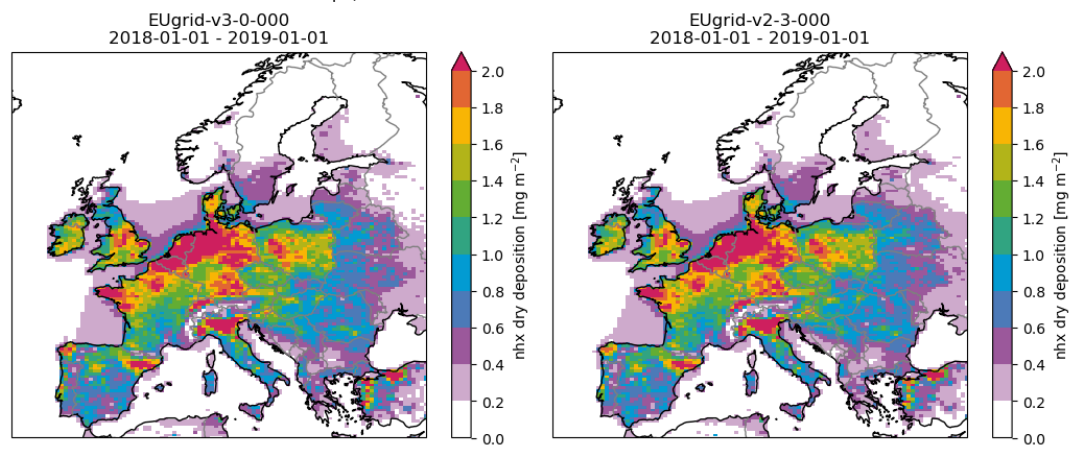


Figure 70: Total dry deposition of NHx.

) TNO Public 50/67

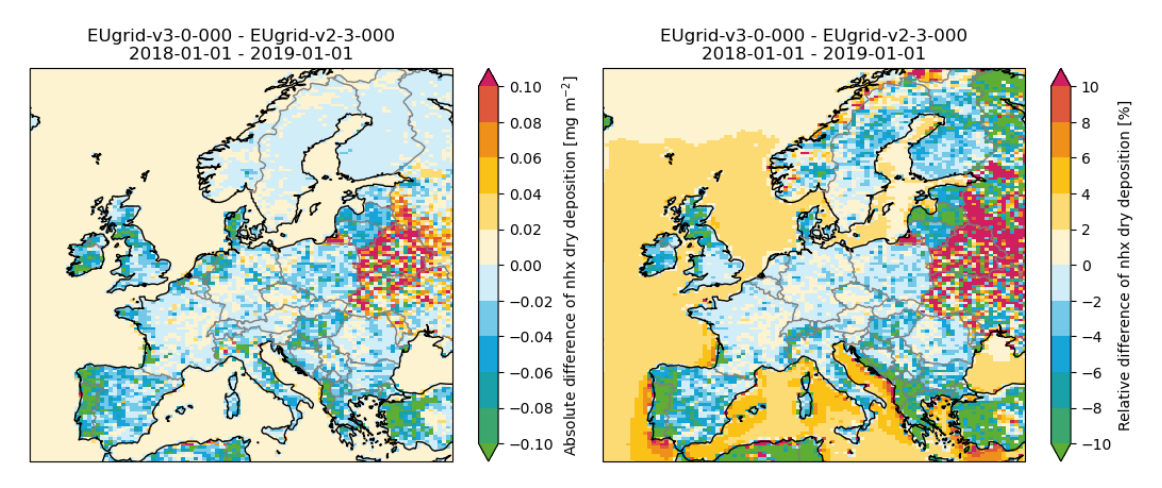


Figure 71: Absolute and relative difference of total dry deposition of NHx.

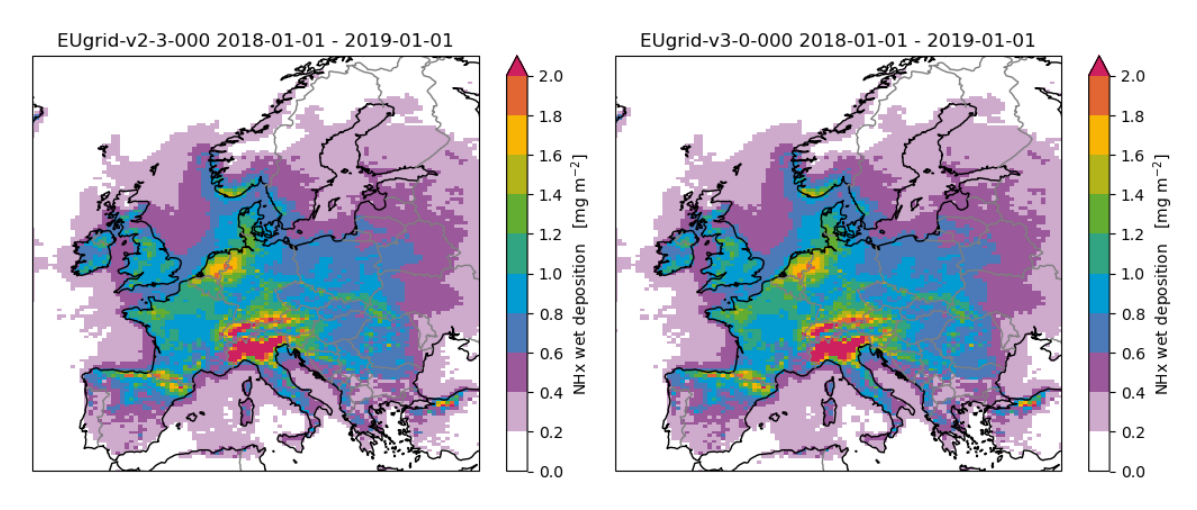


Figure 72: Total wet deposition of NHx.

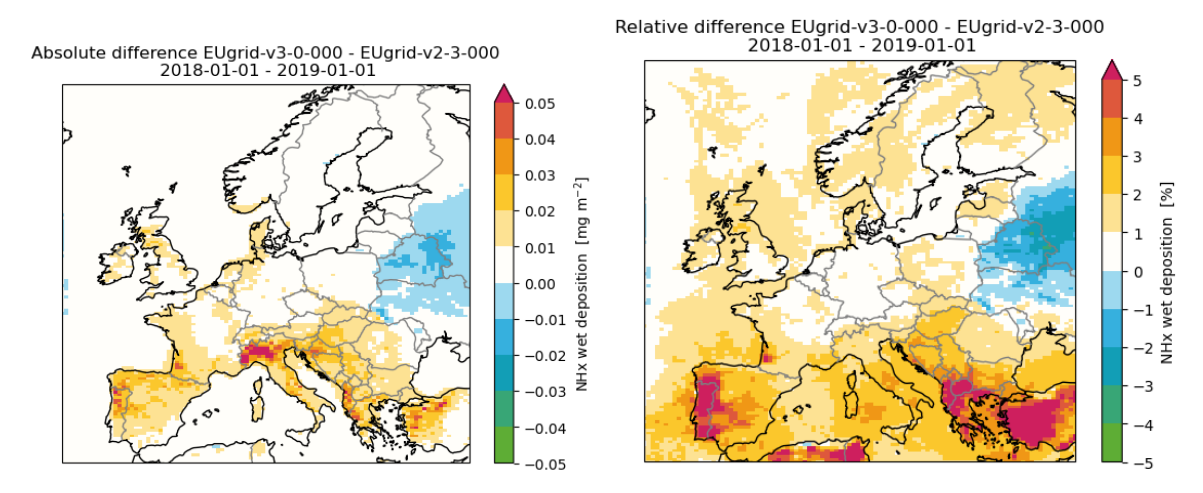


Figure 73: Absolute and relative difference of total wet deposition of NHx.

TNO Public 51/67

#### 4.5.2. NOy Deposition

NOy is composed of the species NO,  $NO_2$ ,  $HNO_2$ ,  $HNO_3$ ,  $NO_3$ a,  $N_2O_5$ , and PAN for which the species  $HNO_3$  and  $NO_2$  are the largest absolute contributor in units of mass to the dry and wet deposition. Note that  $HNO_3$  is formed from  $NH_3$  and  $NO_2$ , and therefore related to both of them.

First of all, the relative change of dry deposition in Figure 75 partly coincides with the biogenic NO emission increases in Figure 5, namely in Scandinavia, Spain, Turkey, Alps, Scotland and Greece.

Second, the changed forest fractions (Figure 84) play a big role in the deposition of NOy. In regions with more forest, Russia/Belarus shows increased NOy dry depositions of 0.10 mg/m $^2$  ~10%. North of Africa and in the areas of the transitional woodland-shrub class (parts of France, Portugal, Turkey and Albania) forest changed into the seminatural class (Figure 82) leading to decreased NOy dry depositions of -0.10 mg/m $^2$  or 5-10%.

The wet deposition is strongly related to the concentrations of NO<sub>2</sub> shown in section 4.3.2.

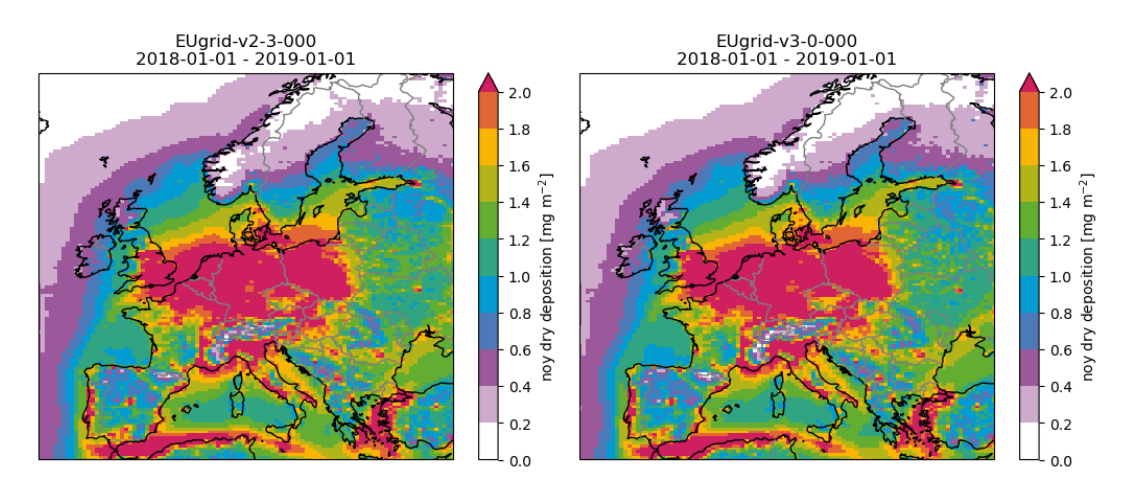


Figure 74: Year total dry deposition of NOy.

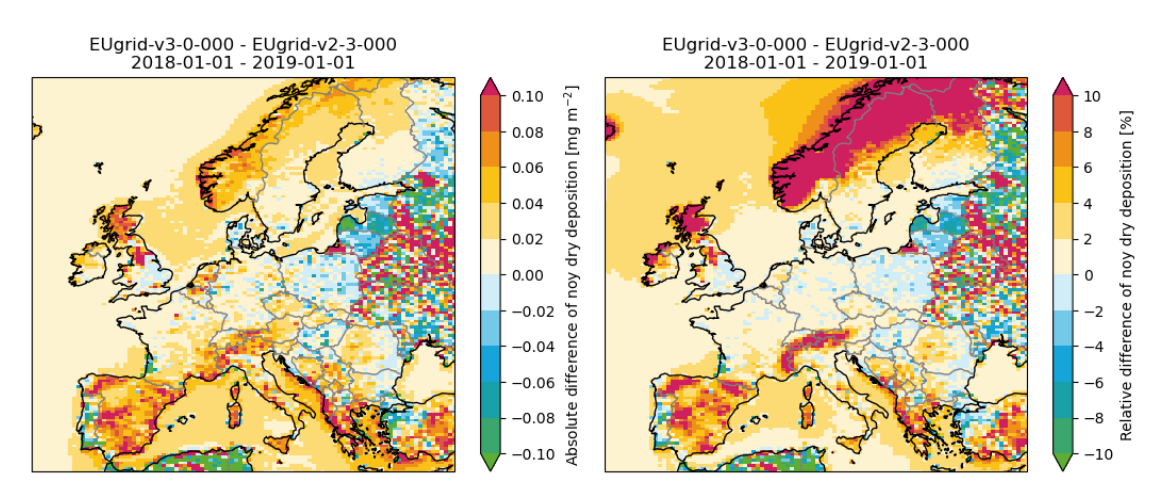


Figure 75: Absolute and relative difference of total dry deposition of NOy.

TNO Public 52/67

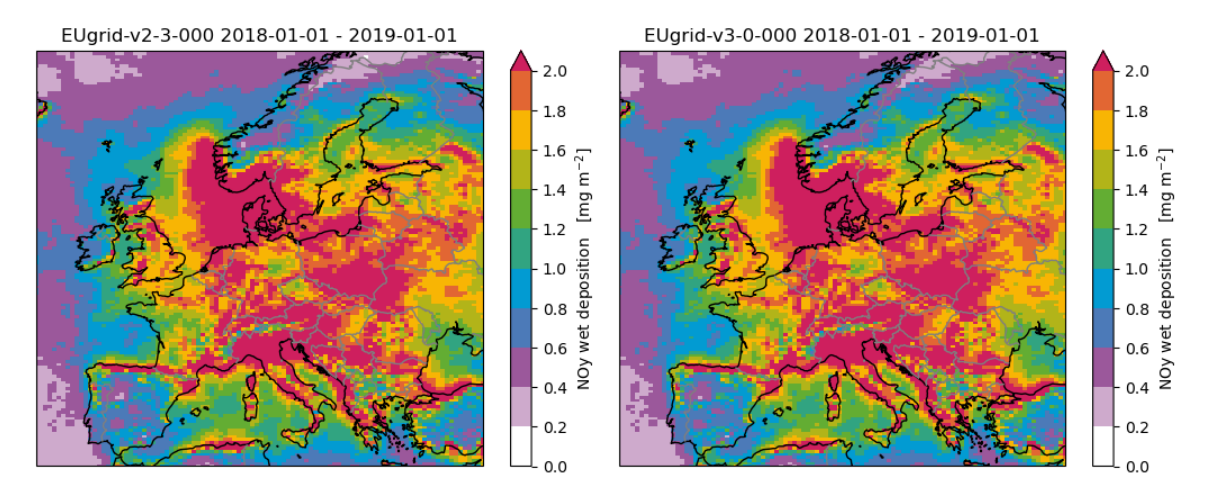


Figure 76: Total wet deposition of NOy.

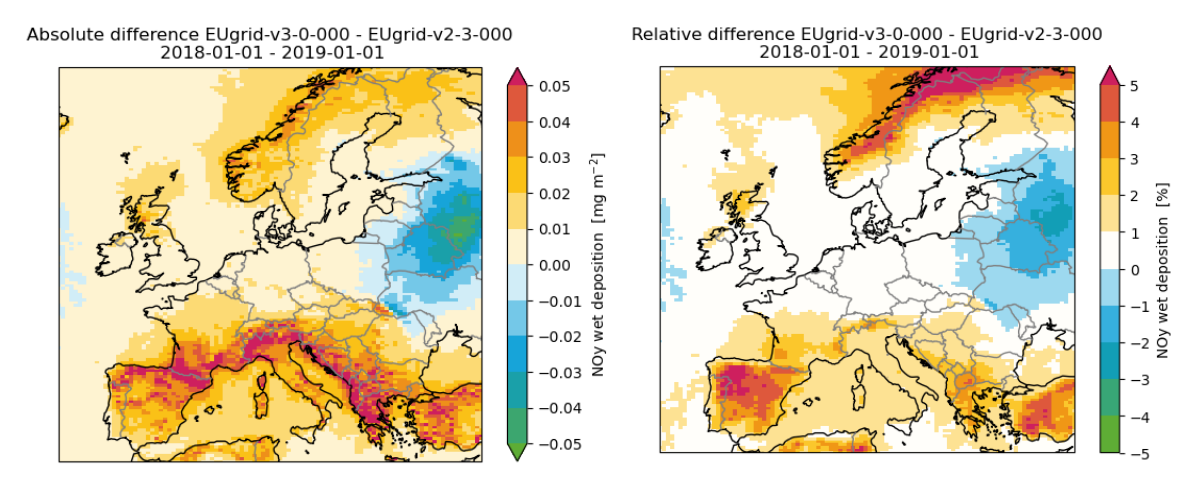


Figure 77: Absolute and relative difference of total wet deposition of NOy.

) TNO Public 53/67

### 4.5.3. SOx Deposition

SOx mainly consist of  $SO_2$  which' concentration maps are shown in section 4.3.4. Discussed in section 4.4.3 was the chemical reactivity of  $SO_2$  in air. In section 4.3.4, the dry deposition of  $SO_2$  is discussed in detail and shown in Figure 34. Comparing Figure 34 and Figure 79, we observe no significant differences.

The wet deposition of SOx follows the concentration trends in Figure 33 and is not greatly impacted; over the whole domain less than 2%.

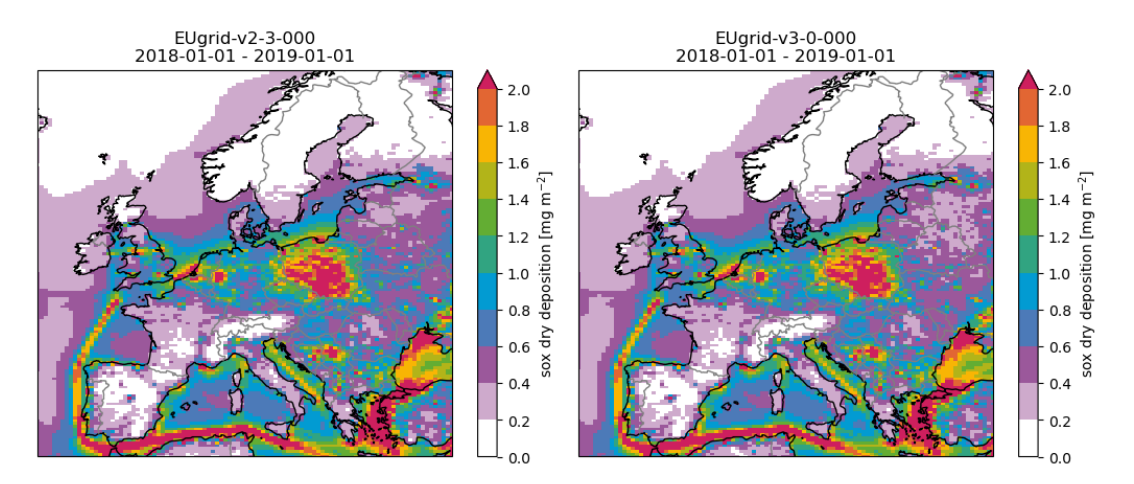


Figure 78: Total dry deposition of SOx.

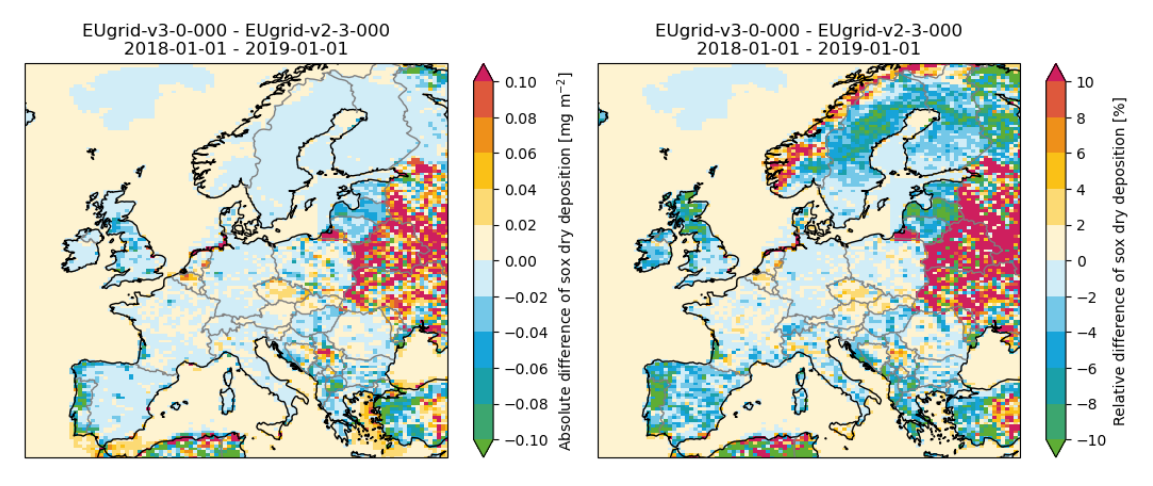


Figure 79: Absolute and relative difference of total dry deposition of SOx.

TNO Public 54/67

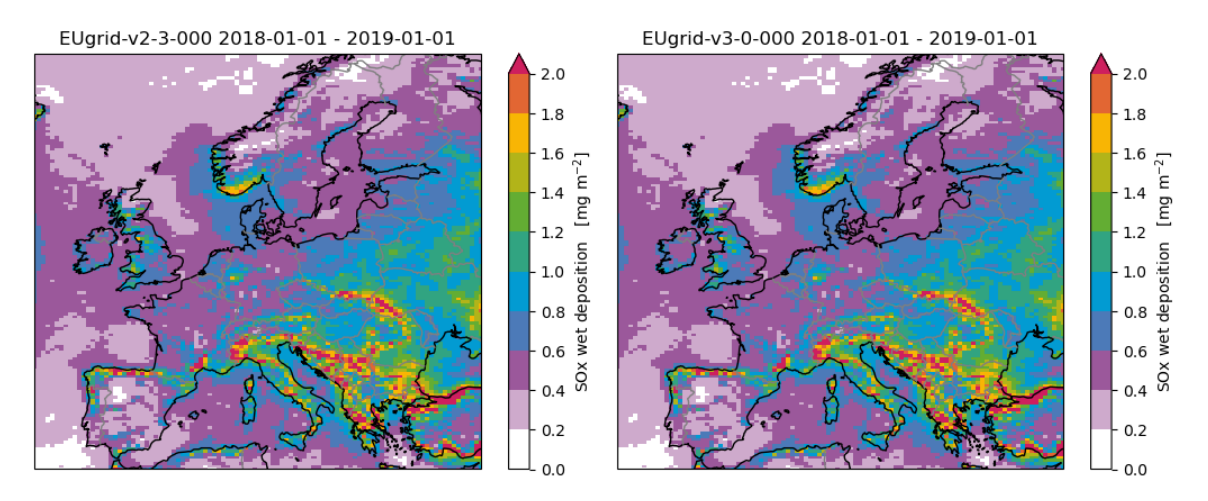


Figure 80: Total wet deposition of SOx.

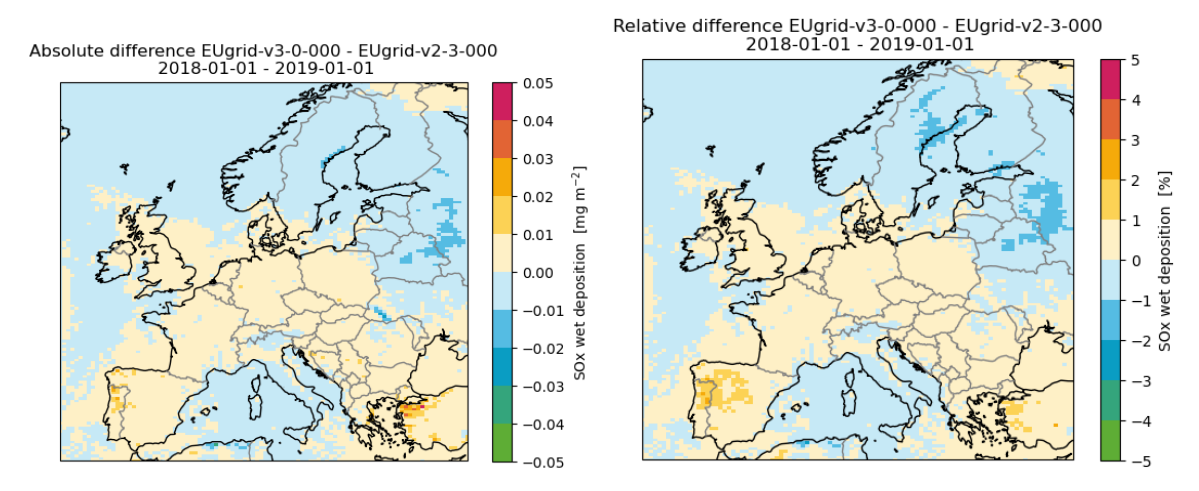


Figure 81: Absolute and relative difference of total wet deposition of SOx.

TNO Public 55/67

# 4.6. Statistics

Below in Table 3 and Table 4, the averaged statistics over the EBAS and EEA measurement stations are show. Overall, the statistics, i.e. RMSE, R2 and NMB, of v2.3 and v3.0 are very similar.

Table 3 Pollutant statistics (RMSE, R2 and NMB) compared to EBAS data with a threshold of 15%. For each pollutant, the time resolution (delta time), average number of measurements per measurement station (<N>) is given. Data is shown for the ref (v2.3.000) and test (v3.0.000).

pollutant	delta time	<n></n>	v2.3.000		v3.0.000			
			RMSE	R2	NMB	RMSE	R2	NMB
NH3	1h	7076	4,23	0,11	0	4,24	0,11	0,01
NH3	1d	358	2,25	0,32	0,68	2,25	0,32	0,68
NH4a (PM total)	1d	349,67	0,60	0,44	0,09	0,61	0,44	0,10
NH4a (PM2.5)	1d	353	0,90	0,35	0,17	0,91	0,35	0,19
NO2	1h	8436,02	5,74	0,34	0,17	5,79	0,33	0,2
NO2	1d	358	3,43	0,35	0,47	3,54	0,33	0,69
NO3a (PM10)	1d	336,38	1,50	0,25	0,58	1,60	0,25	0,69
NO3a (PM2.5)	1d	353	3,02	0,20	7,31	3,07	0,19	7,50
03	1h	8353	18,51	0,51	0,05	18,45	0,52	0,04
O3 MDA8	1d	8353	14,02	0,58	0,06	13,66	0,59	0,05
PM10	1h	8321,77	9,54	0,19	-0,14	9,55	0,19	-0,13
PM10	1d	345,44	8,74	0,27	-0,17	8,76	0,27	-0,15
PM2.5	1h	8429,07	6,69	0,31	-0,08	6,72	0,31	-0,07
PM2.5	1d	344,16	6,62	0,31	-0,11	6,69	0,3	-0,09
SO2	1d	362,25	2,05	0,19	2,23	2,04	0,19	2,21
SO2	1h	8331,1	1,11	0,10	1,67	1,11	0,1	1,68
SO4a (corrected)	1d	349,83	1,09	0,25	-0,07	1,09	0,25	-0,06
SO4a (corrected, PM10)	1d	358,5	0,80	0,49	-0,20	0,80	0,49	-0,19
SO4a (corrected, PM2.5)	1d	353	1,40	0,30	-0,21	1,39	0,3	-0,20
SO4a (total)	1d	349,83	1,21	0,18	0,47	1,20	0,18	0,48
SO4a (total, PM10)	1d	336,38	0,95	0,50	-0,23	0,96	0,5	-0,22
SO4a (total, PM2.5)	1d	353	1,39	0,29	-0,19	1,39	0,29	-0,18

Table 4 Pollutant statistics (RMSE, R2, and NMB) compared to EEA data with a threshold of 15%. Same type of table as Table 3.

pollutant	delta time	<n></n>	v2.3.000		v3.0.000			
			RMSE	R2	NMB	RMSE	R2	NMB
NO2	1h	7881,4	13,24	0,29	-0,33	13,27	0,28	-0,33
03	1h	8074,5	20,70	0,56	0,13	20,81	0,56	0,13
O3 MDA8	1h	8074,5	15,39	0,58	0,07	15,34	0,58	0,07

TNO Public 56/67

PM10	1h	8177,4	13,46	0,24	-0,19	13,45	0,24	-0,19
PM2.5	1h	7837,0	9,93	0,33	-0,12	9,99	0,33	-0,12
SO2	1h	8061,0	4,26	0,09	0,05	4,26	0,09	0,04

# 5. Conclusions and recommendations

To conclude, the major update in LOTOS-EUROS from v2.3 to v3.0 is the introduction of the three-tiered land use approach which gives the user the freedom to adapt the deposition parameters as function of land use class themselves. Along with this technical update, which in principle would not change simulation results, there are updates done on the land use map and deposition parameters in the default version of LOTOS-EUROS.

The updates of the land use map are due to (1) an update of the underlying land use maps, (2) the seminatural land is added to the LOTOS-EUROS lu-classes, and (3) improved translations from the Corine, and ESA classifications to LOTOS-EUROS classifications. The largest observed effect on the concentration of various species stem from the new seminatural class which is assigned to the Corine classes transitional woodland-shrub, sparsely vegetated areas, and sclerophyllous vegetation. This change to the seminatural class causes biogenic NO emissions changes affecting the NO2 concentrations, and following chemical reactivities. Outside the Corine map domain, major updates are observed in Belarus and its border with Russia where a large fraction of the arable land and grassland is changed into forest. In addition, in the north of Africa, a large fraction of the arable land and forest is now assigned to grassland.

The vegetation deposition parameters in the Mediterranean climate zone vapor pressure deficit vpd and temperature T were updated according to literature values. As in the Mediterranean climate zone the biogenic NO emissions were also largely affected leading to lowered ozone concentrations, the effect of the vegetation deposition parameters was not significantly observed. However, when inspecting the ozone dry deposition fluxes an increase of >10% is observed in the mediterranean climate. Over the European domain, we observe concentration and deposition differences between v2.3 and v3.0. However, for the inspected measurement stations, the changes are minor, up to a few percent. For background information and how to use the three-tiered land use approach in LOTOS-EUROS v3.0, we refer the reader to Ref. [1] and [2]. In addition, information on CB7, the newly implemented chemistry scheme, can also be found there.

# 6. References

- 1. LOTOS EUROS Reference Guide v3.0.000 (TNO 2025 R10849)
- 2. LOTOS EUROS User Guide v3.0.000 (TNO 2025 R10850)
- 3. Zanten, M.C. van, F.J. Sauter, R.J. Wichink Kruit, J.A. van Jaarsveld, W.A.J. van Pul, and R.J. Wichink Kruit (2010). Description of the DEPAC module. Dry deposition modelling with DEPAC GCN2010. Tech. rep. Bilthoven, The Netherlands: Rijksinstituut voor volksgezondheid en Milieu, RIVM report 680180001. URL: https://www.rivm.nl/bibliotheek/rapporten/680180001.pdf.
- 4. Wallace, J. M. 1., & Hobbs, P. V. (2006). *Atmospheric science: an introductory survey.* 2nd ed. Elsevier Academic Press.
- 5. Gina Mills et al. "Mapping critical levels for vegetation". In: LRTAP Conventions. Apr. 2017. Chap. Revised Chapter 3 of the Manual on Methodologies and Criteria for Modelling and Mapping Critical Loads and Levels and Air Pollution Effects, Risks and Trends

TNO Public 57/67

# 7. Appendix

In Table 5, the underlying land use maps of the open-source versions of LOTOS-EUROS v2.3 and v3.0 are listed. The main differences between v2.3 and v3.0 are outside the European domain which includes Belarus, Ukraine, and parts of west Russia. In addition, the water land use map, including inland waters and coasts, has changed. Now, the waters are based on their definition of the Corine 2018 map which is mostly visible along the coastline of Europe.

In Table 6, the extension of the land use classes are shown. The forest classes are extended to evergreen and deciduous broadleaf and coniferous forests, and the desert class into barren land which has same the deposition velocities as dsr default and seminatural which has different deposition velocities from dsr default. Extensions are indicated in yellow; name changes in green.

In Table 7, the translations between the Corine map classification and LOTOS-EUROS classifications are shown. Classification changes between v2.3 and v3.0 are indicated in red; name changes in green. In Figure 82 and Figure 83, the changed lu-classes with most (expected) impact are shown.

Outside the EU domain, the update of the ESA map (Table 5) leads to a significant change of the forest lu-fraction, namely the deciduous (dec) and coniferous (cnf) forests, showing mostly changes in Russia/Belarus and north of Africa as depicted in Figure 84.

In Figure 85 to Figure 89, the land use fraction in v2.3 and v3.0 for the selected locations in Figure 1 are shown illustrating the changes of land use fractions. For each category in v2.3 on the x-axis, the blue colored bar illustrated its lu-fraction in v2.3. Next to this blue bar, the light-to-dark colored orange bars correspond to the three-tiered land use category in v3.0. A small shift of the orange bars to the right indicates that multiple climate zones are present at this location. In the legend, all three-tiered land use categories are shown.

For more details, we refer to the LOTOS-EUROS Reference Guide of v3.0.

Domain	V2.3	V3.0	Remark
Outside EU	Corine 2000,	ESA 2015 <sup>6</sup>	Belarus, Ukraine, and
	EEA2000 <sup>5</sup>		parts of west Russia
			are defined by
			ESA2015
Water	Specific waterbody file <sup>7</sup>	Corine 2018 <sup>8</sup>	Only visible at
			coastline
Europe	Corine 2018	Corine 2018	Translation to model
			classes changed

Table 6: Main land use classifications for version v2.3 and v3.0. The shading shows: no change (white), name change (green), and new classes (yellow).

v2.3		v3.0	v3.0		
grs	Grass	grs	Grass		
ara	Arable land	ara	Arable land		
crp	Permanent Crops	crp	Permanent crops		
dec	Deciduous Forest	fbd	Forest: Broadleaved		
			deciduous		

<sup>&</sup>lt;sup>5</sup> EEA (2000). CORINE Land Cover 2000. URL: dataservice.eea.eu.int

TNO Public 58/67

<sup>&</sup>lt;sup>6</sup> https://www.esa.int/ESA\_Multimedia/Images/2018/09/2015\_global\_land\_cover\_map

<sup>&</sup>lt;sup>7</sup>World Water Bodies", version 2011, last updated 10-2-2015. Created by Delorme Publishing and distributed by ESRI, http://library.duke.edu/data/files/esri/esridm/2013/world/data/hydropolys.html

<sup>8</sup> https://land.copernicus.eu/en/products/corine-land-cover/clc2018

		fbe	Forest: Broadleaved
			evergreen
		fcd	Forest: Coniferous
			deciduous
cnf	Coniferous Forest	fce	Forest: Coniferous
			evergreen
urb	Urban areas	urb	Urban areas
wai	Inland water	ilw	Inland water
wat	Sea water	sea	Sea water
dsr	Desert	brn	Barren land
		sem	semi natural land
oth	Other	oth	Other

Table 7: Translation from Corine classes to LOTOS-EUROS land use types. The shading shows: no change (white), name change (green), and changed LOTOS-EUROS-class (red).

Corine class	v2.3	v3.0
Continuous urban fabric	urb	urb
Discontinuous urban fabric	urb	urb
Industrial or commercial units	urb	urb
Road and rail networks and associated land	urb	urb
Port areas	urb	urb
Airports	urb	urb
Mineral extraction sites	urb	oth
Dump sites	urb	oth
Construction sites	urb	urb
Green urban areas	grs	urb
Sport and leisure facilities	grs	grs
Non-irrigated arable land	ara	ara
Permanently irrigated land	ara	ara
Rice fields	ara	ara
Vineyards	crp	crp
Fruit trees and berry plantations	crp	crp
Olive groves	crp	crp
Pastures	grs	grs
Annual crops associated with permanent crops	ara+crp	crp
Complex cultivation patterns	ara	ara
Land principally occupied by agriculture with		
significant areas of natural vegetation	ara+crp	crp
Agro-forestry areas	crp	crp
Broad-leaved forest	dec	fbd
Coniferous forest	cnf	fce
Mixed forest	dec+cnf	fbd
Natural grasslands	oth	grs
Moors and heathland	oth	sem
Sclerophyllous vegetation	oth	sem
Transitional woodland-shrub	dec+cnf	sem
Beaches dunes sands	dsr	brn
Bare rocks	dsr	brn

TNO Public 59/67

Sparsely vegetated areas	dsr	sem
Burnt areas	dsr	brn
Glaciers and perpetual snow	wat	ilw
Inland marshes	dec+wai	sem
Peat bogs	grs+wai	sem
Salt marshes	dsr+wat	sea
Salines	dsr+wat	sea
Intertidal flats	dsr+wat	sea
Water courses	wai	ilw
Water bodies	wai	ilw
Coastal lagoons	wat	sea
Estuaries	wai	sea
Sea and ocean	wat	sea

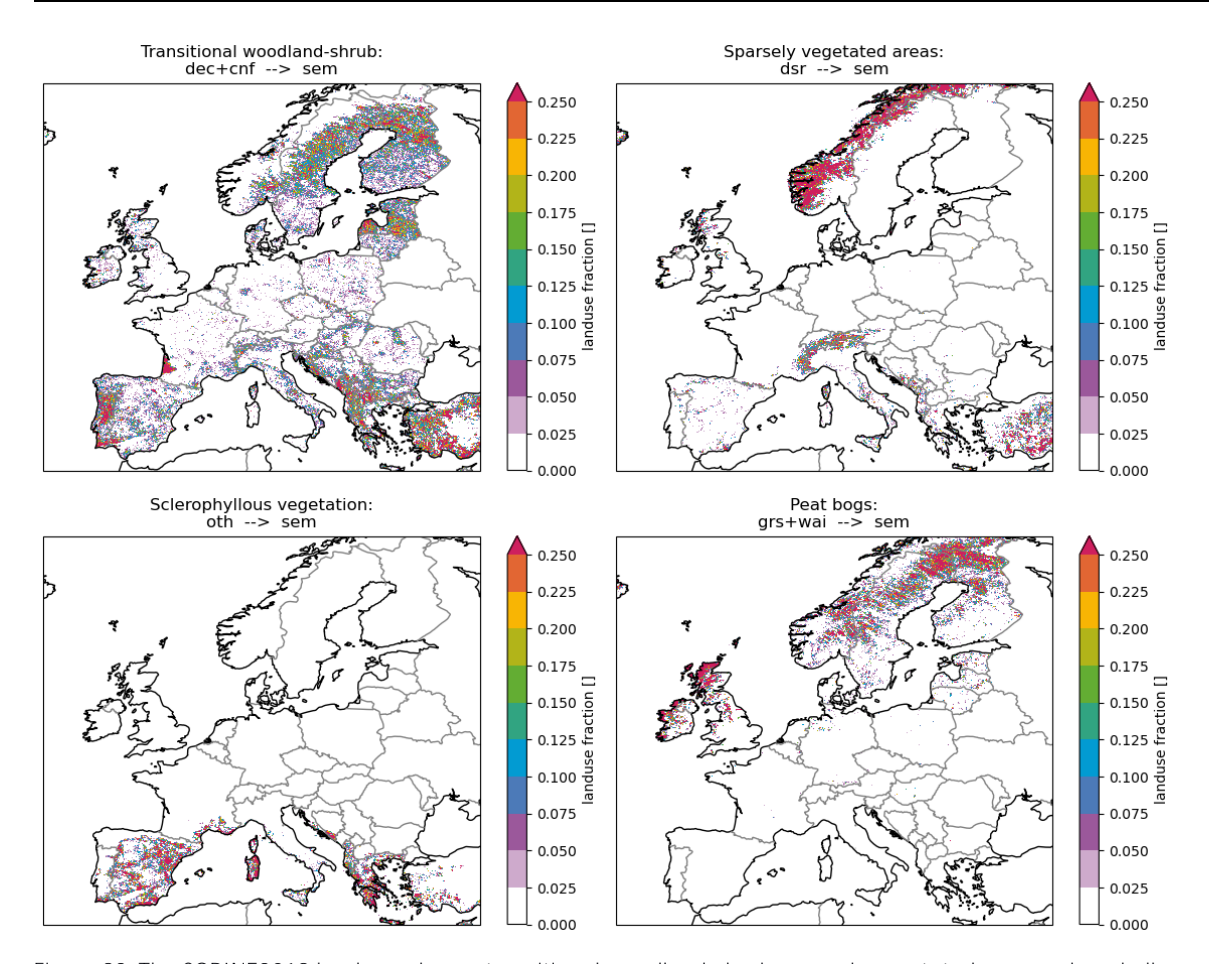


Figure 82: The CORINE2018 land use classes transitional woodland-shrub, sparsely vegetated areas, sclerophyllous vegetation, and peat bogs which changed LOTOS-EUROS land use classification (Table 7) and have significant lu-fraction throughout the domain. The CORINE classes are written in the title, including the LOTOS-EUROS land use class change as the subtitle as "old class --> new class".

TNO Public 60/67

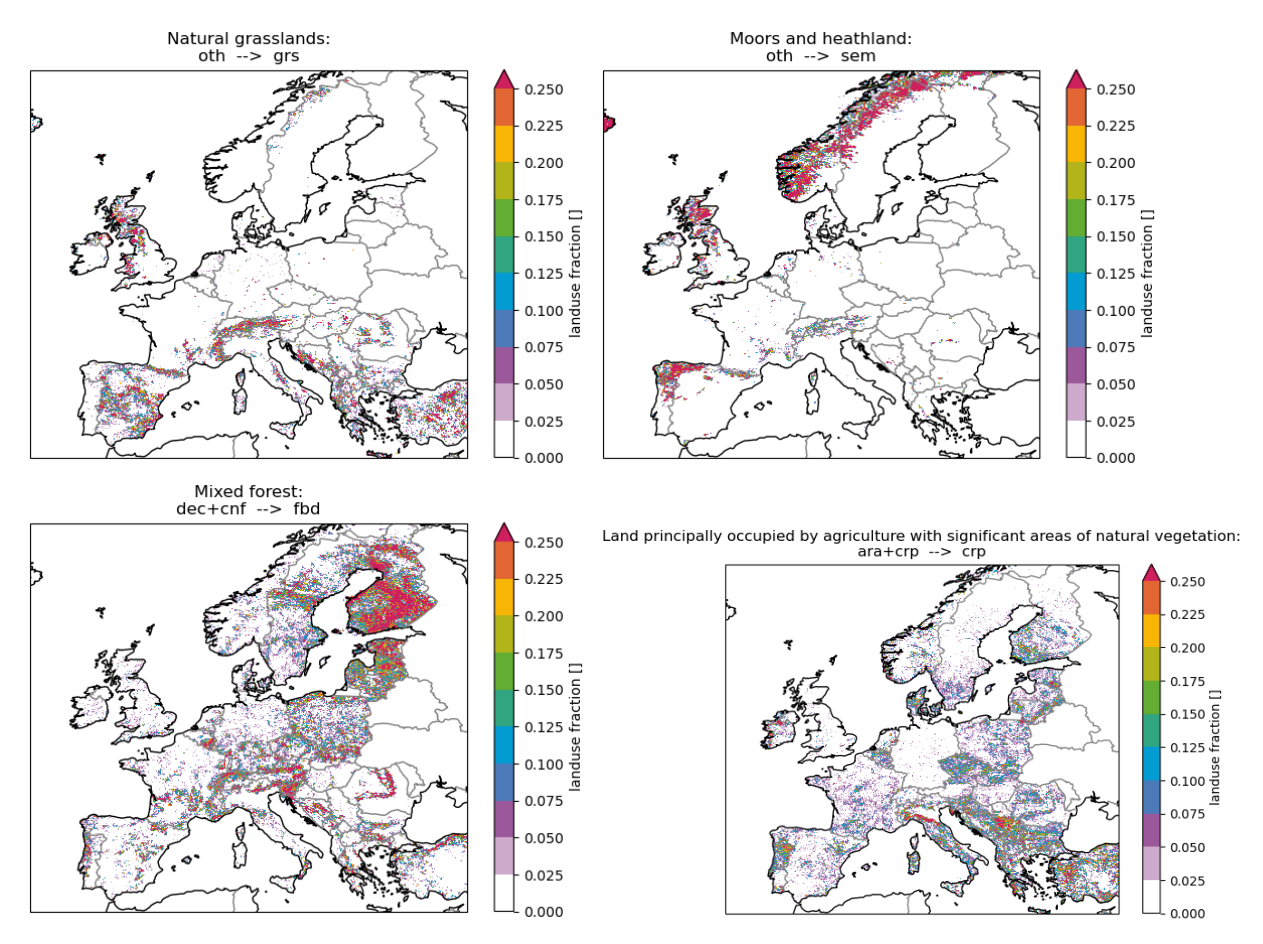


Figure 83: The CORINE2018 land use classes natural grassland, moors and heathland, mixed forest, and land principally occupied by agriculture with significant areas of natural vegetation which changed LOTOS-EUROS land use classification (Table 7) and have significant lu-fraction throughout the domain. The CORINE classes are written in the title, including the LOTOS-EUROS land use class change as the subtitle as "old class --> new class".

TNO Public 61/67

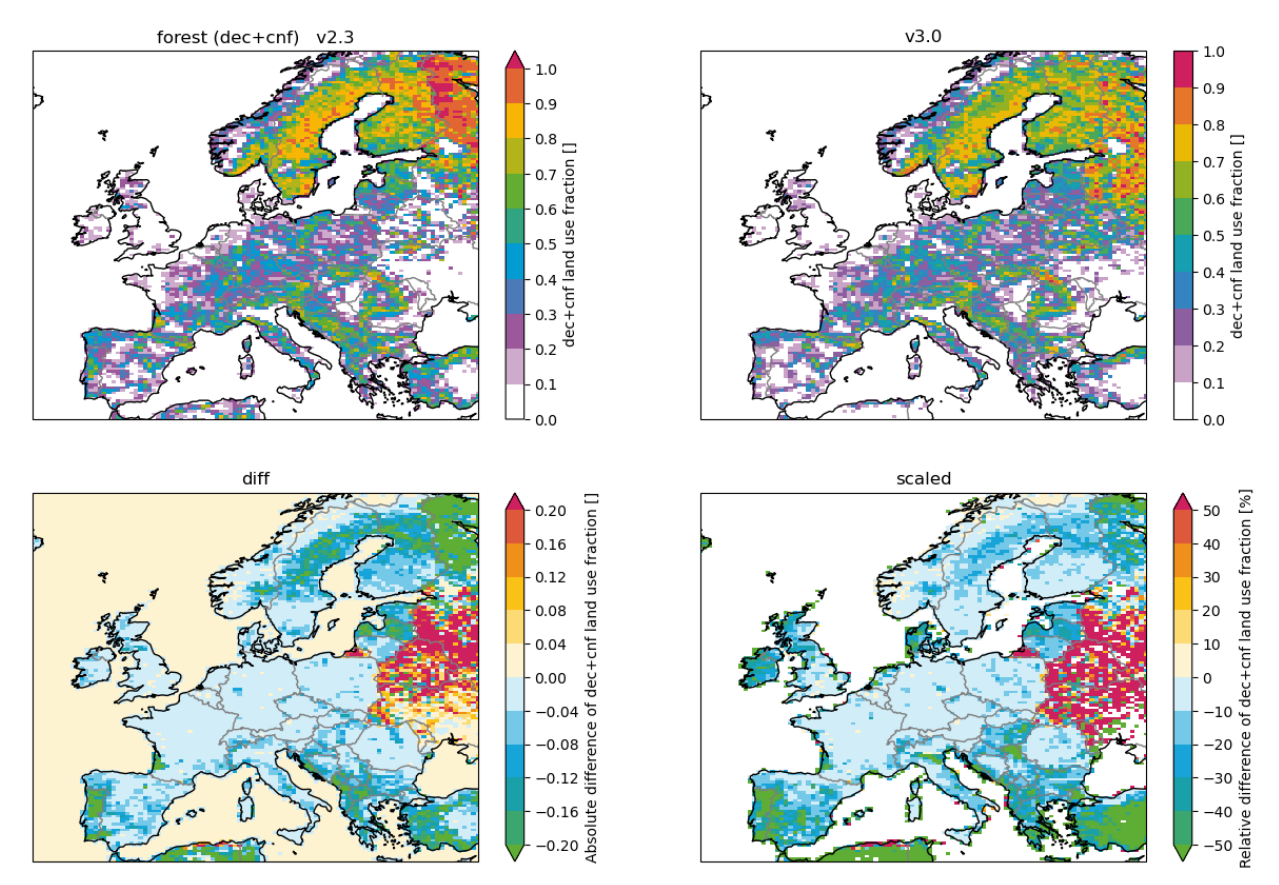


Figure 84 (top) The forest land use classes (dec+cnf) in v2.3 and v3.0. (bottom) The absolute and relative difference between the forest classes in v2.3 and v3.0.

TNO Public 62/67

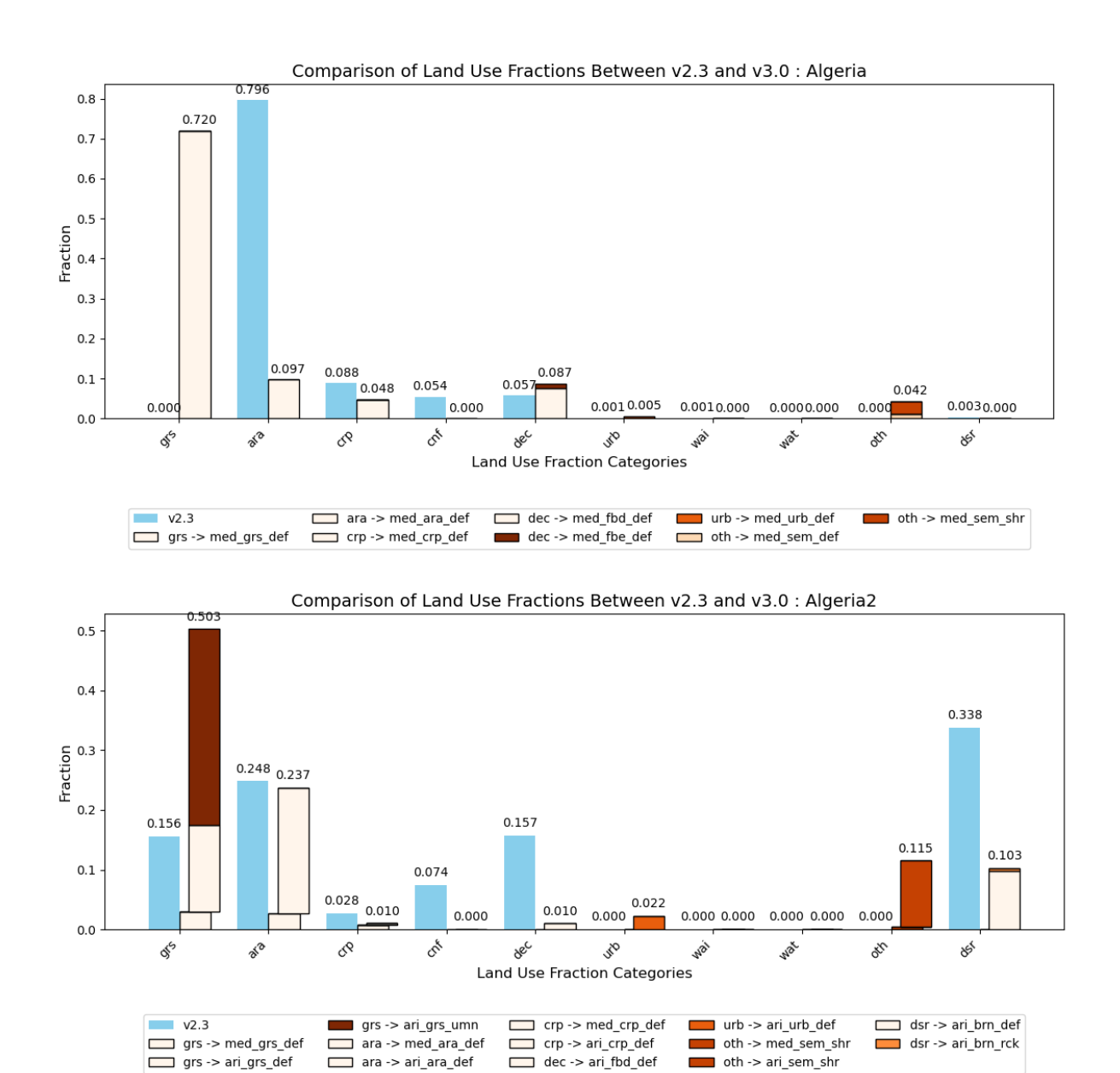
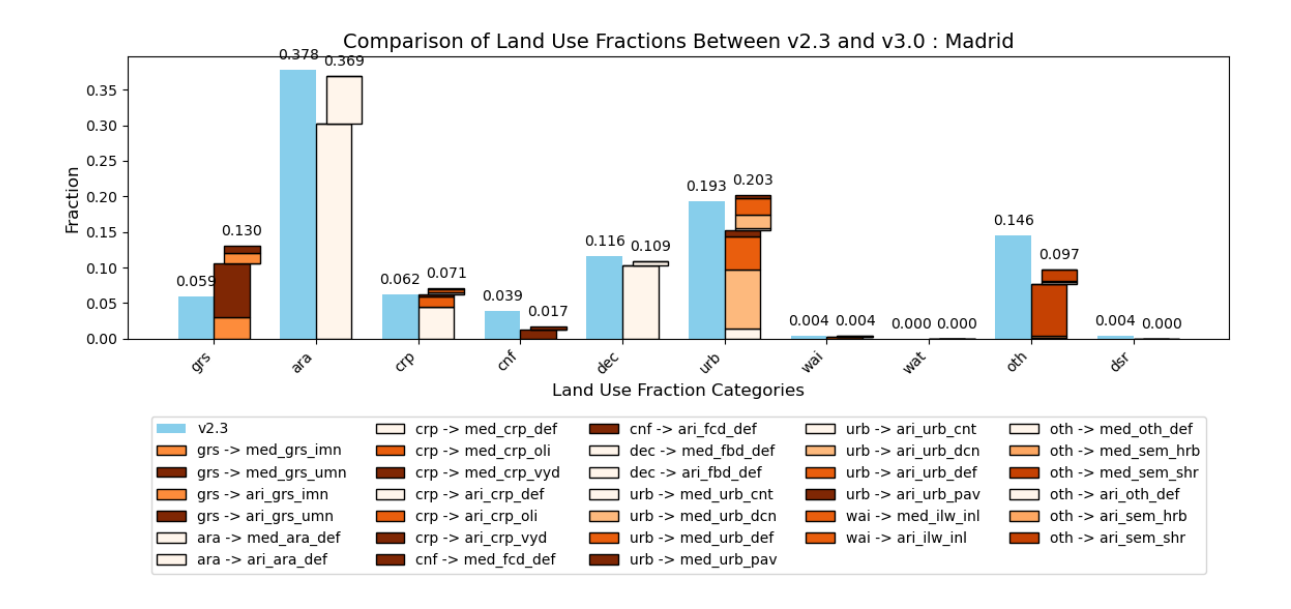


Figure 85: Bar plots of the land use fraction in v2.3 (blue bars with the old lu-class written on the x-axis) and the three-tiered land use classification in v3.0 in light to dark orange. The locations, written in the title of the plot, can also be seen on the map in Figure 1.

TNO Public 63/67



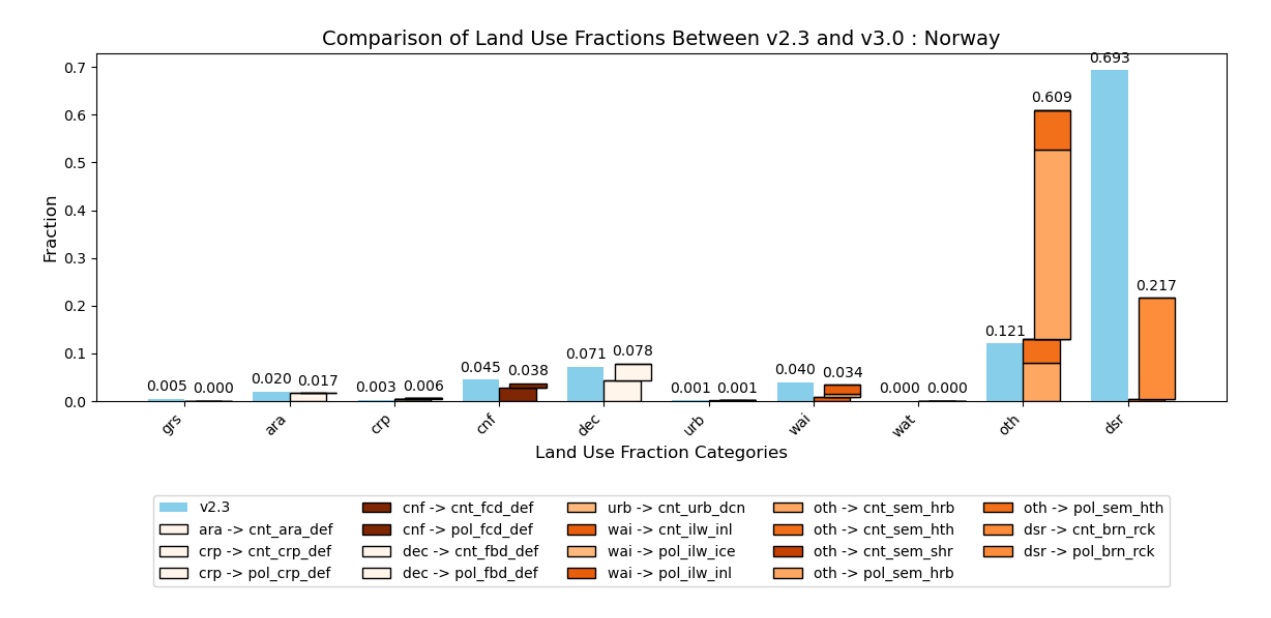
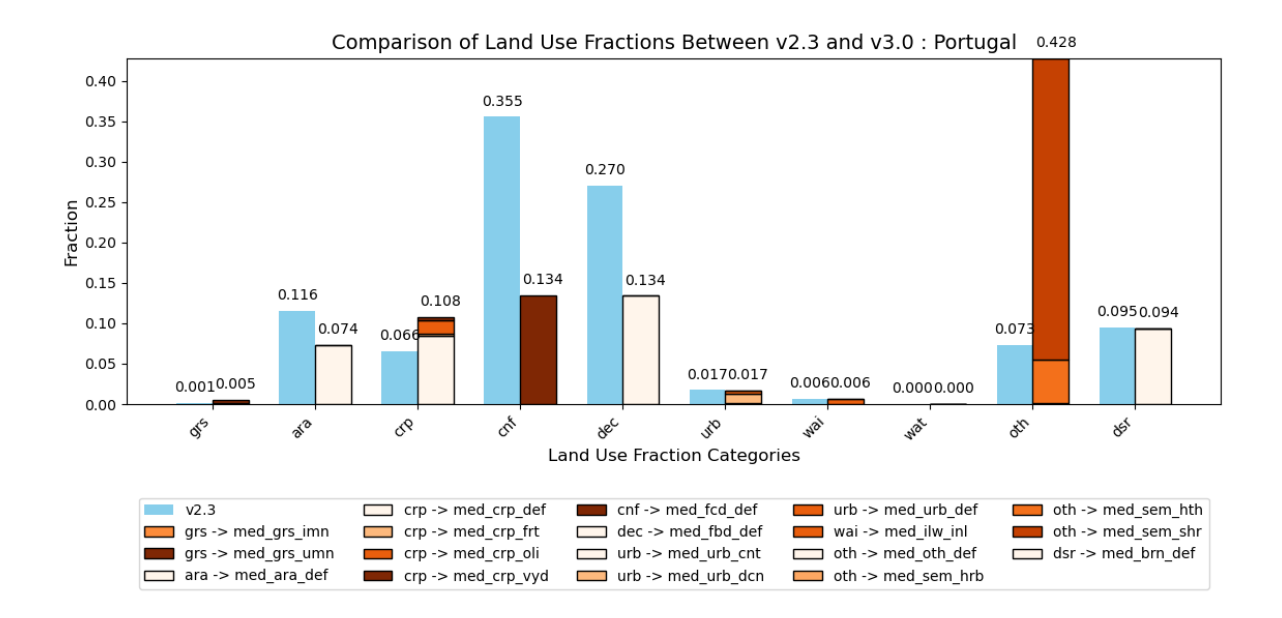


Figure 86: Bar plots of the land use fraction in v2.3 (blue bars with the old lu-class written on the x-axis) and the three-tiered land use classification in v3.0 in light to dark orange. The locations, written in the title of the plot, can also be seen on the map in Figure 1.

TNO Public 64/67



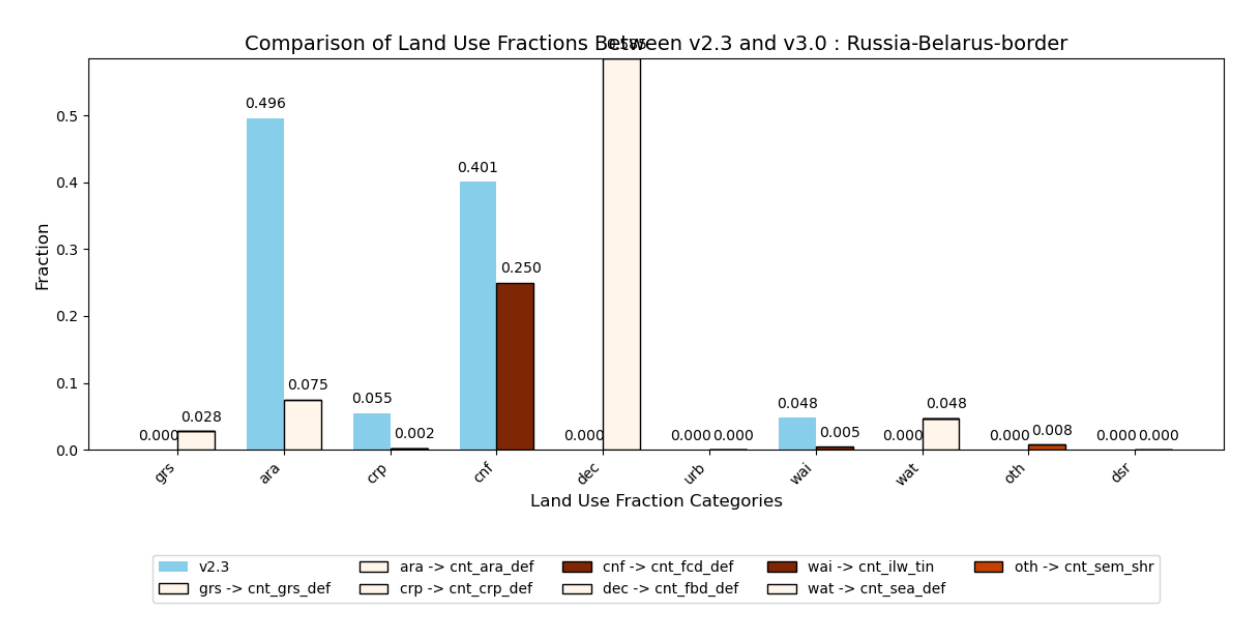
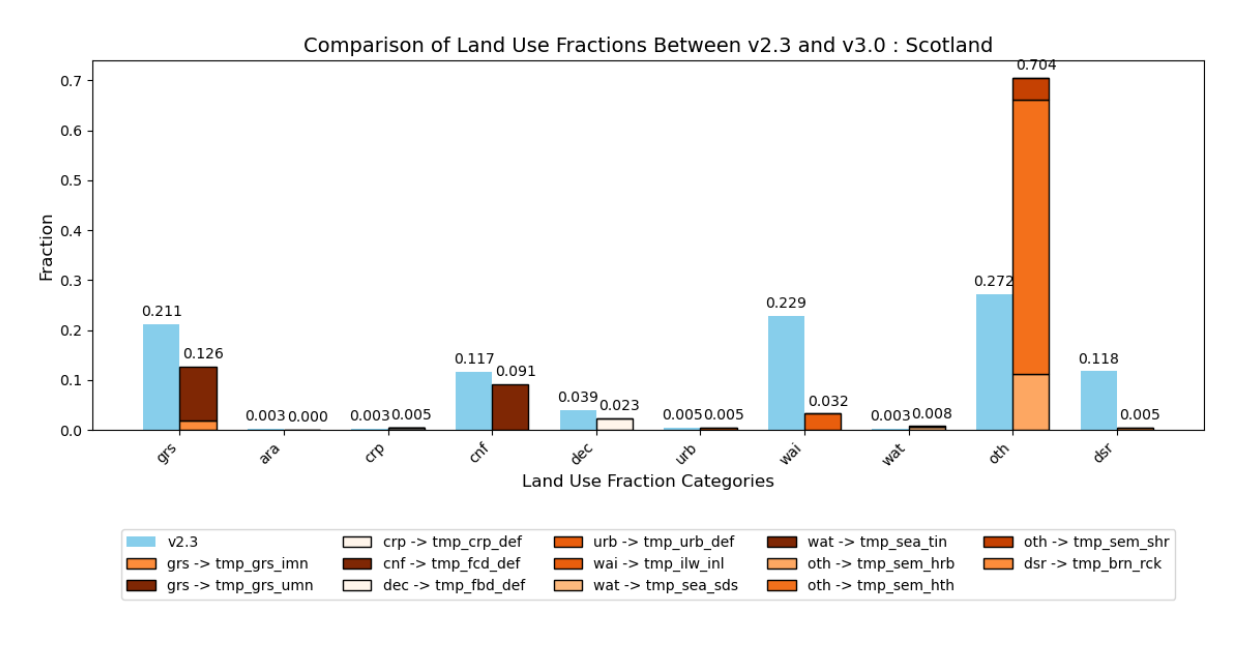


Figure 87: Bar plots of the land use fraction in v2.3 (blue bars with the old lu-class written on the x-axis) and the three-tiered land use classification in v3.0 in light to dark orange. The locations, written in the title of the plot, can also be seen on the map in Figure 1.

TNO Public 65/67



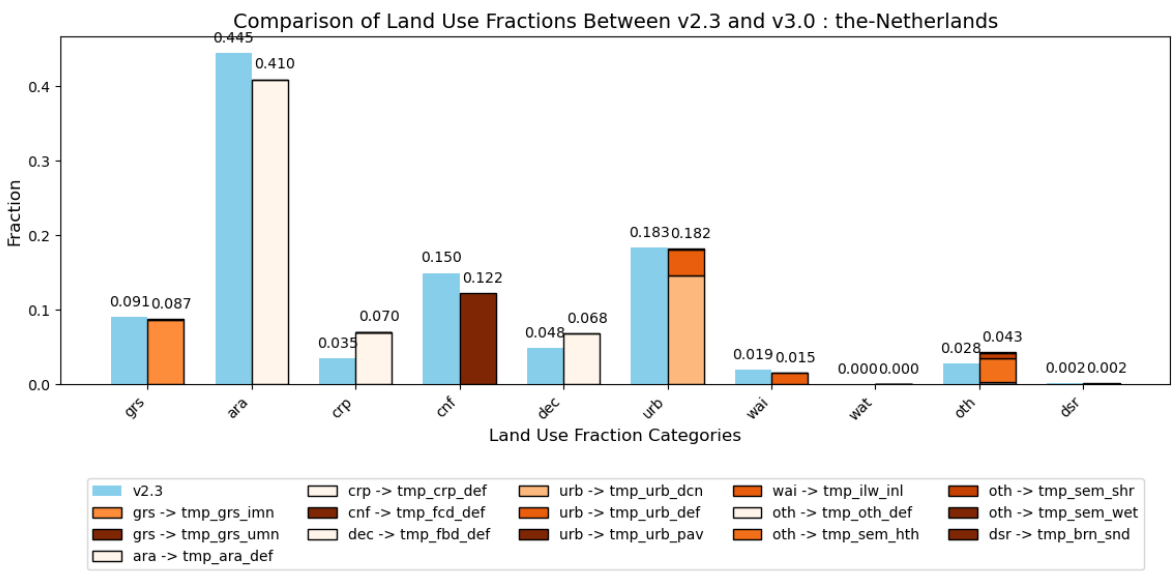


Figure 88: Bar plots of the land use fraction in v2.3 (blue bars with the old lu-class written on the x-axis) and the three-tiered land use classification in v3.0 in light to dark orange. The locations, written in the title of the plot, can also be seen on the map in Figure 1.

TNO Public 66/67

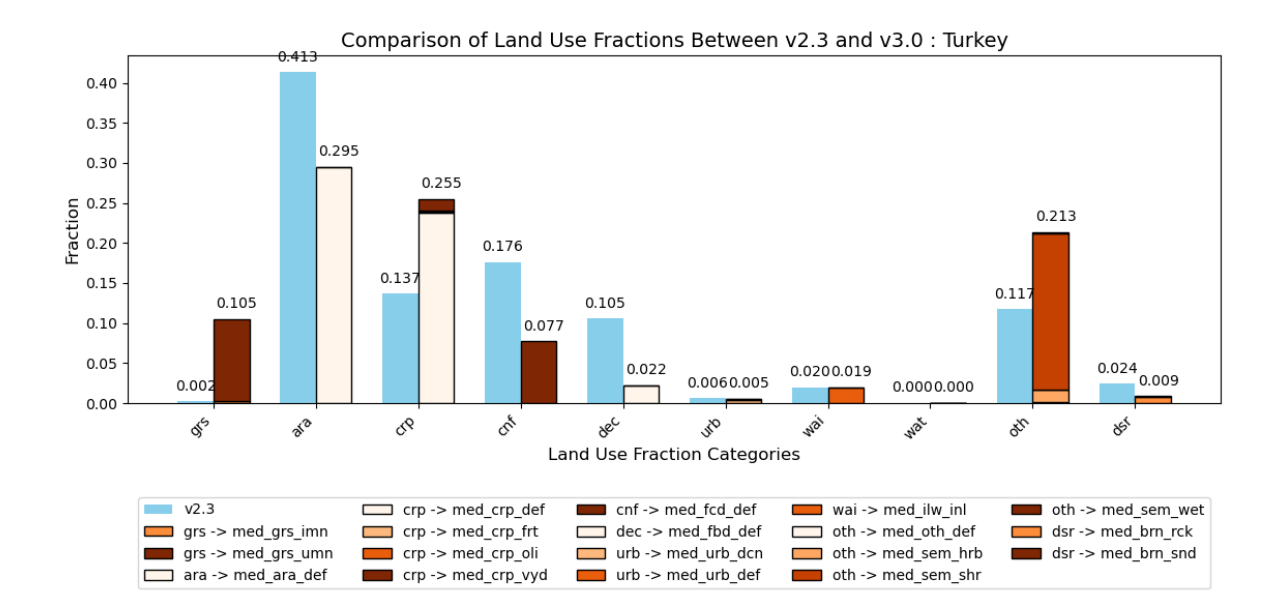


Figure 89: Bar plots of the land use fraction in v2.3 (blue bars with the old lu-class written on the x-axis) and the three-tiered land use classification in v3.0 in light to dark orange. The locations, written in the title of the plot, can also be seen on the map in Figure 1.

# 8. Signature

TNO - Energy & Materials Transition - Utrecht, 8 May 2025

Sam van Goethem Research manager Diane Pétillon Project manager

) TNO Public 67/67